TECHNISCHE UNIVERSITÄT MÜNCHEN

Institut für Entwicklungsgenetik

Analysis of the function of the polarity factors aPKCi and MPP5 in migration and differentiation of granule cells in the cerebellum of *Danio rerio*

Anna-Lena Kerner

Vollständiger Abdruck der von der Fakultät
Wissenschaftszentrum Weihenstephan für Ernährung, Landnutzung und Umwelt
der Technischen Universität München zur Erlangung des akademischen Grades eines

Doktors der Naturwissenschaften

genehmigten Dissertation.

Vorsitzender:		Univ.-Prof. Dr. K. Schneitz
Prüfer der Dissertation:	1.	Univ.-Prof. Dr. W. Wurst
	2.	apl. Prof. Dr. J. Adamski

Die Dissertation wurde am 20.09.2012 bei der Technischen Universität München eingereicht und durch die Fakultät Wissenschaftszentrum Weihenstephan für Ernährung, Landnutzung und Umwelt am 21.01.2013 angenommen.

I. Summary

Impaired migration of neurons to ectopic locations often results in diseases such as Lissencephlay, Polymicrogyria and Heterotopia. In order to divide, to migrate and also to terminally differentiate, cells need an intrinsic polarity to accomplish these tasks in the correct orientation. The proteins aPKCi and MPP5 are crucially involved in orchestrating polarity in many cell types and tissues, but their influence on neuronal differentiation and neuronal migration is not well understood. To investigate their contribution to establish and maintain neuronal polarity we chose the cerebellum, because it is a highly conserved brain compartment among vertebrates including the zebrafish.

For both polarity factors mutant zebrafish lines are available, *heart&soul* (*apkci*) and *nagie oko* (*nok, mpp5*). Neuronal migration in these mutants was addressed by investigating the most numerous neuronal population in the cerebellum, the granule cells (GCs) which migrate long distances from their origin of birth to their final position within the mature cerebellar network. First cerebellar morphology in *apkci* and *nok* mutants was analysed, to elucidate whether cerebellar development is actually affected in these mutant lines. Cellular membrane staining clearly showed a disrupted tissue architecture and a disorganized cellular pattern. Subsequent whole-mount mRNA *in situ*-hybridizations and fluorescent immuno-histochemistry confirmed expression of both, *apkci* and *nok* in the developing cerebellum and in the GC population or its precursors. The following analysis revealed that GC differentiation was impaired in both mutants. In $apkci^{-/-}$ embryos terminal differentiation was found to be missing completely. Because *apkci* mutants showed the stronger phenotype than $nok^{-/-}$ embryos with respect to GC development, subsequent experiments concentrated on the function of aPKCi. Within this work it turned out that the number of GCs is significantly reduced in the mutants, which could be traced back to a decrease of cell proliferation and an increased cell death rate, which was consonant with research studies in other tissues revealing a function of aPKCi in proliferation and cell survival. Confocal time-lapse recordings revealed a proper motility of GCs in *apkci* mutants, however their migration was not directed, but rather unoriented with many directional changes. GCs migrated to ectopic positions and sometimes crossed the posterior morphological border of the cerebellum to migrate into the hindbrain. GCs could most probably cross the apical cerebellar border, because of its interrupted organization, revealed by a fluorescent immune-staining of apical junctions. In order to specifically target GCs, electroporation in combination with cell specific Gal4:UAS

expression was used to block aPKC function in a mosaic cell autonomous manner. Loss of aPKC function seemed to be rescued by the *wild-type* environment, because single affected GCs were able to migrate in a directed fashion, indicating a tissue-specific function rather than a cell-autonomous role of aPKCi in directing GC migration. In summary, this work supports the importance of aPKCi and Nok in cerebellar development. Further I demonstrated that aPKCi is important for GC differentiation and essential to maintain cerebellar tissue integrity, which in turn is necessary for directed GC migration.

II. Zusammenfassung

Eine fehlerhafte neuronale Migration verursacht häufig neurologische Erkrankungen, wie Lissencephalie oder Polymikrogyrie. Damit eine Zelle sich gerichtet fortbewegen kann, aber auch um sich zu teilen und terminal zu differenzieren, muss eine intrinsische Polarität zur korrekten Zellorientierung während dieser Prozesse vorliegen. Die Polaritätsproteine aPKCi und Nok (MPP5) spielen eine wichtige Rolle, um in Zellen und Geweben Polarität zu etablieren und aufrechtzuerhalten. Jedoch ist bisher wenig über ihre Beteiligung an neuronaler Migration oder an der Differenzierung von Nervenzellen bekannt. In dieser Arbeit habe ich die Funktionen beider Proteine während der Entwicklung des Kleinehirns (Cerebellum) untersucht. Das Kleinhirn ist innerhalb der Vertebraten, und somit auch im Zebrabärbling evolutionär stark konserviert, d.h. die neuralen Zelltypen, sowie deren Anordnung und Vernetzung sind nahezu identisch.

Die Funktion von aPKCi oder Nok während der Entwicklung des Cerebellums wurde mit Hilfe von Zebrabärbling-Mutanten dieser Gene (*heart & soul* (*has*, *apkci*) und *nagie oko* (*nok*, *mpp5*)) untersucht. Die morphologische Untersuchung von *apkci* und *nok* Mutanten zeigte eine starke Fehlorganisation des Kleinhirns, gekennzeichnet durch eine zum Teil ungeordnete Zellanordnung und eine diffuse Abgrenzung zum Hinterhirn. Die Expression beider Gene im Cerebellum wurde durch *in situ*-Hybridisierungen und Antikörperfärbungen nachgewiesen. Diese ersten Ergebnisse bestätigten, dass beide Proteine eine wichtige Rolle während der Entwicklung des Cerebellums wahrnehmen. Die nachfolgende Analyse neuronaler Entwicklung in den Mutanten wurde an den Granulärzellen (GCs), den am häufigsten vorkommenden Neuronen im Kleinhirn, durchgeführt. GCs wandern lange Strecken von

ihrem Entstehungsort bis zu ihrer letztendlichen Position innerhalb des Cerebellums. Die Untersuchung der GC-Entwicklung ergab, dass in Embryonen beider Mutations-Stämme (*apkci* und *nok*) die Differenzierung der GCs gestört ist. In *apkci*$^{-/-}$ Embryonen blieb eine terminale Differenzierung sogar vollständig aus. Da die GCs in *apkci*$^{-/-}$ Embryonen stärker betroffen waren als in *nok*$^{-/-}$ Embryonen, konzentrierte sich die weitere Arbeit auf die Rolle von aPKCi während der neuronalen Entwicklung. Es stellte sich heraus, dass die Anzahl an GCs in *apkci*$^{-/-}$ Embryonen stark reduziert war, was auf eine niedrigere Zellproliferationsrate und einen Anstieg an apoptotischen Zellen im Vergleich zu Wildtyp Embryonen zurückgeführt werden konnte. Durch konfokale Zeitrafferaufnahmen GFP-markierter GCs hat sich gezeigt, dass GCs in *apkci*$^{-/-}$ Embryonen nicht in ihrer Beweglichkeit eingeschränkt sind, aber dass ihre Migration wenig gerichtet ist. Viele GCs bewegten sich ziellos mit vielen Richtungsänderungen und wanderten dabei häufig zu ektopischen Positionen, sogar über die caudale Kleinhirn-Grenze hinweg ins angrenzende Hinterhirn. Eine Färbung apikaler Tight Junctions zeigte eine lückenhafte Organisation apikaler Strukturen auf, die höchstwahrscheinlich ein Entweichen von fehlerhaft migrierenden GCs ins Hinterhirn ermöglichte. Ein weiteres Ziel dieser Arbeit, aPKCi mosaikhaft ausschließlich in GCs zu blockieren, wurde mithilfe von Elektroporation erreicht, kombiniert mit zelltyp-spezifischer Gal4-Expression. Es stellte sich heraus, dass derart manipulierte GCs trotz blockierter aPKCi Funktion zielgerichtet wandern konnten. Der in Mutanten beobachtete Phänotyp, die ziellose Migration von GCs, wurde hier offenbar durch die wildtypische Umgebung kompensiert. Daraus ließ sich schließen, dass aPKCi in Bezug auf neuronale Migration wohl keine zellautonome, sondern eher eine übergeordnete gewebsspezifische Funktion ausübt. Zusammengefasst konnte ich mit dieser Arbeit zeigen, dass aPKCi und Nok notwendig für die Entwicklung des Cerebellums sind. Weiterhin konnte ich demonstrieren, dass aPKCi wahrscheinlich eine zellautonome Funktion während der Differenzierung von Granulärzellen ausübt und notwendig ist, um die Gewebsintegrität aufrechtzuerhalten, was wiederum eine gerichtet Migration von GCs ermöglicht.

III. Index

1 Introduction

1.1 The cerebellum of zebrafish as model to study neuronal development

The cerebellum is an evolutionary highly conserved brain compartment among vertebrates. Cell types, neuronal connections, development and cerebellar functions are very similar (fig. 1). Despite the large number of neurons (the cerebellum contains about 50% of all neurons of the vertebrate brain) only few different neuronal cell types build up the layered structure of the cerebellum, which therefore possesses a rather simple neuronal circuitry ideally suited to study neuronal development. The cerebellum is the control centre to fine-tune movements of the locomotor system, proprioception, it regulates and controls body posture, balance and motor-learning. During the past years several investigations also proved the involvement of the cerebellum in higher cognitive and emotional tasks, and subsequently revealed cerebellar abnormalities as a potential cause for psychological disorders, like autism and schizophrenia (for review see Ito 2008; Hibi and Shimizu 2012).

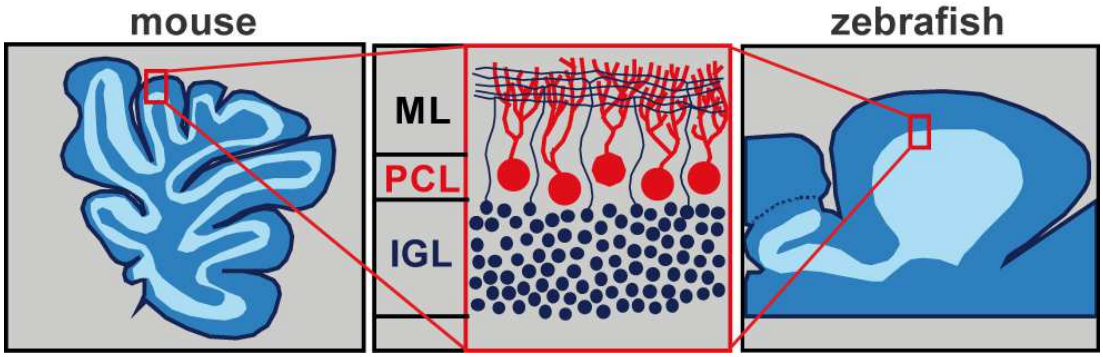

Figure 1.1: The cerebellum is an evolutionary highly conserved brain region.
The scheme shows a comparison between mouse and zebrafish cerebellum and its layered organization. Image by courtesy of R.W. Köster (adapted from Köster, 2006).

Studies in the goldfish indicate, that the cerebellum in teleost is also involved in higher cognitive tasks, for example in eyeblink-like conditioned responses, spatial cognition, memory, learning, ‘emotional’ responses and heart rate conditioning (Rodríguez et al. 2005; Gómez et al. 2010; Hibi and Shimizu 2012). Teleost like the model organism Danio rerio (zebrafish) are therefore well suited for studying cerebellar development. In addition the

external development and the transparency of the embryo allow live imaging in vivo without harming the embryo, and the small size of the embryos enables nonetheless the imaging through the whole cerebellum by confocal laser scanning microscopy. Because of the large numbers of eggs, enough genetically altered embryos like homozygous mutants can be obtained in short time, as well as enough successful manipulated eggs by injection or electroporation of nucleic acid.

1.2 Origin of the cerebellum

The position of the vertebrate cerebellum along the anterior-posterior axis of the neural tube is defined by signals from the Isthmic organizer (IsO), a signaling center within the neural plate, which is localized at the junction between mesencephalon and metencephalon. Induction of the IsO is controlled by the expression of the homeodomain transcription factors orthodenticle homologue 2 (Otx2) and gastrulation brain homeobox 2 (Gbx2). During gastrulation the border between the expression domains of Otx2 and Gbx2 is still diffuse. But during early neurulation the expression domains of Otx2 on the anterior and Gbx2 on the posterior site of the mid-hindbrain junction create a clear border, shown for zebrafish (Gbx1) (Rhinn et al. 2003) and mosue (Joyner et al. 2000).

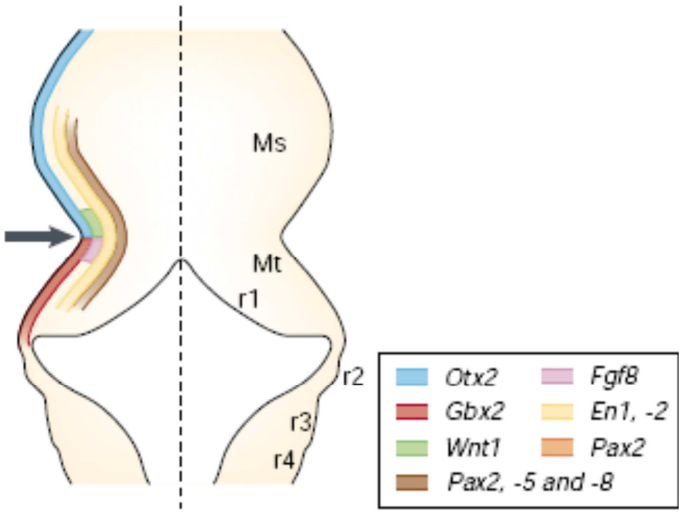

Figure 1.2: The position of the cerebellum is defined by the Isthmic Organizer
The schematic drawing of the mouse mid-hindbrain represents the expression of distinct genes along the IsO to define the boundary between and the positioning of the mid- and hindbrain. Expression of all genes is confirmed for the zebrafish IsO. Image adopted from Wurst and Bally-Cuif, 2001.

Two other genes are strictly separated at the IsO, Wnt1 and Fgf8, which are expressed in a narrow domain just anterior and posterior to the IsO, respectively (fig. 1.2) (Krauss et al. 1992; Joyner 1996; Wurst and Bally-Cuif 2001; O'Hara et al. 2005). Transplantation experiments in chicken embryos and mutation analysis in zebrafish and mouse revealed that Fgf8 is crucial and sufficient to induce the development of mesencephalic and cerebellar structures and to maintain them (Wurst and Bally-Cuif 2001; Sato et al. 2004). The further regionalization of the metencephalon into 7 rhombomeres in zebrafish is orchestrated by specific expression of Hox genes (Moens and Prince 2002). Rhombomere 1 finally gives rise to the cerebellum and rhombomeres 2-7 become the hindbrain.

1.3 Ventricle inflation

During brain development, the neural tube opens at the midline at several hinge points to form the brain ventricles. The hinge point of the 4th ventricle, or hindbrain ventricle, lies at the border between rhombomere 1 (cerebellar primordium) and rhombomere 2.

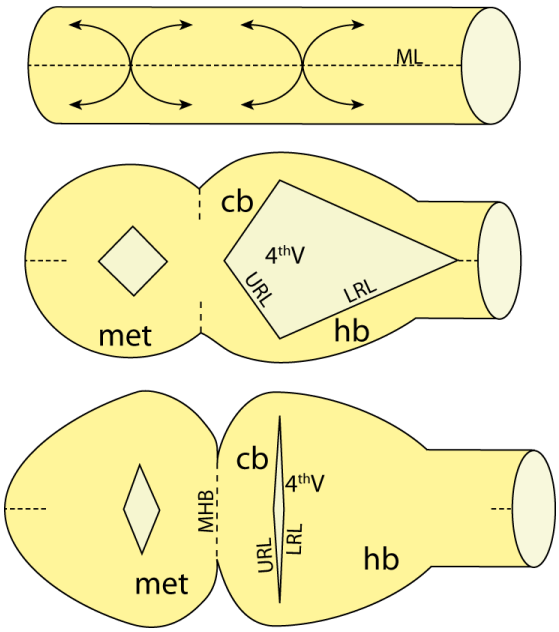

Figure 1.3: Rotation of cerebellar anlage during ventricle inflation
During embryonic development the neural tube opens at distinct hinge point along the dorsal midline starting from 18 hpf onwards and reaches its widest expansion at 24 hpf. Thereby the cerebellar primordium rotates from an anterior-posterior to a medio-lateral orientation. Upon continuous growth of the future brain the ventricles start to close. In case of the rhombencephalon the apical surfaces, i.e. the upper and lower rhombic lip of the ventricles adjoin, creating a morphological border between cerebellum and hindbrain.

Because of the ventricle inflation but continued attachment of midline cells at the IsO, the cerebellar anlage rotates around 90° from an anterior-posterior towards a medial-lateral orientation (fig. 1.3) (Sgaier et al. 2005; Distel et al. 2006). Upon subsequent ventricle closure, caused by continued neuronal proliferation and therefore continued enlargement of the brain, the ventricular surfaces of the cerebellum (upper rhombic lip, URL) and the posterior hindbrain rhombomeres (lower rhombic lip, LRL) adjoin, creating a morphological border between both brain compartments.

1.4 Structural organization of the cerebellum

The cerebellar primordium is a neuroepithelium and hence, cells span the whole radial width connecting to the apical ventricular site and basal lamina, here the mid-hindbrain boundary (MHB) by thin processes. With other words, the early primordium is only a single cell layer forming a proliferative epithelium. But because of interkinetic nuclear movement (INM, s. chapter 1.7), the position of the nuclei within the apical-basal axis varies from cell to cell, which leads to a pseudostratified appearance of the neuroepithelium. Only when first postmitotic cells disconnect from the apical lamina, the site of proliferation, the cerebellar anlage becomes actually multi-layered, being subdivided into zones of proliferating progenitors and regions of neural differentiation.

The mature cerebellum of mammals comprises the archicerebellum, which is the phylogenetic oldest part, the paleocerebellum and the neocerebellum (or cerebrocerebellum). The mature zebrafish cerebellum is divided into three lobes – the valvula cerebelli, only present in ray finned fish; the corpus cerebelli, homologuous to the paleocerebellum; and the vestibulolateral lobe, which is homologuous to the archicerebllum and subdivided into eminentia granularis and lobus caudalis cerebelli (Wullimann 1998). The anterior positioned valvula cerebelli and the medial corpus cerebelli consist of three layers, which are from superficial to deep, the molecular layer (ML), the Purkinje cell layer (PCL) and the internal granule cell layer (IGL). In contrast the lateral eminentia granularis and the posterior located lobus caudalis cerebelli contain only granule cells (GCs) in teleost (Wullimann et al. 1996). The ML is mainly comprised by the large dendritic trees of PCs and the axons of GCs, called parallel fibers. Interspersed are small interneurons, basket and stellate cells in mammals and only stellate cells in zebrafish. The PCL is only one cell thick containing the cell somata of PCs and Bergmann glia cells. Contrary, in the early zebrafish cerebellum no glial cells are

evident (Rieger et al. 2009). The IGL consists mainly of the somata of granule cells, but also of Golgi cells and, in zebrafish, eurydendroid cells which are located close to the PCL (for review (Hibi and Shimizu 2012). In mammals additionally unipolar brush cells reside within the IGL, but in teleost fish they are only reported so far for *Gnathonemus petersii* (Campbell et al. 2007; Mugnaini et al. 2011).

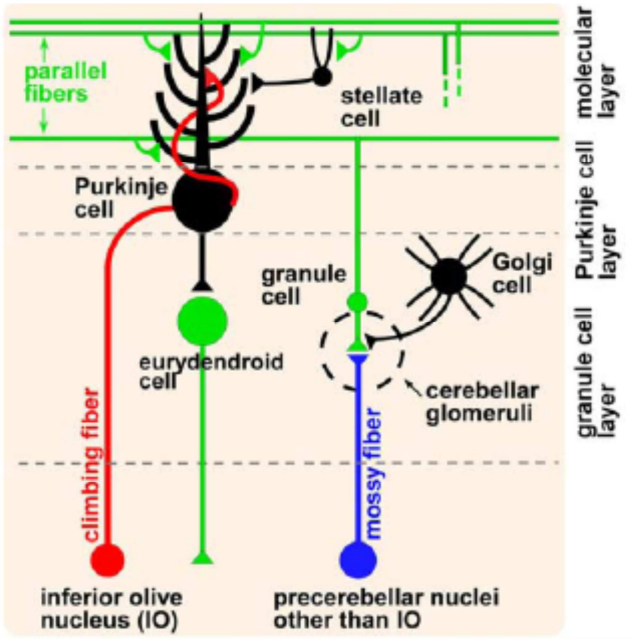

Figure 1.4: Cerebellar circuitry in the zebrafish cerebellum
Precerebellar nuclei provide excitatory input to the cerebellum, most projecting to GCs, except the IO, which send their axons to PCs. GCs develop long axons, called parallel fibers because of their orientation parallel to the cerebellar surface. Parallel fibers synapse onto dendrites of PCs. Thus, PCs integrate finally information from mossy and climbing fibers and generate an inhibitory output signal which is delivered to eurydendroid cells, which then project out of the cerebellum. Schematic drawing adopted from Bae et al., 2009.

The cerebellum receives excitatory input from several pre-cerebellar nuclei. The inferior olive nucleus (IO) is located at the posterior hindbrain and sends climbing fibers to the dendrites of Purkinje cells (PCs). Other pre-cerebellar nuclei project their axons, called mossy fibers, to dendrites of GCs, which subsequently also project on PC dendrites. Therefore, signals from climbing and mossy fibers are finally integrated by PCs, which generate the main output signal of the cerebellum. The inhibitory output signals by PCs are delivered to other PCs and, in zebrafish, to eurydendroid cells, which are located in close vicinity to PCs. Excitatory eurydendroid cells than project out of the cerebellum. In mammals there are no eurydendroid

cells; however PCs send their axons to the homologous functioning deep cerebellar nuclei. They are, in contrast to eurydendroid cells, located far from PCs in more ventral regions (Bae et al. 2009; Wullimann et al. 2011; Hibi and Shimizu 2012). Figure 1.4 illustrates schematically cerebellar neuronal cell types and their connections in the zebrafish cerebellum.

1.5 Origin of cerebellar neurons

Neurons of the cerebellum arise from two distinct proliferative zones along the ventricle. The dorsal most part, called upper rhombic lip (URL), defined by the expression of *atoh1*; and below the ventricular zone (VZ), expressing *ptf1a*. Inhibitory GABAergic neurons, i.e. Purkinje cells and interneurons like Golgi and stellate cells, are derived from *ptf1a* expressing progenitors of the VZ. Excitatory glutamatergic neurons, like granule cells, are derived from URL progenitors expressing the proneural gene *atoh1*. Interestingly neurons of the IO projecting to PCs are also derived from *ptf1a* expressing progenitors of the VZ; and mossy fiber-type pre-cerebellar nuclei projecting on GCs are derived from URL progenitors expressing *atoh1*. Suggesting a simple mode of how connections among neurons are already determined by the dorsoventral origin of their progenitors (Wingate 2005; Wullimann et al. 2011).

In mice the different types of neurons originating of one proliferative zone are generated in a sequential mode. For example, in the URL, tegmental hindbrain nuclei are generated first, than deep cerebellar nuclei and finally granule cells (Wingate 2005). In zebrafish also tegmental hindbrain nuclei are born first and subsequently GCs are delineated (Volkmann et al. 2008; Volkmann et al. 2010; Wullimann et al. 2011). In contrast most of the eurydendroid cells in zebrafish seem to origin from the VZ (Babaryka, 2009; Kani et al. 2010) though a small population also arises from *atoh1* expressing progenitors (Kani et al. 2010).

1.6 The major cell type of the cerebellum: The Granule Cells

Granule cells are the most numerous neurons in the cerebellum. They are glutamatergic excitatory interneurons projecting on PC dendrites. In mammals and chicken, GC precursors (GCPs) arise at the apical side of the most dorsal part of the URL and tangentially migrate to populate the whole surface of the cerebellar primordium, forming the external granular layer (EGL). GCP stay mitotically active in the EGL after leaving the ventricular zone, which is unique for neuronal precursors. Postmitotic GCs further move tangentially in the lower part of

the EGL, displaying a bipolar shape with a leading and a trailing process parallel to the surface oriented along the mediolateral axis.

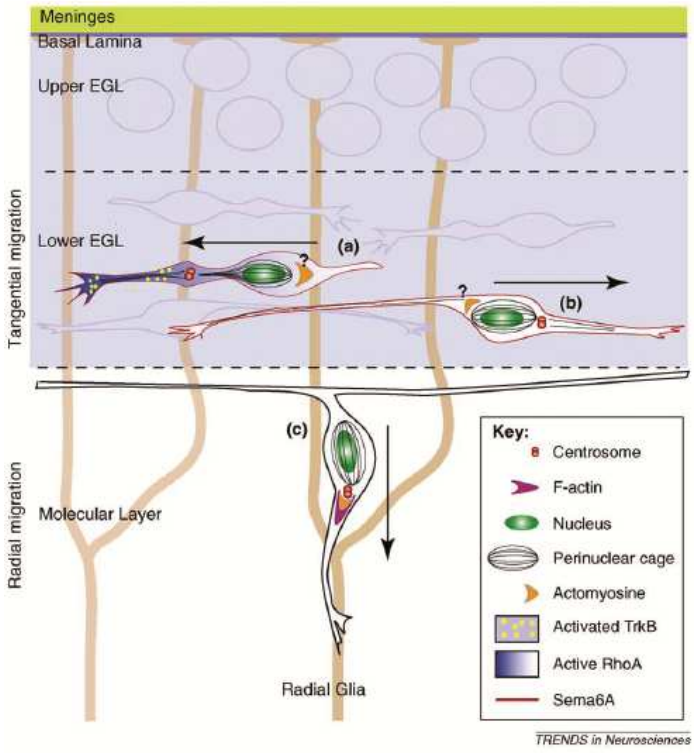

Figure 1.5: Tangential and subsequent radial migration of cerebellar GCs in mammals
GCs migrate tangentially in the transient external granule layer (EGL) before switching to radial migration through the molecular layer in order to reach their final destination in the inner granule cell layer (IGL) where migration ceases. Adopted from A. Chédotal, 2010.

After a certain time the GCs extend a third process perpendicular to the surface projecting to ventral regions and the cell starts to migrate along radial glial fibers (radial migration) through the molecular and the Purkinje cell layer to the IGL. The forward movement of the cell soma with the nucleus occurs by nuclear translocation (described below).

The initial two processes elongate and form the t-shaped parallel fibers, the axons of GCs, which remain in the molecular layer, whereas the cell somata, containing the nucleus, migrate ventrally. Finally, radial migration of GC stops in the IGL, ventral to PCs. The respective final position of the GC is hence determined upon leaving the lower EGL (for review see Chédotal, 2010 and fig. 1.5).

In teleost fish it is controversially debated whether an EGL is existent or not. Chaplin and colleagues stated that no EGL was formed in the zebrafish cerebellum (Chaplin et al. 2010 127). In contrast, a more recent publication in cooperation with our group suggests the presence of an EGL, which is however simpler compared to mammals, as it does not cover the whole surface of the cerebellar primordium, but is rather more restricted to the ventricular site (Wullimann et al. 2011).

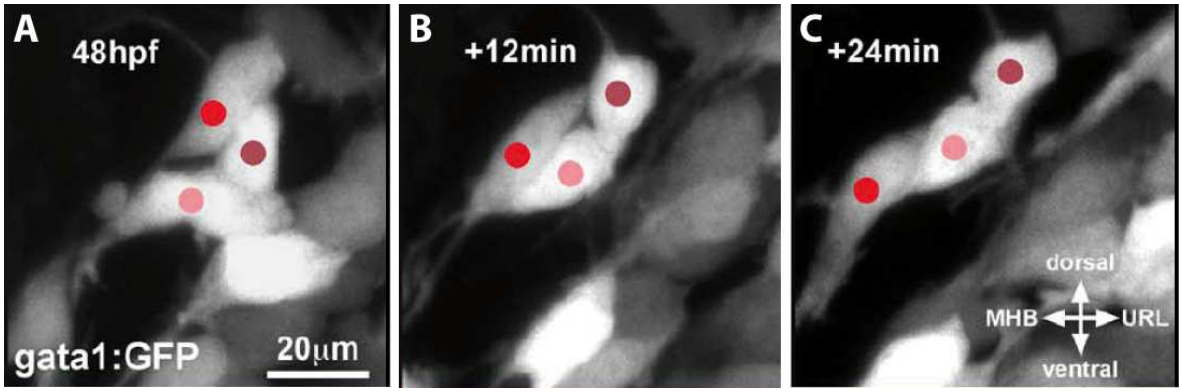

Figure 1.6: Chain-like migration of granule cells in the zebrafish cerebellum
GCs in zebrafish cerebellum migrate tangentially, utilizing each other as substrate and contacting by local temporal adhesion. Adopted from Rieger et al., 2009.

Another major difference, shown by our group, is the absence of radial migration of GCs along glial fibers in the early cerebellum of zebrafish, in contrast to GCs of mammalian cerebelli. GCs rather migrate in a chain like mode along each other, with the cell adhesion protein Cadherin-2 (N-cadherin) playing an important role for this type of migration (Rieger et al. 2009). However in the juvenile and adult cerebellum, newly generated GCs in a medio-ventral located stem cell niche first migrate dorsally along radial processes before turning and migrating lateral and ventral to the IGL by tangential migration (Kaslin et al. 2009).
But independent of the migration mode, cells need to be polarized with a leading site in direction of migration. Also in zebrafish, GCs extend a leading process and migrate by nuclear translocation (for detail s. chapter 1.8). It is not clear however whether the leading or trailing process finally elongates to become the axon when a GC reaches its final destination. It has been shown by our group that GCs migrate into different cerebellar regions to form three clusters. In the transgenic zebrafish strain *Tg(gata1:GFP)*, GFP is expressed in the cerebellum solely by GCs, allowing their tracing during migration by time-lapse recordings.

Depending on the position of birth along the mediolateral axis, GCs migrate to a distinct cluster and therefore finally contribute to a distinct mature functional domain. For example, GCs born near the dorsal midline migrate to the mid-hindbrain boundary (MHB) into the dorsomedial cluster, which later becomes the corpus cerebelli; whereas GCs arising from lateral regions of the cerebellar rhombic lip join the ventrolateral cluster, the future eminentia granularis (fig. 1.7). Therefore, the final position of a GC is already partly determined by its origin of birth in the URL (Volkmann et al. 2008). The same was proven for mice, in which, for example, expression domains of two engrailed genes along the ventrolateral axis of the cerebellar primordium partly define the later position in the mature cerebellum (Sgaier et al. 2005; Sgaier et al. 2007).

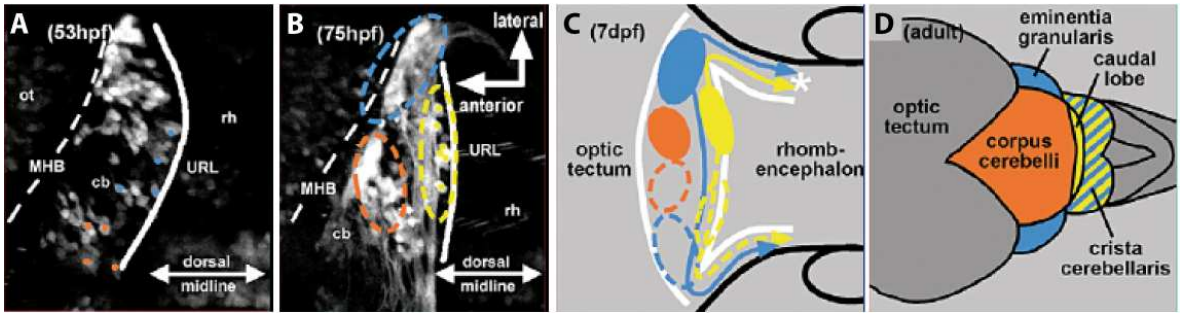

Figure 1.7: Cerebellar GC migration in zebrafish
Cerebellar GCs migrate in different regions to form three clusters, which can be assigned to distinct mature functional domains. For example, GCs migrating to form the dorso-medial cluaster (A, B, C, orange labelling) later contribute to the corpus cerebelli (D, orange area). Image adapted from Volkmann et al., 2008.

1.7 Interkinetic Nuclear Movement

Mitosis of GC progenitors (GCPs) and of every other proliferating neural progenitor in neuroepithelia takes place at the apical membrane. A simple reason for this could be, that the primary cilium and hence the centrioles of the basal body localize apically during G1 and S phase of cell cycle. During G2 and upon entering mitosis the primary cilium is retracted and the centrioles duplicate and separate into two centrosomes to set up the mitotic spindle (Chenn et al. 1998; Tamai et al. 2007; Santos and Reiter 2008). As mentioned already, the early cerebellar primordium is a mono-cell-layer and therefore densely packed by a large number of progenitors, to give rise to the vast numbers of neurons of the mature cerebellum.

Because of the high cell density, not all nuclei can be located at the apical site. To achieve nonetheless, that all nuclei can be mitotically active to further increase the progenitor pool, nuclei move between the apical URL and the basal MHB by interkinetic nuclear movement (INM). After mitosis at the URL the cell soma with the nucleus moves to more basal regions where DNA replication occurs. Successively, the nucleus moves back to the apical site during G2-phase followed again by mitosis. INM is therefore the periodic movement of the nucleus of neuroepithelial cells from apical to basal positions and back to the ventricular surface in concert with cell cycle progression (fig. 1.8, black cell) (Frade et al. 2002; Baye and Link 2007; Tamai et al. 2007).

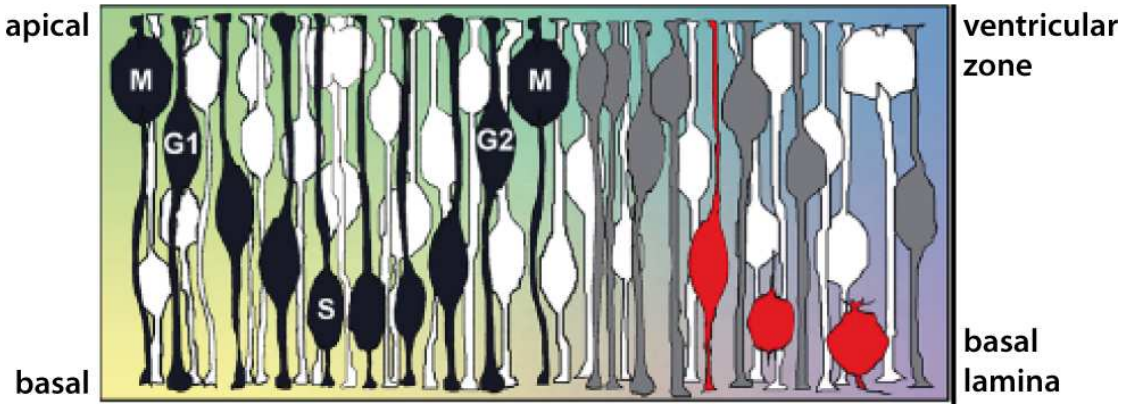

Figure 1.8: Interkinetic nuclear movement
In concert with cell cycle progression the cell soma, containing the nucleus, moves between the apical and basal membrane of the neuroepithelium (black cell). This enables all cells to reach the apical surface having sufficient space to divide and contribute to. Image adopted from Baye and Link, 2007

During INM the nucleus is moved by microtubule motors and actomyosin, but also passive forces like nucleus displacement by neighboring cells are involved. Throughout the entire cell cycle the cells stay attached to the apical and the basal side by characteristic endfeet. On the apical site cells contact each other by tight junctions, which mark the border between apical and basolateral domains of a cell. During division the apical and basal structures and their associated determinants are divided symmetric or asymmetric, resulting in most cases in two progenitors or in one neuron and one progenitor, respectively (Alexandre et al. 2010; Willardsen and Link 2011). Only after a neurogenic division, i.e. when a neuronal differentiation is initiated, the apical process detaches from the ventricular surface (fig. 1.8, red cell) (Baye and Link 2007; Taverna and Huttner 2010; Willardsen and Link 2011). The

cycling exposes the nucleus to different apico-basal protein gradients, which is supposed to play a role in cell fate determination. Depending on how far a nucleus moves basally ahead of division, a cell will either divide asymmetrically generating one neuron and one progenitor, or symmetric differentiative resulting in two neuronal cells, or symmetrically proliferative giving rise to two progenitors (Alexandre et al. 2010; Willardsen and Link 2011).

1.8 Migration of neuronal cells

Upon leaving the ventricular zone, when GCs become postmitotic, they have to migrate to their final destination and interconnect properly with other neuronal cells to build up functional neuronal network circuits. Cell polarity is important for both aspects. Migrating neurons are polarized in the direction of migration and mature neurons need to be polarized to setup axons and dendrites at the proper location for the interconnection with other neurons.

Migration of precursor cells and postmitotic neurons is an important feature to shape the developing brain and total nervous system to its final appearance. Most migrating neuronal cells extend a long thin leading process with a growth cone like shape at its tip. Forward movement of the nucleus occurs in a saltatory pattern and is also called nucleokinesis. First a swelling in the leading process ahead of the nucleus is formed, then the nucleus and the cell body are trans-located into this swelling and the resulting trailing process is retracted. Finally the leading process again elongates and a new migratory cycle is initiated (Tsai and Gleeson 2005; Marín et al. 2010; Valiente and Marín 2010). It was long thought, that the centrosome plays an important role in the forward movement of the nucleus, because in cell culture it was always located first in the swelling of the leading process ahead of the nucleus. However, recent work has shown that the centrosome does not locate necessarily ahead of the nucleus during the entire period of nucleokinesis. In early rhombic lip-derived neurons of the zebrafish cerebellum the centrosome is only leading the nucleus during preparation of a migratory step, but is trailing behind the nucleus after being surpassed by it during nuclear forward movement (Distel et al. 2010). A study on organotypic slices of the mouse cerebellum suggested, that the nucleus was pulled forward by stable microtubules extending into the leading process and anchored directly to the anterior part of the nuclear membrane; rather than being pulled forward by the centrosome (Umeshima et al. 2007). A further study of mouse cerebellar GC culture supports the hypothesis that acto-myosin contractility in the leading process pulls both, the centrosome and the soma forward (Solecki et al. 2009).

Interestingly, radially migrating neurons have a single leading process, whereas the leading process of most tangentially migrating neurons has several branches. This is most useful in order to make fast directional decisions upon binding chemo-attractants and -repellents and to follow a chemically laid down migratory route, rather than having first to retract a single wrong oriented process and to re-establish it towards a new direction (Martini et al. 2009).

1.9 Epithelial polarity

Neuroepithelia, like all epithelia, have a clear separation between apical and basolateral membrane sites, because of the different functions they need to fulfill. The apical membrane of the early neural tube faces to a fluid filled lumen and is sensitive to long range signaling by the primary cilia and transmembrane proteins of the cells. Different diffusible molecules generate gradients to which a cell responds intrinsically, for example to adopt a neuronal fate. The baso-lateral sector of a cell interacts with neighbouring cells and stabilizes cell-cell contact and tissue integrity. Distinct complexes localize specifically to these regions. There are two main apical complexes. One complex contains the proteins Crumbs, PATJ and Pals1 (homologues are *Dros.* Stardust and zebrafish Nagie oko or MPP5); and the other complex consists of Par-3 (*Dros.* Bazooka), Par-6 and aPKC (Margolis and Borg 2005; Assémat et al. 2008). In vertebrate epithelia, these complexes localize to the apical tight junctions (Feigin and Muthuswamy 2009) (fig. 1.9). The two complexes are linked by Par-6 and Pals1 and the connection is stabilized by Crumbs, which can interact with both proteins (Hurd et al. 2003; Lemmers et al. 2004). The protein kinase aPKC can directly interact with Par-3 and Par-6 by phosphorylating them. Par-6 further recruits active Rac1 and Cdc42 to aPKC (Joberty et al. 2000; Johansson et al. 2000; Qiu et al. 2000). Rac1 and Cdc42 are involved in modifying the actin cytoskeleton and hence important players in all kinds of polarity throughout species (Fukata et al. 2003) including directed migration of astrocytes in a wound healing assay, at least shown for Cdc42 in concert with Par6/aPKCζ and GSK-3ß (Etienne-Manneville and Hall 2003). Par-3 is the first protein of the Par-aPKC-complex to arrive at the apical membrane and is thought to target aPKC and Par-6 to this membrane region. In turn Par-6 and aPKC seem to be important to stabilize the association of Par-3 at membrane sites (Harris and Peifer 2005; Suzuki and Ohno 2006).

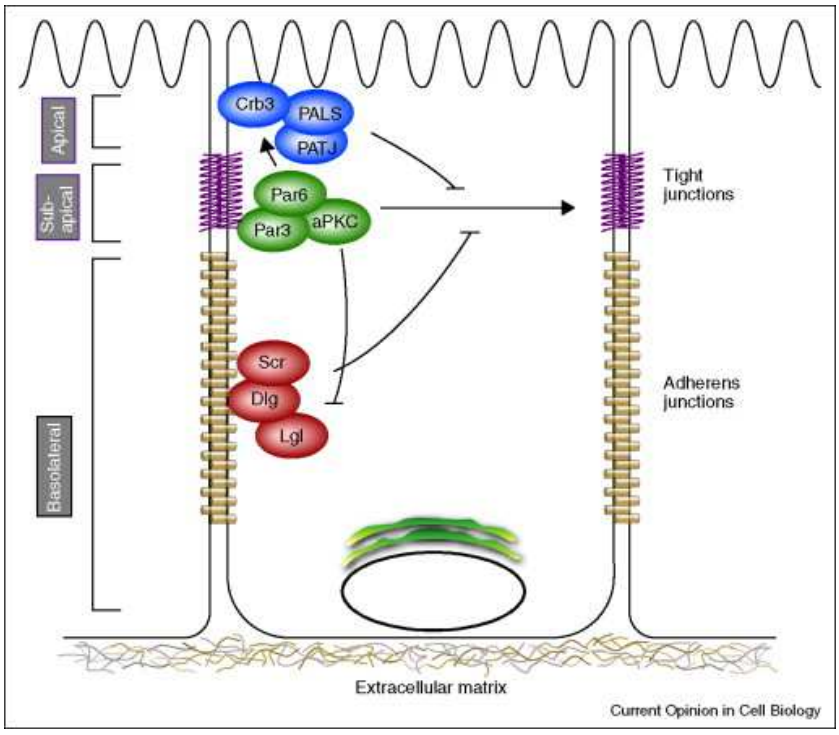

Figure 1.9: Epithelial polarity
Epithelial polarity is maintained by two major complexes. The Crumbs-complex and the Par-aPKC-complex; the latter antagonizes baso-lateral located proteins like Par-1. Adopted from Feigin, 2009.

A basally localized protein establishing polarity is Par-1 antagonizing the Par-aPKC-complex. Par1 is phosphorylated by aPKC and therefore cannot bind to the apical membrane, but only to the baso-lateral membrane where aPKC is not located. In turn, Par-1 phosphorylates Par-3, which destabilizes the Par-aPKC-complex and prevents its localization to basolateral sites. Therefore polarity is regulated by mutual antagonism of proteins (Benton and Johnston 2003; Hurov et al. 2004; Suzuki et al. 2004).

The apical Par-aPKC-complex is highly conserved throughout species and plays an important role for example in anterior-posterior polarization of the *C. elegans* zygote, the polarization of the *Drosophila* oocyte (Pellettieri and Seydoux 2002), embryonic ectoderm and neuroblasts (Wodarz et al. 2000) and apical-basal polarization of mammalian epithelial cells (Izumi et al. 1998; Suzuki et al. 2001). Polarity is also important for cell proliferation, cell migration and to establish the polarity of mature neurons. The Par-aPKC-complex seems to be involved in all of these processes, whereas the Crumbs-complex (containing MPP5) seems to be more restricted to epithelial polarity by recruiting the Par-aPKC-complex to apical domains (Margolis and Borg 2005; Suzuki and Ohno 2006; Assémat et al. 2008).

Interestingly, it was shown for the zebrafish hindbrain, that during asymmetric division of a progenitor (s. chapter 1.7) the cell inheriting the apical proteins aPKC and Par-3 most often becomes a neuron. The cell receiving the basal process stays in a progenitor mode (Alexandre et al. 2010), contrary to what was predicted from studies in the mouse cortex (Kosodo et al. 2004). This might explain the results that loss of aPKC shifts the mode of divisions to more proliferative than neurogenic in the retina, i.e. less neurons and more progenitors are generated (Baye and Link 2007; Alexandre et al. 2010). The same results were obtained with two other mutant zebrafish lines deficient for apical localizing proteins, *mpp5* (*nagie oko*, *nok*) and *N-cadherin* (*ncad*). In the retina of both mutants the rate is shifted to proliferative at the expense of neurogenic division (Yamaguchi et al. 2010). Contrary, in Drosophila the loss of aPKC causes earlier cell cycle exit of neuroblasts (neuronal progenitors) resulting in fewer progeny cells. Further, imaginal disc epithelia are clearly reduced in size (Rolls et al. 2003). And also in mice the loss of Par3 causes premature cell cycle exit and the gain of Par3 or Par6 function promotes the generation of self-renewing progenitors (Costa et al. 2008). The same was shown for a conditional knockout of Pals1 (MPP5) in the medial cortex of the mouse brain, which first led to a premature exit of cell cycle resulting in a massive increase of early-born neurons and then to severe cell death of the entire cortical neuronal cell population (Kim et al. 2010). Together these data point out an important role for apical proteins in regulating the mode of division.

Another *in vitro* study of 3D culture of Madin-Darby canine kidney (MDCK) cells also suggests a role for aPKCλ and Par6 in regulation of cell death of epithelial morphogenesis (Kim et al. 2007). This result indicates a further role of aPKC in cell survival besides regulating proliferation and establishing cell polarity.

In vertebrates there are two isoforms of aPKC, aPKCi and aPKCζ. For mouse it is reported that aPKCi is essential for early embryogenesis and cytoskeletal functions, whereas aPKCζ is supposed to mediate signal transduction of the innate immune system (Soloff et al. 2004). Mice homozygous for a loss-of-function allele of *apkci* are embryonic lethal (Soloff et al. 2004) as well as *apkci*$^{-/-}$ zebrafish embryos (Malicki et al. 1996; Schier et al. 1996; Lowery et al. 2009); own data). *C. elegans* and *Drosophila* embryos possess only one aPKC variant and a functional knockout of this protein also results in embryonic lethality (Tabuse et al. 1998; Wodarz et al. 2000; Cox et al. 2001). In contrast, mouse embryos lacking aPKCζ develop rather normal, with defects only in secondary lymphoid organs (Soloff et al. 2004). In zebrafish no aPKCζ mutant strain is available. Molecular approaches to knockout specifically

aPKCζ are difficult, because pseudosubstrates inhibitors or kinase-dead versions likely inhibit also the function of aPKCi as the kinase domain of both variants is highly conserved. Nevertheless, a morpholino approach specifically targeting either *apkci* or *apkcζ* showed that both variants have partially redundant function in retinal development and a rescue experiment of the *apkci* retinal phenotype with *apkcζ* mRNA revealed that transgenic expressed aPKCζ can compensate for the function of aPKCi to a great extend (Cui et al. 2007).

1.10 Nagie Oko and Heart and Soul

The mutant zebrafish strains *nagie oko* (*nok*) and *heart and soul* (*has*) were first identified and described in a large ENU-mutagenesis screen (Malicki et al. 1996; Schier et al. 1996; Stainier et al. 1996). Following studies identified the encoding protein of the gene *nagie oko* as a membrane-associated guanylate kinase (MPP5, also known under the synonym Pals1) (Wei and Malicki 2002; Rohr et al. 2006); and the protein encoded by the gene *heart and soul* as an atypical protein kinase C (aPKCi in mouse and zebrafish and aPKCλ in humans) (Horne-Badovinac et al. 2001).

nok mutant embryos (fig. 1.10 c, c') possess a curved body axis, reduced and patchy eye pigmentation, disorganized retina, severely reduced ventricle inflation and abnormal brain shape, reduced circulation (Malicki et al. 1996; Schier et al. 1996), failure in heart tube elongation (Rohr et al. 2006) and failure in gut looping (Horne-Badovinac et al. 2003). In the developing brain of *nok* mutant embryos, midline separation and subsequent ventricle inflation does not occur or only poorly, and the neural tube seems to be stuck. Labeling with junctional markers at 22 hpf displays a highly disorganized neuroepithelium and a midline, which is not continuous and already impaired following neural tube closure. Although, junctional proteins localize apical, no cohesive actin belts characteristic for epithelial cells are formed (Lowery and Sive 2005; Lowery et al. 2009). It has been therefore proposed, that Nok is necessary for early epithelial integrity and continuous midline formation in one plane for correct midline separation along the neural tube (Lowery et al. 2009).

Embryos with a mutant allele of *has* (fig. 1.10 a, a'), possess a very similar phenotype like *nok* mutants. They display a curved body axis, reduced eye pigmentation and retinal degeneration, a very small defective heart with no distinctive chambers, reduced brain ventricle inflation and an abnormal brain shape (Malicki et al. 1996; Schier et al. 1996;

Stainier et al. 1996) and also impairment in digestive organ morphogenesis (Horne-Badovinac et al. 2001; Horne-Badovinac et al. 2003).

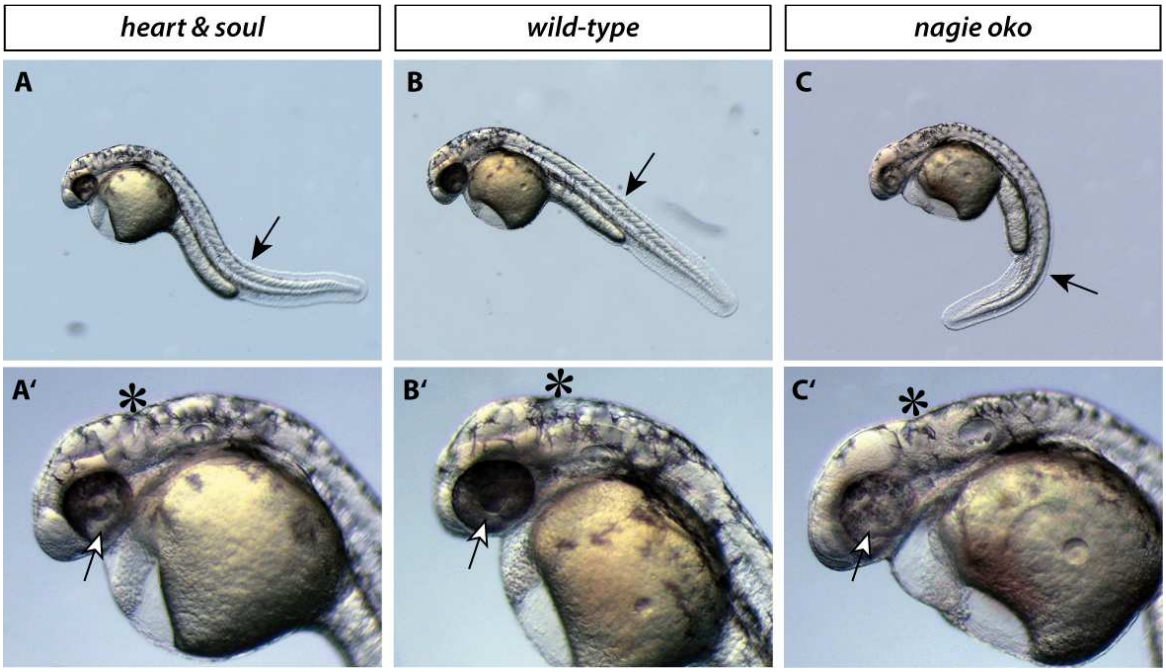

Figure 1.10: Phenotype of 24 hpf old heart & soul, wild-type and nagie oko embryos
B, B') At 24 hpf *wt* embryos possess a straight body axis (black arrow), an inflated hindbrain ventricle (asterisk), and a nearly complete pigmented eye (white arrow). A, A') The 4th ventricle of *has* embryos is not inflated properly, eye pigmentation is patchy and the body axis is curved. C, C') The phenotype of *nok* is most severe, i.e. all brain ventricle are not inflated, especially recognizable at the 4th ventricle, the eye pigmentation is missing in many areas and the body axis is curved. The curvature of the body axis of *has* and *nok* embryos varied strongly within one clutch.

The neural tube midline in *has* mutants is continuous, nevertheless fails to open in its full extent and stays adjoined at several sites in the hindbrain. The fore- and midbrain are less affected, and ventricle opening in those regions occurs rather normally. Midline separation defects indicate abnormalities in neuroepithelial cells. However, junctions appear normal at early stages around 22 hpf (Lowery et al. 2009), but they are progressively lost during development and are almost completely lacking in the retina as well as in the neural tube at 60 hpf (Horne-Badovinac et al. 2001).

Taken together, it has been shown for both mutants, that epithelial integrity and tissue morphogenesis of several distinct organs, also the hindbrain neuroepithelium is impaired, suggesting both mutant zebrafish strains suitable to investigate aspects of early cerebellar development.

1.11 Aim of the study

Migration of neurons to ectopic locations causes severe neurological diseases. Neuronal migration disorders are for example Lissencephlay, Polymicrogyria and Heterotopia, which are often associated with mental retardation or epileptic seizures (Spalice et al. 2009). Because the cerebellum is a highly conserved brain compartment regarding its principle neuronal network, it is well suited to be investigated in the model organism zebrafish. The zebrafish enables us to image neuronal migration and therefore morphogenesis in vivo, thereby excluding artificial cell behaviour often reported for *in vitro* cell culture studies when compared to results of *in vivo* analysis.

This work aims to determine a possible role of the polarity proteins aPKCi and MPP5 in neuronal migration and maturation, as polarity is crucial for directed migration. As already mentioned, well-described mutant zebrafish lines exist for both genes *apkci* and *mpp5*, but nothing so far is known of their role and expression in the development of cerebellar neurons, which is the project of this work.

First the morphogenesis of the cerebellum of those mutant lines compared to *wt* was investigated, followed by the analysis of gene expression in *wt* embryos to clarify whether *apkci* and *mpp5* could play a role in cerebellar development. Consequently, the next step needed to reveal whether both genes are expressed in GCs.

Subsequently, the development of GCs in the mutant lines compared to *wt* was addressed, to get a first hint whether our designated neuronal cell type for further investigations was affected by the loss-of-function mutation of *apkci* or *mpp5*. In addition, the migration behaviour of GCs in both mutant lines was studied. Therefore, the transgenic line *Tg(gata1:GFP)*, which expresses GFP in cerebellar GCs, was crossed into the mutant lines and surveyed *in vivo* by confocal laser scanning microscopy.

During this research it turned out that the number of GCs in the cerebellum of the mutants was clearly reduced. To investigate possible reasons cell proliferation, cell death and cell differentiation were analysed.

In order to inhibit selectively the function of aPKCi or MPP5 to answer the question if both proteins acted cell- or rather tissue-autonomous, an electroporation approach combined with injection of a dominant-negative version of the proteins was conducted. To achieve this, electroporation first needed to be established and its optimal settings determined in our laboratory.

2 Material and Methods

2.1 Materials

2.1.1 Equipment

Binocular	Zeiss Stemi SV 11 (Zeiss, Jena, Germany)
Centrifuges	Sorvall Evolution, GSA rotor (Thermo Scinetific, Waltham, MA, USA)
	Table centrifuge (Eppendorf, Hamburg, Germany)
	Varifuge 3.0R, rotor #8074 (Heraeus, Hanau, Germany)
Electroporator	ECM 630 (BTX Harvard Apparatus, Holliston, MA, USA)
Fluorescent Stereomicroscope	MZ 16FA (Leica, Wetzlar, Germany)
Gel electrophoresis chamber	Shelton Scientific (Deisenhofen, Germany)
Gel documentation	Herolab gel system (Herolab, Wiesloch, Germany)
Microinjectors	FemtoJet and FemtoJet express (Eppendorf, Hamburg, Germany)
Micromanipulator	MN-151 (Narishige, London, UK)
Microinjection needle puller	PC-10 (Narishige, London, UK)
Microscopes: upright	Axioplan 2, Zeiss (Zeiss, Jena, Germany)
confocal laser scanning	LSM510, (Zeiss, Jena, Germany)
	LSM510 Meta, (Zeiss, Jena, Germany)
	TCS SP5 (Leica, Wetzlar, Germany)
Microscope camera	Axiocam HRc digital camera, (Zeiss, Jena, Germany)
Photometer	Biophotometer, (Eppendorf, Hamburg, Germany)
PCR machine	PTC-100 (MJ Research, Waltham, MA, USA)

2.1.2 Chemicals and Consumables

Standard chemicals were obtained from Sigma-Aldrich, Fluka, Merck, Roth GmbH, Biozym. Plastic ware was used from Eppendorf, Nunc, Roth GmbH. Glassware was obtained from Schott.

2.1.3 Enzymes, Dyes and Kits

Acridine Orange (SYTOX®)	Invitrogen, Darmstadt, Germany
Alkaline Phosphatase (1U/µl)	Roche Diagnostics, Mannheim, Germany
Bodipy FL C_5-ceramide	Invitrogen, Darmstadt, Germany
DIG RNA-Labelling mix	Roche Diagnostics, Mannheim, Germany
DNaseI	Roche Diagnostics, Mannheim, Germany
dNTPs	Roche Diagnostics, Mannheim, Germany
mMESSAGE mMACHINE® SP6 Kit	Ambion, Darmstadt, Germany
Nucleic Acid and Protein Purification Kit	Macherey-Nagel, Düren, Germany
NucleoBond Finalizer Large	Macherey-Nagel, Düren, Germany
Pfu Ultra II DNA-Polymerase	Stratagene, La Jolla, CA, USA
Proteinase K	Roche Diagnostics, Mannheim, Germany
QIAquick Gel Extraction Kit	Qiagen, Hilden, Germany
QIAquick Nucleotide Removal Kit	Qiagen, Hilden, Germany
QIAquick PCR Purification Kit	Qiagen, Hilden, Germany
Restriction Endonucleases	MBI Fermentas, St. Leon-Rot, Germany
	New England Biolabs, Frankfurt/M, Germany
	Roche Diagnostics, Mannheim, Germany
RNasin Plus RNase Inhibitor (40U/µl)	Promega, Mannheim, Germany
RNeasy Mini Kit	Qiagen, Hilden, Germany
SP6 RNA-Polymerase (20U/µl)	MBI Fermentas, St. Leon-Rot, Germany
T3 RNA-Polymerase (20U/µl)	MBI Fermentas, St. Leon-Rot, Germany
T4 DNA-Ligase (5U/µl)	MBI Fermentas, St. Leon-Rot, Germany
T7 RNA-Polymerase (20U/µl)	MBI Fermentas, St. Leon-Rot, Germany
6x loading dye	MBI Fermentas, St. Leon-Rot, Germany
6x orange loading dye	MBI Fermentas, St. Leon-Rot, Germany
1kb standard DNA-ladder	MBI Fermentas, St. Leon-Rot, Germany
Ultra low gelling agarose (Type IX-A)	Sigma-Aldrich, St. Louis, MO, USA

2.1.4 Solutions

2.1.4.1 Zebrafish Media

Anaesthetic	0.002 g/ml Tricaine in 30%/Danieau
Egg Water	0.3 g/l Instant Ocean Salt Mix/dH_2O
300% Danieau stock solution	174 mM NaCl, 2.1 mM KCl, 1.2 mM $MgSO_4$, 1.8 mM $Ca(NO_3)_2$, 15 mM HEPES (pH 7.2) → dilute 1:10 for working solution (30% Danieau)
100x PTU stock solution (anti-pigmentation agent)	0.3 % 1-phenyl-2-thiourea (m/v) → dilute 1:100 in 30% Danieau for working solution

2.1.4.2 Bacteria Media

LB-Medium	10 g Bacto-Trypton, 5 g yeast extract, 10 g NaCl in 1l dH_2O, pH 7.4; autoclaved
LB-Agar	15g Agar in 1 L LB-Medium; autoclaved

2.1.4.3 Histology Buffer

Fixative (PFA)	4 % paraformaldehyde in PTW (v/v)
Glycerol 90%	90 % glycerol in ddH_2O
Glycine	20 mg / 1 ml PTW
ISH Hybridization Buffer	50 % formamide (v/v), 25 % 20x SSC (v/v), 50mg/ml Heparin, 100 mg/ml Torula-RNA, 0.1% Tween20 (v/v)
ISH Staining Buffer	0.1 M NaCl, 0.1 M Tris-HCl (pH 9.5), 50 mM MgCl2, 0.1 % Tween20 (v/v)
ISH Staining Solution	187.5 µg BCIP + 250 µg NBT per 1ml staining buffer
NGS (blocking solution)	10 % normal goat serum (v/v) in PTW/ 1% DMSO
PTW	0.1 % Tween20 in PBS (v/v)
SSC 20x	3 M NaCl, 0.3 M NaCitrat; pH 7.0

2.1.4.4 Gel Electrophoresis Buffer

Agarose Gel	0.8 % agarose in 1x TAE
TAE stock solution, 50x	100 ml 0.5M Na_2EDTA (pH8) + 57.1 ml glacial acetic acid + 242 g Tris in 1 L dH_2O → dilute 1:50 in dH_2O for working solution

2.1.4.5 Electroporation Buffer

Electroporation buffer	180 mM NaCl, 5 mM KCl, 1.8 mM $CaCl_2$, 5mM Hepes; pH 7.2
Agarose	0.7 % low melting agarose in electroporation buffer

2.1.5 Plasmids

Table 1: DNA Cloning Vectors

Plasmid	**Constructor**
pCSII+	Ralf Rupp (Rupp et al. 1994)
pCSII+/GI (Globin Intron)	R. Köster
pBluescript+ (pBS)	Stratagene Inc., La Jolla, CA, USA
pCS-B	Blunt PCR Cloning Vector, Stratagene Inc.
pBS/4xUAS	M. Distel, R. Köster lab
pSC-B/apkci (reverse orientation)	A-L Kerner, R. Köster lab
pCSII/apkci; pCSII/apkci-GI	A-L Kerner, R. Köster lab
pCSII/apkci2A	A-L Kerner, R. Köster lab
pCSII/UncVenus	R. Köster
pCSII/UncVenus-T2A-NmycTS	R. Köster
pBS/4xUAS-UncVenus	A-L Kerner, R. Köster lab
pBS/4xUAS-UncVenus-T2A-apkci	R. Köster
pBS/4xUAS-UncVenus-T2A-apkci2A	R. Köster
pCS-B/nagie-oko (wrong ORF, but used for probe)	A-L Kerner, R. Köster lab
pCSII/nagie-oko; pCSII/nagie-oko-GI	A-L Kerner, R. Köster lab

2.1.5.1 Cloning strategy to obtain the full length ORF of *nok*, *apkci* and *apkci2A*

pCS-B/nagie-oko and pCSII/nagie-oko:

The open reading frame (ORF) of *nagie oko* (*nok*) was isolated from zebrafish embryonic cDNA by PCR using primer pair nok5-3 and nok3-5 (Primers are listed in Table 2 under chapter 2.2.4.1) with including the sequence of start and stop codon, respectively. Subsequently the blunt end fragment was cloned into pSC-B. Because no continuous correct ORF was achieved, the final *nok* ORF was combined from two different PCR products. The 5'prime part of 1705bp was restricted by EcoRI / PstI from one PCR product and the remaining 407bp of the 3'prime part by PstI / XhoI restriction from another amplicon. Both fragments were finally cloned by a triple ligation into pCSII+ (and pCSII+/GI).

pSC-B/apkci and pCSII/apkci:

The ORF of *apkci* was isolated by PCR from zebrafish embryonic cDNA using primer pair aPKCup and aPKClo including the sequence of start and stop codon, respectively. Subsequently the blunt end fragment was cloned into vector pSC-B. Sequencing revealed a reverse orientation of apkci in the plasmid. To insert the ORF in correct orientation into pCSII+, pSC-B/apkci was digested with Xba1, blunted by Klenow polymerase followed by a Xho1 digest and inserted into the pCSII+ backbone opened with EcoRI/ blunt/ XhoI. (The same strategy was applied to obtain pCSII/apkci-GI).

pCSII/apkci2A:

The mutant variant apkci2A was created using site directed mutagenesis, which is described in detail in chapter 2.2.4.4.

2.2 Experimental procedures

2.2.1 Maintenance and breeding of Zebrafish

Breeding and maintaining of zebrafish lines was performed as described before (Westerfield 1995). Embryonic and larval stages were determined according to Kimmel et al. (Kimmel et al. 1995).

2.2.2 Zebrafish Strains

Following wild type, mutant and transgenic zebrafish strains were used during the course of this project:

- *wild type* AB (ZIRC, Eugene, OR, USA)
- *wild type* EKK (EkkWill Waterlife Resources, Gibbonston, FL, USA)
- *brass* (EkkWill Waterlife Resources, Ruskin, FL, USA)
- *Tg(gata1:GFP)*, strain 781 (Long et al. 1997)
- *has*^{m567} (Abdelilah-Seyfried; Malicki et al. 1996)
- *nok*^{s305} (Abdelilah-Seyfried; Malicki et al. 1996)
- *Tg(zic4:Gal4,UAS:mCherry)* (M.Distel, R.W. Köster lab)

2.2.3 Fixation of Zebrafish Embryos

Embryos were anesthetized with 5% Tricaine in 30% Danieau / PTU and transferred to the fixative (4% PFA / PTW). Embryos were incubated in the fixative over night at 4°C by continuous shaking; or sometimes 24-48 hpf old embryos were incubated only for 2h at RT. Embryos were then washed 3x 15 min in PTW, 2x 5 min with 100% MeOH, transferred in a 2 ml tube in fresh 100% MeOH and stored at -20°C.

2.2.4 DNA/RNA handling and cloning procedures

2.2.4.1 Standard PCR

To obtain a DNA fragment of interest a standard PCR, using the proofreading Polymerase Pfu Ultra II, was performed. As a template zebrafish cDNA from developmental stages 24 hpf, 30 hpf or adult brain was used. Primers utilised are listed in Table 2. The following approach and cycler protocol were applied:

Reaction components

DNA	1µg cDNA
Primer A	2 µM
Primer B	2 µM
dNTP mix	280 µM
10x Buffer	5 µl
Pfu Ultra II	2 µl
ddH_2O	→ 50µl

Cycler Protocol

95 °C	3 min (denaturation)
95 °C	30 sec (denaturation)
X °C	1 min (annealing; temp. dependent on Primer)
72 °C	1 min/kb fragment length (elongation)
72 °C	10 min (final elongation)

PCR-products were purified using the 'QIAquick PCR Purification Kit' (Qiagen) according to the manufacturer's protocol and the amplicon was stored at -20°C.

Table 2: Primer

Name	Sequence	Amplification of
nok5-3	GCCCTCACACCATGCAGAA	nok from 5' with ATG
nok3-5	CCCATCTCAGCGCAGCCA	nok from 3' with stop-codon
aPKCup	ATGCCCACGCTGCGGGACAGCACCA	aPKC from 5' with ATG
aPKClo	TCACACACACTCCTCCGCAGACATCAGCA	aPKC from 3' with stop-codon

2.2.4.2 Restriction Digest

Restrictions were carried out using an appropriate buffer according to the manufacturer. Reactions were incubated at 37°C for 30 min (standard approach) or 3h up to overnight (preparative restriction).

Standard restriction

In order to verify the result of cloning procedures or ligations an analytical restriction digest was performed using either one or two restriction endonucleases. The following approach was used:

1 µl	purified DNA solution
0.5 µl	of each restriction endonuclease
1 µl	restriction buffer suitable to enzymes
x µl	ddH_2O to a total volume of 10 µl

Preparative restriction

To obtain restricted DNA fragments, plasmid-DNA or PCR-products for further cloning steps; a preparative restriction was carried out using the following reaction protocol:

x µl	DNA solution (up to 10 µg)
3 µl	per enzyme
3 µl	restriction buffer
x µl	ddH_2O to a total volume of 30 µl

Restriction digests were purified using either the 'QIAquick Nucleotide Removal Kit' (Qiagen) following the manufacturer's protocol or by gel-extraction (s. 2.2.4.5).

2.2.4.3 Ligation

Different DNA fragments were joined together using T4 DNA-ligase. Standard reaction mixtures had a total volume of 15 µl and contained following components:

x pmol	insert DNA
x pmol	plasmid DNA
1.5 µl	T4 ligase
1.5 µl	T4 ligase buffer
x µl	ddH_2O to a total volume of 15 µl

Ligations were incubated either for 30 min at RT or overnight at 16°C. For optimal outcome the molar ratio of insert to plasmid DNA should be 1-3:1 using sticky ends or 1:1 using blunt end ligation. Ligations were purified using the 'QIAquick Nucleotide Removal Kit' (Qiagen) and stored at 4°C, or for longer storage at -20°C.

2.2.4.4 Site directed mutagenesis of aPKCi

Site directed mutagenesis was performed using the QuikChange Lightning Site-Directed Mutagenesis Kit (Stratagene, Agilent Technologies, #210518) according to the manufacturer's instructions. The primers aPKCmutagen1 and aPKCmutagen2 (s. Table 3) were used to insert two point mutations in the sequence of aPKCi, which leads to a change in the highly conserved 'APE' motif of subdomain VIII of the protein, which is important for the recognition of substrates (Hanks and Hunter 1995) (fig. 1).

Wild type sequence: 5'-…cccaattacattgcaccagagattctgagaggagaag…-3'
Mutagen sequence: 5'-…cccaattacattgcagcagcgattctgagaggagaag…-3'

Wild type sequence: N'-…PNYIAPEILRGE…-P'
Mutagen sequence: N'-…PNYIAAAILRGE…-P'

Figure 2.1: Comparison of the wildtype and mutant variant sequence of aPKCi

To verify the success of site directed mutagenesis, a control PCR was performed using either the primer aPKCmutaContr or the primer aPKCwtControl. If the mutagenesis was successful the latter primer would bind and amplified DNA would be visible on a subsequent agarose gel electrophoresis. If the mutagenesis was not successful amplified DNA would be obtained with the other primer.

Table 3: Primers used for site directed mutagenesis and control-PCR

Name	Sequence	Purpose
aPKCmutagen1	CCCAATTACATTGCAGCAGCGATTCTGAGAGGAGAAG	Insertion of 2 point mutations
aPKCmutagen2	CTTCTCCTCTCAGAATCGCTGCTGCAATGTAATTGGG	Insertion of 2 point mutations
aPKCmutaContr	CTTTCTGTGGAACTCCCAATTACATTGCAGCAGC	To check success of mutagenesis
aPKCwtControl	CTTTCTGTGGAACTCCCAATTACATTGCACCAGA	To check success of mutagenesis

2.2.4.5 DNA Gel Electrophoresis

DNA fragments of different length can be separated using agarose gel electrophoresis. DNA is negatively charged because of its phosphate backbone and the DNA therefore moves to the anode in an electrical field. DNA fragments of different length can be separated in agarose as smaller fragments move faster through the pores of the gel. Standard gel electrophoresis was performed using 0.8 % agarose gels. Samples were mixed with 6x loading dye or 6x orange loading dye and applied into the slots of the gel. In addition, to identify the size of the DNA fragments a 1 kb standard DNA ladder (Invitrogen) was applied. The electrophoresis chamber was filled with 1x TAE. For separating DNA fragments a voltage between 80 and 140 was applied. After electrophoresis gels were soaked for 15 min in an ethidium bromide bath (dilution 1:2000 in 1x TAE). The DNA fragments with the intercalated ethidium bromide were visualized using UV light at 254 nm and the gel was documented using a Herolab gel system.

2.2.4.6 RNA Gel Electrophoresis

RNA gel electrophoresis was performed like DNA gel electrophoresis (s. 2.2.4.5) but with some changes in order to prevent rapid denaturation of the RNA due to RNase activity. The gel chambers and combs were washed with soap and dH_2O ahead of electrophoresis. The gel was pre-run without RNA for 10 min at 55 V. Electrophoresis was then performed between 120 and 160 V as short as possible. The staining of RNA fragments occurred in an ethidium bromide bath reserved for RNA gels.

2.2.4.7 Gel-Extraction of DNA

In order to extract the desired DNA fragments out of a restriction digest or to purify a PCR-product, a preparative agarose gel electrophoresis was performed. A sample volume up to 50 µl was loaded onto the gel and electrophoresis was conducted. The desired DNA fragments were cut out as small agarose blocks and transferred into a 2 ml tube. Extraction was performed using the ‘QIAquick Gel Extraction Kit’ (Qiagen) following the manufacturer’s manual.

2.2.4.8 Transformation of Bacteria

During this work only chemo-competent (heat shock) bacteria were used. Bacteria were thawed on ice for 10 min. Plasmid DNA (1-5 µl of a standard ligation or ~ 0.1 µl of a Maxi-

Prep with a concentration of 1µg/µl) was added to 100µl of competent bacteria. Cells were incubated on ice for 30 min and then a heat shock was applied for 45 sec at 42°C. Directly after the heat shock bacteria were placed on ice for 2 min. 500 µl of LB-medium was added and cells were incubated at 37°C for 30 min. The bacteria were spread on agar plates containing an antibiotic corresponding to the selection cassette encoded by the backbone plasmid, using either glass beads or a spatula, and incubated over night at 37°C.
Following E. coli bacteria strains were used for transformation:

- XL1-Blue (Bullock et al. 1987)
- GM4 Dam negative (Bolivar et al. 1979)
- StrataClone SoloPack competent cells (Stratagene, LaJolla, CA, USA)

2.2.4.9 Low Scale Plasmid Preparation

To identify successful cloning events and to obtain a small amount of purified DNA a low scale plasmid preparation ('Mini-prep') was performed from individual bacterial colonies. Mini-preps were performed using the solutions from the 'Nucleic Acid and Protein Purification' - Kit (Macherey-Nagel). All centrifugation steps were performed using a table centrifuge. After the transformation of the bacteria and incubation overnight (s. 2.2.4.8) individual colonies were picked and transferred into 5 ml LB-medium with the respective antibiotic and incubated overnight on a shaker at 37°C. In addition, bacteria of the picked colonies were also transferred onto a culture plate (master plate) and incubated overnight at 37°C. The next day the plates were put at 4°C to stop bacterial growth and the fluid bacteria cultures were centrifuged in 2 ml tubes for 5 min at 10 000 rpm. The supernatant was removed and the bacterial pellet re-suspended in 200 µl S1 buffer. 200 µl S2 alkaline lysis buffer was added and the tubes were inverted immediately several times, and the cells were incubated for 2 min in order to lyse. To neutralize the solution and stop the lysis reaction 200 µl of the buffer S3 was added. By adding S3 also the proteins precipitate. To remove the proteins the solution was centrifuged for 10 min at 13 200 rpm. The supernatant was transferred into a new 1.5 ml tube. 400 µl Isopropanol was added in order to precipitate the DNA. The mixture was centrifuged at least for 20 min at 4°C. Afterward the supernatant was removed and the DNA pellet was washed by adding -20 °C cold 70% EtOH and centrifuging 10 min at 4°C. For further washing of the DNA this step could be repeated. The final centrifugation step lasted for 10 min at 4°C after adding -20°C cold 100% EtOH. The EtOH was removed completely and the pellet dried at room temperature or at 60°C in an incubator. The pellet was resolved in ddH_2O.

2.2.4.10 Large Scale Plasmid Preparation

To obtain a large amount of highly purified DNA a large scale plasmid preparation ('Maxi-prep') was performed using the 'Nucleic Acid and Protein Purification' - Kit (Macherey-Nagel). Individual colonies with the desired Plasmid-DNA were transferred from the master plate (s. 2.2.4.9) into 200 ml LB-medium with an antibiotic corresponding to the resistance of the plasmid and cultured overnight on a shaker at 37°C. The next day the 200 ml culture was centrifuged for 15 min at 6000 rpm at 4°C (Sorvall Evolution, GSA rotor) in a closed beaker and the supernatant was removed. The bacterial pellet was resolved in 10 ml S1 buffer. 10 ml S2 alkaline lysis buffer were added, the solution mixed well and incubated to lyse the bacteria. Then 10 ml S3 buffer were added and the suspension was incubated in the fridge for 10 min to precipitate the proteins. Meanwhile the column was equilibrated with 6 ml N2. After 10 min the lysed bacterial solution was filtered to remove the proteins, before the solution was transferred onto the column where the DNA would bind to the matrix of the column. To wash the bound DNA the column was filled completely with N3. After the washing buffer had passed through, the column was filled with 15 ml N5 buffer to elute the DNA. The eluate was captured and 11 ml Isopropanol were added to precipitate the DNA. To finally obtain the DNA, the mixture was either centrifuged at 4°C, 11 000 rpm for 30min (Varifuge 3.0R, Heraeus, rotor #8074), then the supernatant was removed, and the DNA pellet was washed with 5 ml -20°C cold EtHO, air-dried and resolved in 200 µl ddH_2O. Alternatively, the solution was filtered through a large NucleoBond Finalizer (Macherey-Nagel), the bound DNA was washed with EtOH, dried by pressing air through the filter and eluted with 200 µl ddH_2O. The concentration of the DNA was measured using a standard photometer. The plasmid-DNA solution was stored at -20°C.

2.2.4.11 Synthesis of Sense mRNA for Injection

To obtain a template for mRNA-synthesis, a preparative restriction digest of plasmid-DNA containing the desired cDNA fragment was conducted (s. 2.2.4.2). The restricted DNA was purified using the 'QIAquick Nucleotide Removal Kit' (Qiagen), according to the manufacturer's instructions. Subsequently the reaction for capped mRNA synthesis was set up using the mMESSAGE mMACHINE® SP6 Kit (Ambion) and following reaction approach:

6 µl restricted plasmid-DNA template
2 µl Enzyme Mix

2 µl buffer

10 µl dNTP mix

→ incubate for 2h, 37°C

→ add 1 µl DNase (Roche) and incubate for another 20 min, 37°C

The reaction was then purified using the 'RNeasy Mini Kit' (Qiagen) according to the manufacturer's protocol. The mRNA was eluted with RNase free water and the integrity was controlled by RNA gel electrophoresis (s. 2.2.4.6). The mRNA concentration was measured with a Photometer. The mRNA solution was stored at -20°C.

2.2.5 *In situ*-Hybridization

Visualization of expression profiles of genes can be achieved using mRNA *in situ*-hybridization. In this approach Digoxigenin conjugated UTP is incorporated into antisense riboprobes. Digoxigenin subsequently serves as an epitope for an antibody conjugated to Alkaline Phosphatase (AP). AP then catalyses the conversion of a chromogenic substrate, resulting in a blue precipitate.

2.2.5.1 In vitro transcription of antisense riboprobes

For synthesizing riboprobes, plasmids containing the gene of interest were digested at a single restriction site and transcribed by a RNA-polymerase suited for the distinct plasmid to achieve the synthesis of an antisense RNA strand. In addition to the polymerase, DIG RNA-Labelling mix (Roche) was added, containing UTP conjugated to Digoxigenin.

Preparative digest	RNA synthesis
10 µg DNA	10 µl linearized DNA
3 µl enzyme	1 µl RNasin
3 µl reaction buffer	2 µl transcription buffer 10x
x µl dH_2O	2 µl RNA polymerase
→ 30 µl total volume	2 µl DIG labeling mix
	3 µl dH_2O RNase free

The synthesis reaction was incubated for 2-3 h at 37°C. Optional an additional 1 µl of polymerase was added to the reaction after 1 h.

In order to digest the template DNA 1.5 µl DNaseI was added to the reaction and incubated for 20 min at 37°C. The purification of the RNA was performed using the 'RNeasy Mini Kit'

(Qiagen) according to the manufacturer's manual. To verify the integrity and yield of the synthesised riboprobe, a RNA gel electrophoresis (s. 2.2.4.6) was carried out. RNA-probes were stored at -20C.

2.2.5.2 Preparation of embryos for further hybridization steps

All steps were performed at RT in 6-well-tissue-culture-plates. Fixed embryos (s. 2.2.3) stored in MeOH at -20°C were rehydrated stepwise 5 min each in 75% MeOH, 50% MeOH, 25% MeOH, 2x PTW. Proteinase K was added at a concentration of 10 µg per 1 ml PTW, using 5 ml solution per each batch of embryos. Only very gentle shaking was applied. The duration of digestion varied between the stages of embryonic development and persisted according to following table:

24 hpf	→	7 min
36 hpf	→	20 min
48 hpf	→	25 min
72 hpf	→	30 min
4 dpf	→	40 min
5 dpf	→	50 min

To terminate the enzyme reaction, the embryos were carefully rinsed twice with 1x Glycine solution. Embryos were then refixed with 4% PFA/PTW for 20 min (gentle shaking) and finally washed 5x 5 min using PTW (shaking).

2.2.5.3 RNA Hybridization

Embryos were transferred into 2 ml tubes. The subsequent steps were performed at 60°C using a water bath. Embryos were incubated at least 1h at 60°C in prehybridization buffer containing torula-mRNA to block unspecific riboprobe binding. For hybridization approximately 4 µl riboprobe (depending on the RNA concentration and experience) were added to 200 µl prehybridization buffer per each batch of embryos. This hybridization mixture was denatured at 90°C for 10 min prior adding it to the embryos, which were then incubated overnight at 60°C. The next day embryos were washed 45 min each at 60°C in 50% Formamide/2x SSC/0.1% Tween20 (twice), 2x SSC/0.1% Tween20 and 0.2x SSC/0.1% Tween20 (twice). Finally embryos were washed twice for 5 min at RT using PTW.

2.2.5.4 Antibody detection and staining reaction

PTW was removed from the embryos, 10 % NGS/PTW was added and the embryos were incubated at least 1 h at RT on a rotator to block unspecific antibody binding sites. Sheep-anti-DIG antibody was diluted in 10% NGS/PTW (dilution 1:2000) and 1 ml of this dilution was applied into each vial and the embryos were incubated over night at 4°C on a rotator.

The following steps were performed at RT. Embryos were transferred to 6-well-tissue-culture-plates and washed on a shaker 5x 15 min in PTW followed by two 5 min washing steps in staining buffer. The staining buffer was removed and 5 ml of staining solution was added to each batch of embryos. Embryos were shaken for 1 min and subsequently incubated in darkness until the desired staining intensity was reached, which was controlled under a stereomicroscope. To stop the staining reaction the embryos were washed 3x 15 min in PTW and transferred into 90% glycerol.

Table 4: Antibodies

Antibodie for ISH	**Host species**	**Dilution**	**Obtained from** (Catalogue-Nr.)
anti-Digoxigenin	Sheep	1:2000	Roche Applied Science (11093274910)
IHC Primary Antibodies	**Host species**	**Dilution**	**Obtained from** (Catalogue-Nr.)
anti-GFP	Chicken	1:500	Aves Labs (1020)
anti-ZebrinII	Mouse	1:500	R. Hawks
anti-phospho-Histone H3	Rabbit	1:150/1:200	Millipore (06-570)
anti-PCNA	mouse	1:250	Santa Cruz (sc-25280)
anti-PKCζ	Rabbit	1:200	Santa Cruz (sc-216)
anti-PKCλ	Mouse	1:200	BD Transduction Laboratories (610207)
anti-ZO-1	Mouse	1:200	Invitrogen life technologies (339100)
anti-nok	Rabbit	1:50/1:100	S. Abdelilah-Seyfried
IHC Secondary Antibodies	**Host species**	**Dilution**	**Obtained from** (Catalogue-Nr.)
FITC anti-chicken	Donkey	1:200	Jackson Immuno Research (703 095 155)
Alexa 488 anti-mouse	Chicken	1:500	Invitrogen life technologies (A21200)
Cy3 anti-mouse	Goat	1:200	Jackson Immuno Research
Alexa 647 anti-rabbit	Goat	1:500	Invitrogen life technologies (A21244)
Cy3 anti-rabbit	Donkey	1:200	Jackson Immuno Research (711-166-152)

2.2.5.5 Imaging of embryos

Embryos should be kept in 90% glycerol at least over night before taking images. For facilitated adjustment of the embryo on the glass slide and in order to obtain better images, the tail, the yolk and, for lateral images of 3-5 dpf embryos, also one eye were removed using precision forcipes (Carl Roth, type 5). Prepared embryos were transferred with a small drop of 90% glycerol onto a glass slide and covered with a cover slip. In order to avoid strong pressure to the embryos the object slides were modified with spacers made either of cover slips or sticky tape according to the thickness of the embryo. Images were recorded using a Zeiss Axioplan microscope with Plan-Neofluar 10x/0.30, 20x/0.50 and 40x/1.3oil objectives and Axio Vision Software 4.5 SP1.

2.2.6 Immunhistochemistry

To detect the expression profile of genes on the protein level specific antibodies were used. Staining reactions were performed on whole-mount preparations of zebrafish embryos. A primary antibody (AB) was targeted against the desired protein and a secondary AB coupled with a fluorochrome was used to detect the bound primary antibody.

2.2.6.1 Staining procedure

Fixed embryos (s. 2.2.3) stored at -20°C at least overnight were either transferred directly in -20°C cold Acetone for 7 min or washed with PTW/1% DMSO. After Acetone treatment embryos were transferred to dH2O for approximately 5 min followed by trnasfere to PTW/1% DMSO. Embryos were washed in PTW/1% DMSO 3x 5 min and incubated for at least 1 h in 10% NGS/PTW/1% DMSO in order to block unspecific antibody binding sites. Primary antibodies were diluted at concentrations according to Table 4: Antibodies in 10% NGS/PTW/1% DMSO and embryos were incubated over night at 4°C on a shaker. On the next day, embryos were rinsed 2x with PTW/1% DMSO and washed with PTW/1% DMSO 4x 15 min. Secondary antibodies were diluted at concentrations according to Table 4 in 10% NGS/PTW/1% DMSO and embryos were incubated again over night at 4°C on a shaker. The next day, embryos were rinsed 2x with PTW/1% DMSO and washed with PTW/1% DMSO at least 4x 15 min or as long as possible to reduce background signal.

2.2.6.2 Imaging of embryos

For image recording embryos were embedded in 1.2% ultra-low gelling temperature agarose/PBS and images were recorded using a confocal laser scanning microscope (Zeiss LSM510).

2.2.7 Vital Dyes

2.2.7.1 BODIPY FL C_5 ceramide

Bodipy ceramide (BC) outlines cellular boundaries without harming the living embryo making it an excellent tool to compare for example morphological differences between wt and mutants during development. The use in living embryos abolishes the risk of artefacts like in fixated embryos. The dye is easy to handle because it can be added directly to the embryo medium. Different colours are available but only the green fluorescent version (BODIPY FL C_5 ceramide) was used during this thesis.

To obtain a stock solution BC was dissolved in DMSO at a concentration of 1 mM. For working solution the stock was diluted 1:2000 for embryos at 24 and 48 hpf and 1:1000 for all older stages in 30% Danieau / PTU. Embryos of all stages were incubated overnight in BC. The next day embryos were washed extensively with 30% Danieau / PTU (at least 5x 5 min), mounted in 1.2% ultra-low gelling temperature agarose and imaged using a Zeiss LSM510 confocal microscope.

Because of the strong formation of oedema of 4 and 5 dpf old *apkci*$^{-/-}$ embryos it was difficult to obtain images of the brain as the dye accumulated in the oedema and outshined the labelled tissue. Therefore also 4 and 5 dpf fixed embryos of wt and mutant phenotype were used to obtain better images. The embryos were fixed according to 2.2.3 and the skin in the brain region of *apkci* mutants was removed to deflate the oedema. Fixed embryos were incubated and imaged using the same protocol but using PTW as diluent instead of Danieau.

2.2.7.2 Acridine Orange

Acridine Orange (AO) can be used to investigate cell death in living animals, because it can only enter the nucleus when the nuclear membrane breaks down as a consequence of cell death. AO then binds to nucleic acid, i.e. DNA and RNA, by intercalation or electrostatic

attractions. Excitation and emission maxima differ from AO coupled to DNA (502/525 nm) or RNA (460/650 nm). In this approach only the emission of AO bound to DNA was detected.
Living embryos at the age of 24 and 48 hpf were incubated 20 min and embryos of 3 and 4 dpf were incubated 30 min in Acridine Orange solution at a concentration of 5 µg per 1 ml 30% Danieau / PTU / 5% Tricaine. Embryos were quickly washed several times with 30% Danieau / PTU / 5% Tricaine and immediately mounted in 1.2% ultra-low gelling temperature agarose. For image recording a Zeiss LSM510 confocal microscope was used.

2.2.8 Injection of mRNA into One Cell Stage Embryos

Transient ectopic gene expression can be achieved by injecting either RNA or DNA into a living organism, for example to block or enhance the function of an endogenous gene. In the course of this project, mRNA was injected into one cell stage embryos. Injection of mRNA leads to a ubiquitous expression, as it gets distributed to both daughter cells during cell division. However, mRNA degrades faster than DNA; therefore expression is guaranteed only until approximately 48 hpf and it is also dependent on the stability of the expressed protein.
For injections 1.5 % agarose was filled into petri dishes and a special comb floated on top to spare free lines in which the embryos were embedded with the animal pole up. A needle filled with injection solution was pushed through the chorion and into the cytoplasm of the zygote with the help of a micromanipulator and a binocular. Then a small amount of injection solution was applied into the cell, by help of a microinjector. Phenol red was added to the solution for better observance of the injected volume.

A standard injection mixture was prepared as followed:

50-500 ng mRNA
1 µl phenol red
x µl RNase free ddH_2O to a total volume of 10 µl

2.2.9 Electroporation

Electroporation of plasmid-DNA was used to obtain mosaic expression of different aPKCi variants in the GCs of the cerebellum of zebrafish starting at an age of around 36 hpf. Compared to one-cell-stage injection cells are not affected by transgene expression in their early development, but only starting from the time of electroporation.

Electroporation was performed as described before (Kera et al. 2010) with small modifications. 6-8 embryos at the stage of 36 hpf were mounted in 0.7 % ultra-low gelling temperature agarose solubilized in electroporation buffer, oriented on the lateral side. The agarose was placed on ice until it was solid enough that embryos were not floating away when the agarose was carefully covered with electroporation buffer. Injection solution was injected in the 4th ventricle of the developing brain at a concentration of 900 ng/µl DNA mixed with phenol red (for better visualization) until the maximum capacity of the ventricle was reached. Directly after injection, two electrodes were placed around the head, positioning the anode on the side to which the DNA should move (s. fig. 2.2), and electric pulses were applied (settings see below). The voltage had to be set carefully with every new round of Electroporation to achieve an output of 24 V. 5-7 pulses were applied according to the used plasmid, as some had a superior expression rate and therefore less pulses were needed to obtain the same number of labelled cells in the end. Embryos were removed carefully from the agarose and placed in 30 % Danieau/PTU overnight. The next day, embryos were selected for fluorescence and time-lapse imaging was performed using a confocal LSM (Zeiss LSM510, Leica TCS SP5). Confocal stacks were recorded every 10 or 15 min.

Settings of Electroporator:

- 19-21 Volt (Output: 24 Volt)
- 5-7 pulses
- Pulse: 5 ms (output: 4.5 ms)
- Interval: 1.1 sec

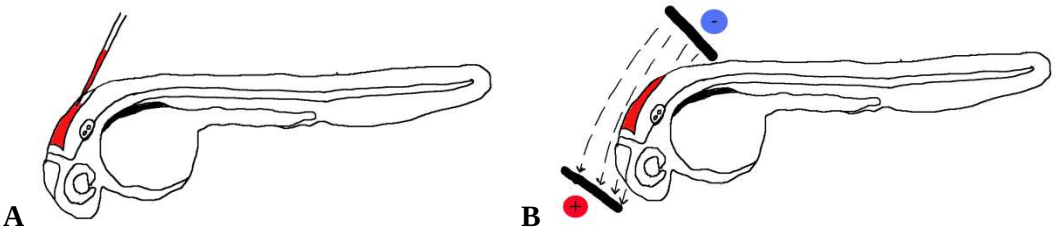

Figure 2.2: Schematic drawing of the principle of electroporation
A) Injection of Plasmid-DNA into the 4th ventricle of the brain at developmental stages 24-48 hpf. B) Placing of the electrodes next to the head, with the anode on the anterior side, so the negatively charged DNA moves in the direction towards the cb. Image by courtesy of Enrico Kühn.

2.2.10 Data processing

2.2.10.1 Statistical analysis

All statistics and graphs were obtained by using Microsoft Excel 2010. Significance was calculated using a two-tailed students t-test with unequal variance.

2.2.10.2 Imaging software and Image processing

Zeiss Axio Vision Software 4.5 SP1 (Zeiss, Jena, Germany)
Zeiss LSM 510 (4.0 SP1); Zeiss LSM Image examiner
Leica LAS AF; Leica LAS AF lite
Adobe Photoshop CS3
ImageJ 1.43u (plugins: Timestamper, Stackreg, Manual Tracking) (http://imagej.nih.gov/ij/)
Apple QuickTime Player Pro Version 7.1.6
Adobe Illustrator CS3

3 Results

3.1 Cerebellar Morphology of *nok* and *apkci* mutant embryos

It has already been shown that the 4th ventricle barely opens in mutants lacking a functional *nok* (*mpp5*) or *aPKCi* allele (Lowery and Sive 2005) (Lowery et al. 2009). However, the further development of the brain was not an issue of investigation so far. The intention of this work was to characterize the role of aPKCi and MPP5 in the development and migration of granule cells (GCs) in the cerebellum. Therefore, a first step was to prove that cerebellar development is actually affected in these mutants. To obtain a first idea about cerebellar morphology, the cerebellum was analysed from day 1 until day 5 post fertilization. The embryos were soaked in 'Bodipy FL C_5 ceramide' overnight. This is a vital dye, which intercalates into cell membranes, visualizing cellular and also tissue morphologies.

In *wildtype* (*wt*) embryos the 4th ventricle was widely open at 24 hpf (fig. 3.1 a, asterisk), and therefore the cerebellar anlage was rotated around 90°, as was described before (Distel et al. 2006). In homozygous *nok*$^{-/-}$ embryos the ventricle did not open, or only to a small extend at the region of rhombomere 1 and 2 (fig. 3.1 b, asterisk); instead it remained fused along the midline (Lowery and Sive 2005; Lowery et al. 2009). In homozygous *apkci*$^{-/-}$ the ventricle opening did not expand completely. Though a separation could be observed very often in the region of rh 1 (cerebellar anlage), the midline always stayed fused at several points from rhombomere 2 toward the posterior (fig 3.1 c, asterisk) (Lowery et al. 2009). Around 48 hpf the ventricles in wt embryos started to close again because of continuous growth. Because of the ventricle closure, the apical sides of the cerebellar and hindbrain neuroepithelia adjoined around 3 dpf, displaying a morphological boundary between both tissues (fig. 3.1 d, arrowhead). On account of the little ventricle opening in the mutants, only a minor rotation of the cerebellar anlage occurred and subsequently the morphological boundary between the cerebellum and hindbrain was incomplete (fig. 3.1 e, f, arrowhead). Despite of this strong divergent morphological development some cerebellar neurons must have been able to develop in this environment based on the appearance of a molecular layer, which is largely formed by Purkinje cell dendrites and parallel fibres of GCs (fig. 3.1 e,f, asterisks). This layer however is less pronounced in both mutants compared to *wt* (fig. 3.1 d, asterisk). Furthermore, parallel fibre projections appeared from 80 hpf onwards (in wt around 58 hpf) forming the

prominent dorsal commissure, clearly visible at 4 dpf (fig. 3.1 g, h, i, arrowhead). This is a very characteristic property of mature GCs (Volkmann et al. 2008).

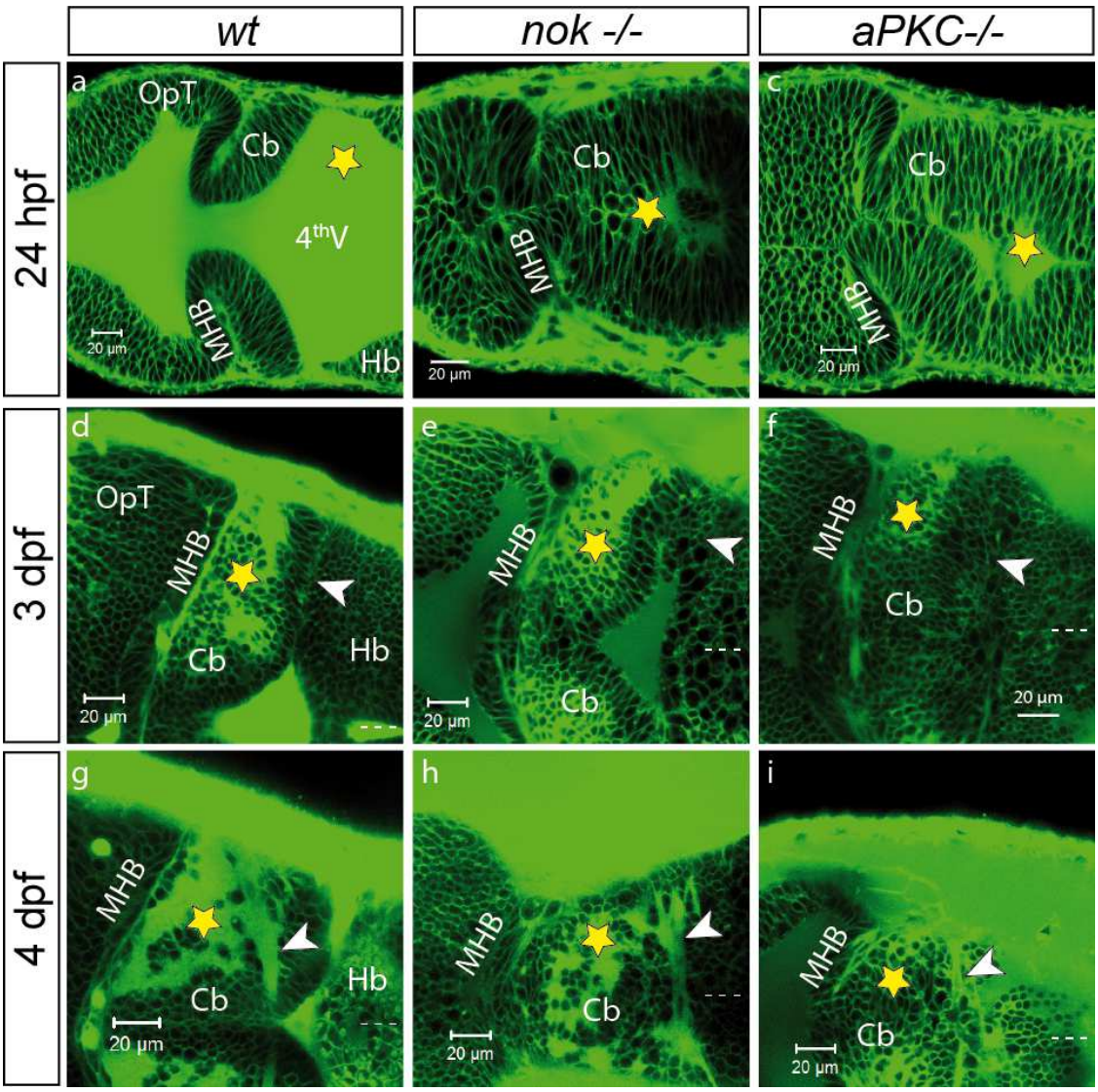

Figure 3.1: Bodipy staining to reveal cerebellar morphology of *wt*, *nok*-/- and *apkci*-/- embryos.
a-i) Single confocal sections of the dorsal cerebellum. a-c) dorsal view of 24 hpf old embryos. a) In *wt* embryos the brain ventricles (asterisk) were inflated and therefore the cerebellar anlage rotated about 90°. b, c) In *nok*-/- and *apkci*-/- the neuroepithelium stayed mostly closed. d-f) Dorsal view of one cerebellar hemisphere of 3 dpf old embryos. d) In *wt* a molecular layer has formed (asterisk) and a clear border between cb and hb was visible (arrowhead). e, f) In the mutants a molecular layer was also formed, but no continuous border between cb and hb existed (arrowheads). g- i) Dorsal view of one cerebellar hemisphere of 4 dpf old embryos. g) In *wt* parallel fiber projections of GCs appeared and formed the prominent dorsal commissure (arrowhead). h, i) Also in the mutants the dorsal commissure created by projections of GCs were visible (arrowheads).
Cb – cerebellum, GC – granule cell, hb – hindbrain, MHB – mid-hindbrain boundary, 4thV – 4th ventricle.

3.2 The cerebellum of mutant embryos is smaller compared to *wt* embryos

Another observation made with the Bodipy Ceramide staining was the reduced size of the cerebellum of both mutant strains, clearly visible at 4 dpf, especially regarding the lateral expansion. Therefore measurements using these recordings were done. The expansion of the cerebellum was measured at two sites on the same z-level; at the anterior site the distance between the most lateral points of the mid-hindbrain boundary (MHB) and at the posterior site the distance between the most lateral points of the dorsal commissure created by the lateral fibres of granule cells (fig. 3.2 b-d).

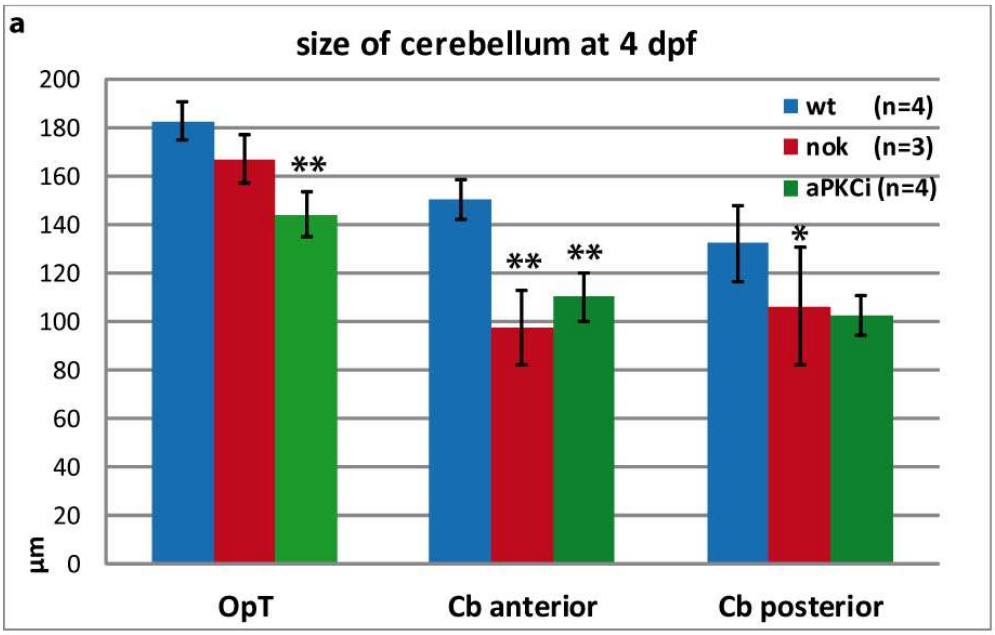

a'	width in µm		
	OpT	Cb anterior	Cb posterior
wt (n=4)	182,87	150,17	132,22
nok (n=3)	166,97	97,68	106,38
aPKCi (n=4)	144,32	110,11	102,55

a''	*p*-value		
	OpT	cb ant	cb post
wt/nok	0,070	0,002	0,041
wt/aPKCi	0,001	0,007	0,095

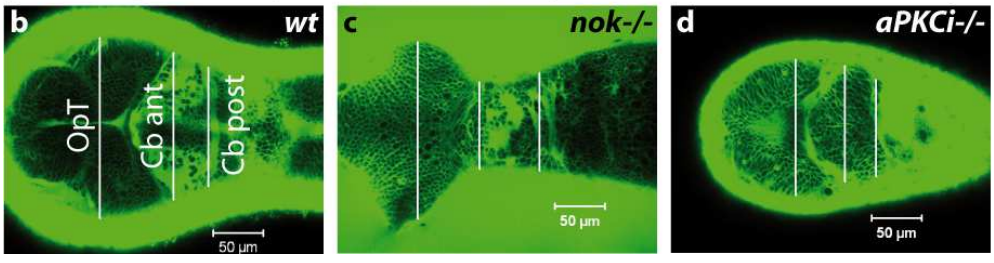

Figure 3.2: Comparison of the cerebellar size between *wt* embryos and mutants.
a-a'') Graphe and tables of mean values of the lateral expansion of the OpT and the cb at an anterior and posterior site. b-d) Images to illustrate the measured distances. The OpT was measured at its widest expansion. The cb was measured between the most lateral points of the MHB and the most lateral points of the dorsal commissure formed by parallel fiber projections. The OpT of *nok-/-*

embryos is in tendency smaller than that of *wt* embryos (p=0.07). The cb of *nok-/-* is highly significantly reduced at the anterior sites (p=0.002) and significantly smaller at the posterior site (p=0.041) compared to *wt*. The OpT of *apkci*$^{-/-}$ embryos is highly significantly smaller than of *wt* embryos (p=0.001) and the cb is significantly reduced at the anterior site (p=0.07) and also in tendency smaller at the posterior site (p=0.095). The p-value was calculated with a two-tailed students t-test with unequal variance. Cb – cerebellum, OpT – optic Tectum, *= significantly reduced , **=highly significantly reduced.

In addition, the optic tectum (OpT) was measured for comparison at the widest expansion on the same z-level as the cerebellum. A comparable z-layer in all embryos was chosen on the dorsal side of the cerebellum, using the dorsal commissure and the MHB as orientation marks. Significance (p-value < 0.05) was calculated using a two-tailed students t-test with unequal variance.

In *nok*$^{-/-}$ embryos the optic tectum is in tendency narrower than in wt (p=0.07). The extent of the cerebellum is significantly reduced at the anterior site (p=0.002) and also significantly reduced at the posterior site (p=0.041). The expansion at the anterior site is by mean value only 97.68 µm wide compared to 150 µm in wt (fig. 3.2 a-a''). In *apkci*$^{-/-}$ embryos the optic tectum and the anterior width of the cerebellum are significantly reduced compared to wt (p=0.01 and p= 0.07, respectively). No significant reduction of the width at the posterior site was determined, however, a trend to a smaller cerebellum could be observed (p=0.095; fig. 3.2 a-a''). A likely explanation for the reduced width of the cerebellum is the incomplete rotation of the cerebellar anlage, due to a failure in ventricle opening, as observed above (s. 3.1).

3.3 *apkci* and *nok* are expressed in the early zebrafish cerebellum

The morphological analysis revealed that the development of the cerebellum is altered in both mutants. In order to address a possible role of Nok or aPKCi in cerebellar development, the expression profile of both genes was analysed in the developing embryo over time by *in situ*-hybridization and antibody staining. Because gaining insight into migration mechanisms of GCs, another aim was to prove the expression of *nok* and *apkci* within GCs.

To obtain the probes for the *in situ*-hybridization, full length zebrafish *apkci* and *nok* were amplified from embryonic zebrafish cDNA, and subsequently ribo-probes were synthezised.

3.3.1 Expression of *apkci*

Whole-mount mRNA *in situ*-hybridization on *wt* embryos with an antisense probe of *apkci* revealed an expression of *apcki* mRNA in the whole brain and hence in the cerebellum (fig. 3.3 a-c'', arrows) in 24-72 hpf old embryos. The negative control with a sense probe of *apkci* confirmed that this was not unspecific staining (fig. 3.3 d-f), as staining in the cerebellum (arrows) was not detectable. Stained areas in 24 hpf embryos subjected to hybridization with the control sense probe were not localized to cellular structures but instead accumulated in tissue cavities such as brain ventricles (fig. 3.3 d).

However, with the mRNA *in situ*-hybridization it was not possible to determine the exact distribution of *apkci* expression within the cerebellum. Hence a fluorescent antibody staining against aPKCi was performed.

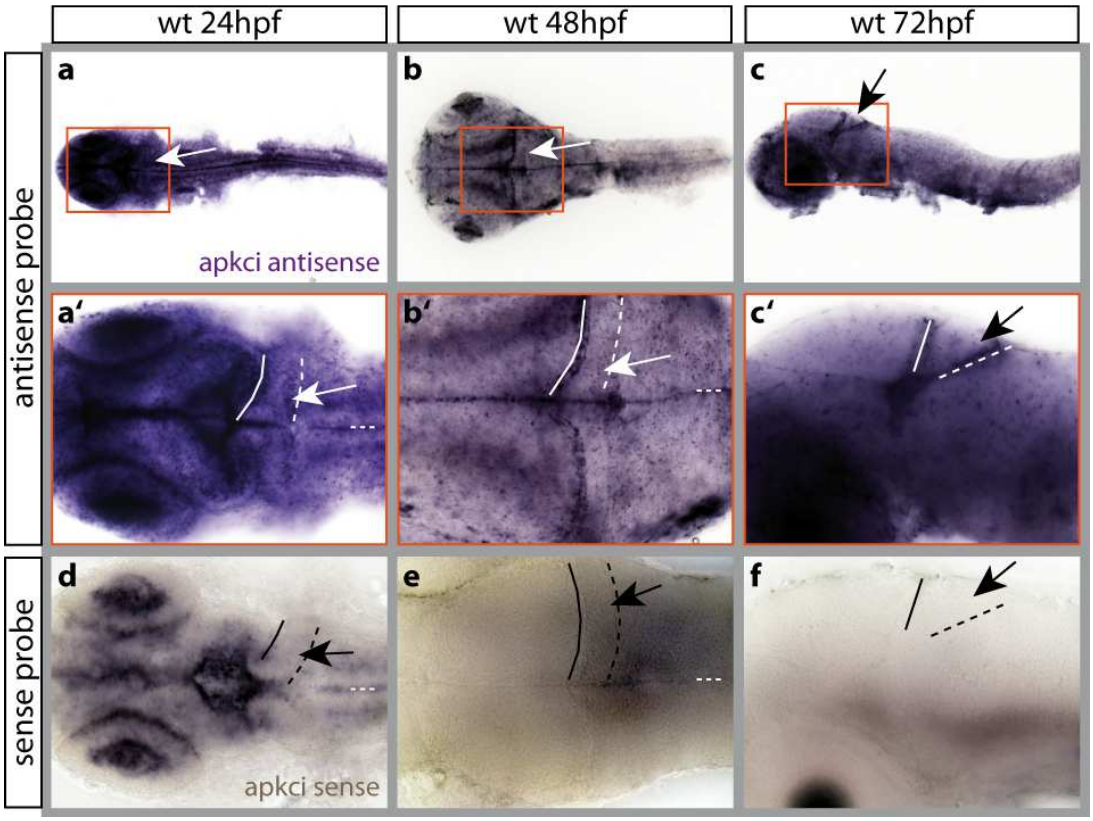

Figure 3.3: *apkci* is expressed throughout the brain of *wt* zebrafish embryos.
Whole-mount *in situ*-hybridization with *apkci* antisense and sense riboprobes on *wt* embryos. Images of 24 hpf and 48 hpf are dorsal view, those of 72 hpf are lateral view. a-c'') Expression of *apkci* mRNA in the cerebellum (arrows) and throughout the brain could be confirmed in 24-72 hpf embryos. d-f) The negative control with a sense probe of *apkci* showed no expression in the cerebellum (arrows). Staining in the 24 hpf negative control is likely artificial accumulation of staining reagents in tissue cavities.
Lines indicate the mid-hindbrain boundary, dashed lines the upper rhombic lip, small dashed lines the midline. a,b,c) 10x; a'-f) 40x objective, Zeiss Axioplan microscope.

Because the only commercially available aPKC antibody reported to work in zebrafish so far was raised against the C-terminus of aPKCζ and detects both isoforms of aPKC, aPKCi and aPKCζ, several antibodies had to be tested. Antibodies directed against epitopes of human aPKCi, called aPKCλ and aPKCι (BD laboratories) were available and so we determined their ability to detect zebrafish aPKCi as follows. By aligning the amino acid sequence of the human and the zebrafish aPKCi a high similarity was observed (sequence alignment fig 5.2 of appendix). In the epitope region recognized by the antibodies, there were only 7 divergent amino acids (95.7% identity and 97.5% similarity). To confirm epitope recognition a western blot analysis was conducted. 293T-cells were transfected with zebrafish aPKCi (expression vector pCSII/apkci) and subsequently the protein lysate was subjected to western blotting, which was then analysed by immunohistochemistry. Both antibodies gave a strong signal at ~ 70 kDa, the size of aPKCi, confirming their ability to cross-react with zebrafish aPKCi (western blot fig. 5.1 of appendix), and were further used for fluorescent whole mount immuno-staining on zebrafish embryos.

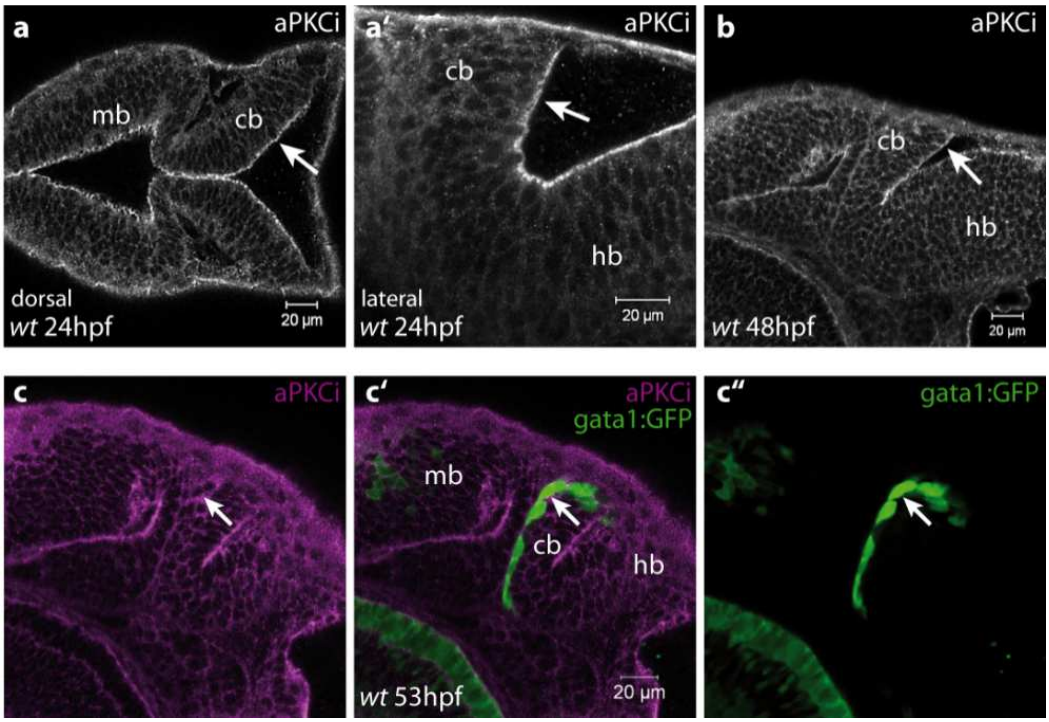

Figure 3.4: aPKCi is expressed throughout the cb and hence in GCs of zebrafish embryos.
Antibody staining against aPKCi (a-b) and double staining against aPKCi and GFP (c-c''). In 24 hpf wt embryos aPKCi was expressed throughout the brain, but was most prominent along the ventricular surface and therefore along the URL (a-a', arrows). The same expression pattern was apparent at 48 hpf (lateral view), also with a strong localization at the ventricle surface (b, arrow). aPCKi was expressed in differentiated and migrating granule cells, which are GFP positive in the transgenic line *Tg(gata1:GFP)*, here shown in a lateral view of 53 hpf old embryos (a-c'', arrows). Cb – cerebellum, hb – hindbrain, mb – midbrain.

The immuno-staining with the tested aPKCi antibody and subsequent analysis by confocal microscopy proved the expression of aPKCi throughout the whole brain from 24 hpf until 3 dpf. Expression was predominant along the apical membranes of the neuroepithelia and therefore along the upper rhombic lip (URL) of the cerebellum (fig. 3.4 a-b, arrows), where tight junctions are present.
In the *gata1:GFP* line (Long et al. 1997; Köster and Fraser 2006), GFP is expressed by GCs in the cerebellum (Volkmann et al. 2008) (see also chapter 3.5). Using this transgenic line, the expression of aPKCi was not only confirmed in GC precursors but also in differentiating GCs, according to antibody signals in green fluorescent cells apart from the URL (fig. 3.4 c-c'', arrows).

Because we then realized, that the aPKCι/λ antibodies were directed against the C-terminus of the protein, we tried to test the specificity of these antibodies in discriminating between aPKCi and aPKCζ. Comparison of the epitope of human aPKCi and zebrafish aPKCζ revealed 82.3% identity and 90.2% similarity, including 4 gaps, compared to 95.7% identity and 97.5% similarity of human and zebrafish aPKCi (s. fig 5.3 of appendix). Performed western blot analysis so far revealed many unspecific protein bands, obtained either with the anti-aPKCι or the anti-aPKCζ antibody (data not shown). Thus, the background made it impossible to come to a conclusion. Yet, combined with our results of an affected brain development and taking into account the distribution of *apkci* expression observed with the above *in situ*-hybridization using a specific *apkci* riboprobe, the antibody staining probably resembles aPKCi expression.

3.3.2 Expression of *nagie oko*

Expression of Nok along the 4th ventricle has been shown by (Lowery and Sive 2005) at least at 22 hpf. However, later stages were not investigated so far.
In situ-hybridization with a *nok* antisense probe confirmed expression of *nok* in the neuroepithelium at 24 hpf, most abundant at the apical side (fig. 3.5 a, arrows). As a negative control an *in situ*-hybridization with a *nok* sense probe was performed. In this negative control no specific staining was observed (fig. 3.5 a'), only artificial accumulations of staining reagents in tissue cavities (fig. 3.5 a', asterisks). At 48 hpf *nok* expression was restricted to cells lining the ventricle (fig. 3.5 b, arrows) and the dorsal midline (fig. 3.5 b, arrowheads).

The antibody-staining against Nok at 3dpf showed the same result, i.e. expression along the ventricle and the midline (fig. 3.5 c, arrows). Expression in GCs was not detectable (fig. 3.5 c, c', arrowheads).

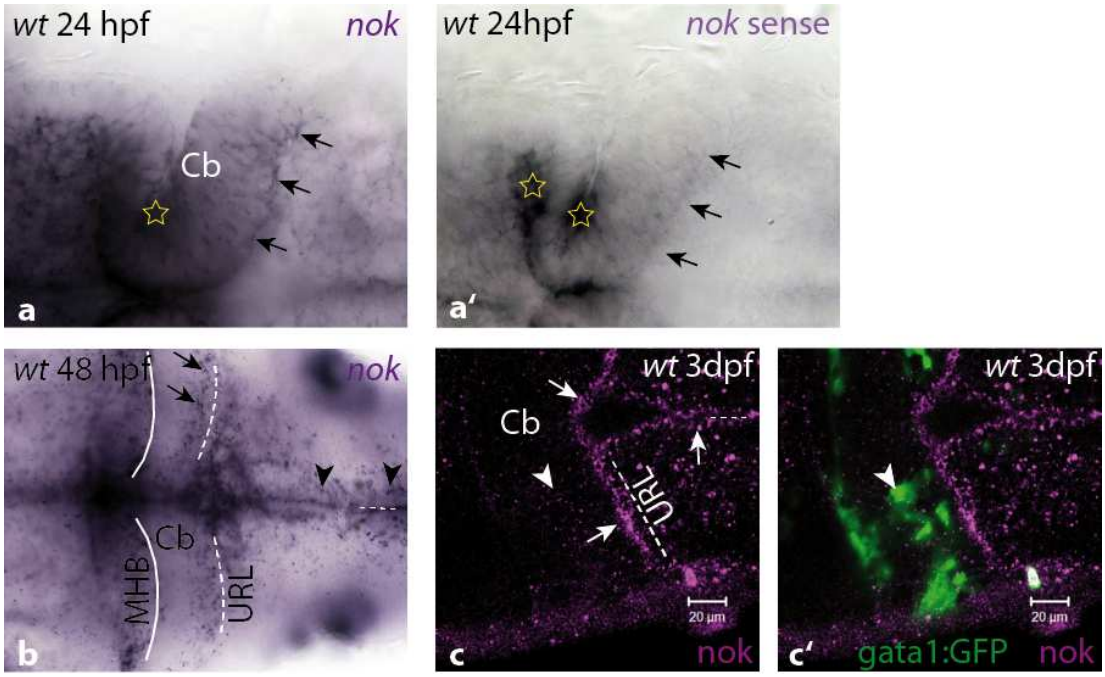

Figure 3.5: *Nok* is expressed along the apical side of the cerebellum.
In situ-hybridization of *nok* mRNA (a-b). At 24 hpf *nok* is expressed in the cb most prominent at the ventricular surface (a, arrows). As a negative control hybridizations with a *nok* sense riboprobe were performed, and no staining was apparent, besides accumulations of staining reagents in cavities, also visible in hybridizations with the *nok* antisense probe (a-a', asterisks). At 48 hpf expression of *nok* concentrated along the ventricular surfaces and the midline of the brain, therefore also at the URL of the cb, the proliferation zone of GCs. An antibody staining against Nok in the transgenic line *Tg(gata1:GFP)* revealed its expression along the ventricle. No expression of Nok was found in GCs distant from the URL. Cb – cerebellum, MHB – mid-hindbrain boundary, URL – upper rhombic lip; a-b) 40x objective, Zeiss Axioplan microscope.

Contrary to Nok, aPKCi was not restricted to the apical membrane of the cerebellum but expressed within the cerebellum itself (compare *in situ*-hybridization). Both proteins play a role in tight junction formation (Feigin and Muthuswamy 2009) and it was no surprise they localized apically. But Nok seems to be more restricted to the function in setting up tissue polarity, whereas aPCKi could be involved in other cellular processes in which polarity plays an important role like directed cell migration (Etienne-Manneville and Hall 2003). Nevertheless, in the early monolayer of the cerebellar neuroepithelium the apical side is the proliferation zone of neuronal cells and expression of *nok* could play a role in proper GC proliferation.

3.4 Differentiation of GCs in *apkci*$^{-/-}$ and *nok*$^{-/-}$ embryos

For both loss-of-function mutants morphological aberrations of cerebellar development were observed, and in addition both genes, *apkci* and *nok*, were found to be expressed in the cerebellum. Therefore a detailed investigation of neuronal differentiation of the most prominent cell type of the cerebellum, the granule cells, was performed. While *apkci* expression could be shown in differentiating GCs, *nok* was restricted to the apical proliferation zone and thus most likely expressed in GC progenitors. To address neuronal differentiation, genes expressed in different stages of granule cell development were investigated regarding their pattern and onset of expression by mRNA-*in situ*-hybridization in whole mount embryos. The selected GC marker genes (see below) are expressed in a time dependent manner during different stages of GC development until terminal differentiation (Volkmann et al. 2008).

Expression of *atonal homolog 1a* (*atoh1a*) defines the rhombic lip, which is a highly proliferative zone of the rhombencephalon, which is further subdivided into a cerebellar part, termed the upper rhombic lip (URL), and a lower rhombic lip (LRL) along the dorsal ventricular side of the remaining hindbrain (Machold and Fishell 2005; Wang et al. 2005). As already mentioned in the introduction the URL not only gives rise to GCs but also to tegmental hindbrain nuclei and deep cerebellar nuclei at an earlier stage (Volkmann et al. 2010). Hence, *atho1a* is not an exclusive marker for GCs, but its expression still provides a first hint whether the proliferation zone, from which GCs arise, is affected in the mutants or not. Expression of *athoh1a* was broad throughout the rhombic lip in both mutants. Comparing mutant with wt embryos (fig. 3.6 a-a’’), the different appearance of the pattern though is immediately obvious. In wildtype embryos the expression of *atoh1a* outlines the trigonal shape of the 4th ventricle, whereas in both mutants only one long stretched expression domain in the centre of the hindbrain region was visible. A reasonable explanation for this finding was presented in chapter 3.1, where Bodipy Ceramide staining revealed that the ventricle remains mostly closed in both mutants. Therefore both proliferation zones of the rhombic lip (URL and LRL) stay in line adjacent to the midline without the rotation of the cerebellar anlage like in *wt*. However, the broad expression of *atoh1a* restricted to a central domain suggested that a rhombic lip *per se* was defined and thus neuronal proliferation was likely taking place in mutant embryos.

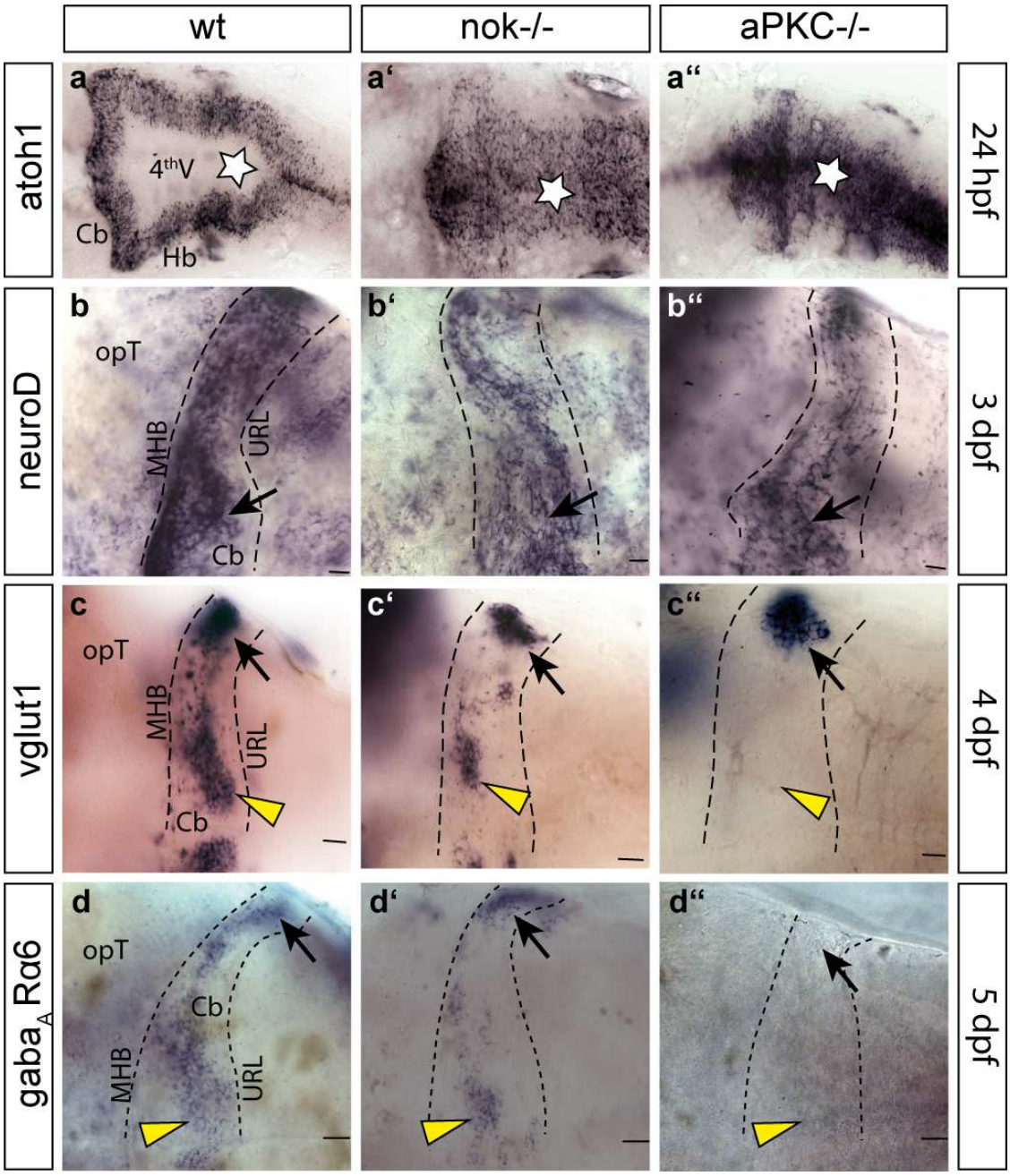

Figure 3.6: Expression of granule cell marker genes in the cb of wt and mutant embryos.
mRNA *in situ*-hybridization on whole mount zebrafish embryos, dorsal view of the mid-hindbrain region, b-d'' only one hemisphere. a-a'') In 24 hpf old *wt* embryos the expression of *atoh1a* outlined the open ventricle. In *apkci*$^{-/-}$ and *nok*$^{-/-}$ expression of *atoh1a* concentrated around the midline without a gap in the middle. b-b'') *neuroD* expression seemed comparable between *wt* and mutants, however less cells expressing *neuroD* were visible. c-c'') The expression profile of *vglut1* showed a clear difference between *wt* and mutants. In *nok*$^{-/-}$ embryos fewer cells expressed *vglut1* in the medial cerebellar region and in *apkci*$^{-/-}$ mutants no expression could be seen in the medial part (yellow arrowhead). Expression in the lateral cerebellar region is comparable between *wt* and mutants. d-d'') Strikingly no expression of the terminal differentiation marker gene *gaba$_A$ Rα6* at all was visible in *apkci*$^{-/-}$ mutants. In *nok*$^{-/-}$ embryos the number of *gaba$_A$ Rα6* expressing cells was clearly reduced compared to wt (arrowheads and arrows).
Cb – cerebellum, MHB – mid-hindbrain boundary, OpT – optic tectum, URL – upper rhombic lip; a-d'') 40x objective, Zeiss Axioplan microscope.

Next, the expression of *neuroD* was analysed, which is a marker gene for early postmitotic neurons and is expressed in differentiating and migrating GCs (Miyata et al. 1999; Schüller et al. 2006; Volkmann et al. 2008; Pan et al. 2009). In *wt* embryos expression was already prominent at 3 dpf (s. fig. 3.6 b, arrow). Compared to *wt* fewer cells were labelled by the hybridization with the *neuroD* riboprobe in the cerebelli of both mutant lines (fig. 3.6 b'-b'', arrows). Possible reasons could have been less cell proliferation, increased cell death, or a postponed onset of differentiation of GCs.

At 4 dpf expression of *vesicular glutamate receptor 1* (*vglut1*) appeared in the cerebellum of *wt* embryos, thus GCs had begun to acquire their neurotransmitter identity as glutamatergic neurons (fig. 3.6 c) (Volkmann et al. 2008). Compared to *wt* embryos the region of *vglut1* expressing cells was markedly reduced in *nok*$^{-/-}$ mutants, especially in the medial cerebellar region (fig. 3.6 c and c', arrowheads), whereas there was only a slight reduction concerning the lateral region (fig. 3.6 c', arrows). Regarding the lateral cerebellar region in *apkci*$^{-/-}$ embryos there was also only a slight reduction in cells marked by *vglut1* expression compared to *wt* (fig. 3.6 c and c'', arrows), but strikingly no expression could be found in the medial region of the cerebellum in *apkci*$^{-/-}$ (fig. 3.6 c'', arrowheads). This points either to a massive cell death during development of GCs in the mutants or to a postponed onset of or even a failure in differentiation.

To further address the question of differentiation, expression of the terminal differentiation marker gene *gaba$_A$ receptor α6 subunit* (*gaba$_A$ Rα6*) was investigated. *Gaba$_A$ Rα6* is solely expressed in cerebellar GCs (Kato 1990; Lüddens et al. 1990; Bahn et al. 1996; Volkmann et al. 2008). Again in the *nok* mutants fewer cells expressed *Gaba$_A$ Rα6* in the medial cerebellar regions compared to *wt* (fig. 3.6 d and d', arrowheads), but the expression in the lateral region was similar (fig. 3.6 d and d', arrows). However, no expression of *gaba$_A$ Rα6* was visible, neither in the medial nor in the lateral regions of the cerebellum of *apkci* mutants (fig. 3.6 d''). This confirms the conclusion made by the observations of the *vglut1* expression. Taken together these findings suggest alterations in GC development in *nok*$^{-/-}$ and *apkci*$^{-/-}$ embryos, caused by cell death or differentiation problems.

3.4.1 Terminal differentiation is not reached by GCs in *apkci* mutants

To test the hypothesis that cell differentiation is postponed, the expression of *neuroD* and *vglut* was reanalysed at later stages in *apkci*$^{-/-}$ embryos, which displayed the stronger phenotype of the mutants. The early postmitotic marker gene *neuroD* was analysed at 4 and 5

dpf. At 4 dpf cells were labelled along the URL in *wt* embryos (fig. 3.7 a). In *apkci*$^{-/-}$ embryos cells were mainly labelled along the URL as well, but in addition cell clusters in ectopic positions could be observed (fig. 3.7 a'). At 5 dpf the expression analysis showed a similar result, confirming that cells were still existing. Nevertheless, the amount of cells expressing *neuroD* was reduced in *apkci* (and *nok*) mutants compared to *wt* embryos. The staining of *vglut1* in 5 and 6 dpf old embryos revealed, that still only GCs in the lateral cerebellar region were expressing *vglut1* (fig. 3.7 c' and d') like at 4 dpf (fig. 3.7 c''). This indicated problems of GCs in the medial clusters of achieving a neurotransmitter identity after cells have become postmitotic.

Interestingly, although no expression of the neurotransmitter marker *vglut1* and the terminal differentiation marker *Gaba$_A$ Rα6* could be observed, still a dorsal commissure of GC parallel fibres was formed (compare fig. 3.1 andFigure 3.8). This suggests that in this case the outgrowth of axons precedes the specification of a neurotransmitter identity and terminal determination as GCs. In summary, GC number was reduced in the mutants and GCs especially in the medial cerebellar regions did not reach a neurotransmitter identity.

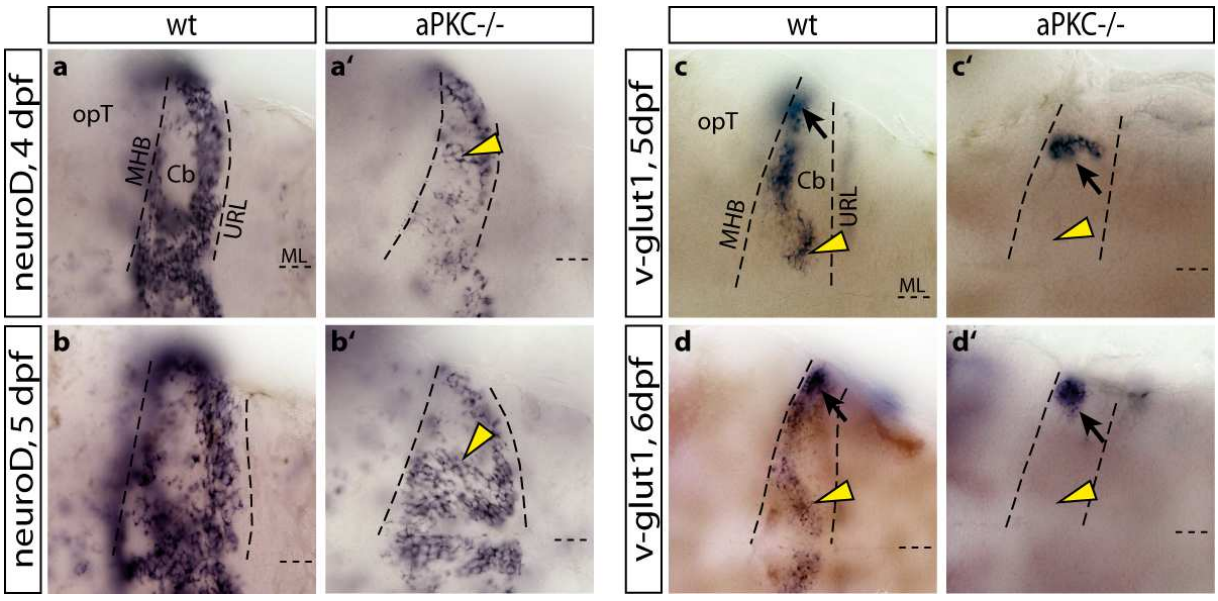

Figure 3.7: Analysis of the expresison of neuroD and v-glut1 at later developmental stages
Whole mount *in situ*-hybridizations; dorsal view of the cerebellum. a-b') Expression of *neuroD* was analysed at 4 and 5dpf in wt and *apkci*$^{-/-}$ embryos. At both stages expression was evident in *apkci* mutants, but the number of *neuroD* expressing cells was less than in *wt*. c-d') Expression of *vglut1* at 5 and 6dps was comparable to 4 dpf. No expression was visible in the medial cerebellar region (arrowheads), only in the lateral part (arrows) expression could be found.
Cb – cerebellum, MHB – mid-hindbrain boundary, OpT – optic tectum, URL – upper rhombic lip;
a-d') 40x objective, Zeiss Axioplan microscope.

3.5 The number of GCs is reduced in the mutants and GCs are localized partly at divergent areas compared to *wt*.

The transgenic line *Tg(gata1:GFP)* was originally established to investigate erythroid cells, as the transcription factor Gata1 is specifically expressed in these cells (Long et al. 1997). However due to a position effect in the *Tg(gata1:GFP)* 781-line, expression of GFP is also driven in other cell types, and particularly in the cerebellum. Our research group could show that these cells represent the granule cell population (Volkmann et al. 2008). Therefore embryos of this transgenic strain represent an excellent tool to investigate migration of GCs in the zebrafish, and their spatio-temporal differentiation throughout the cerebellum.

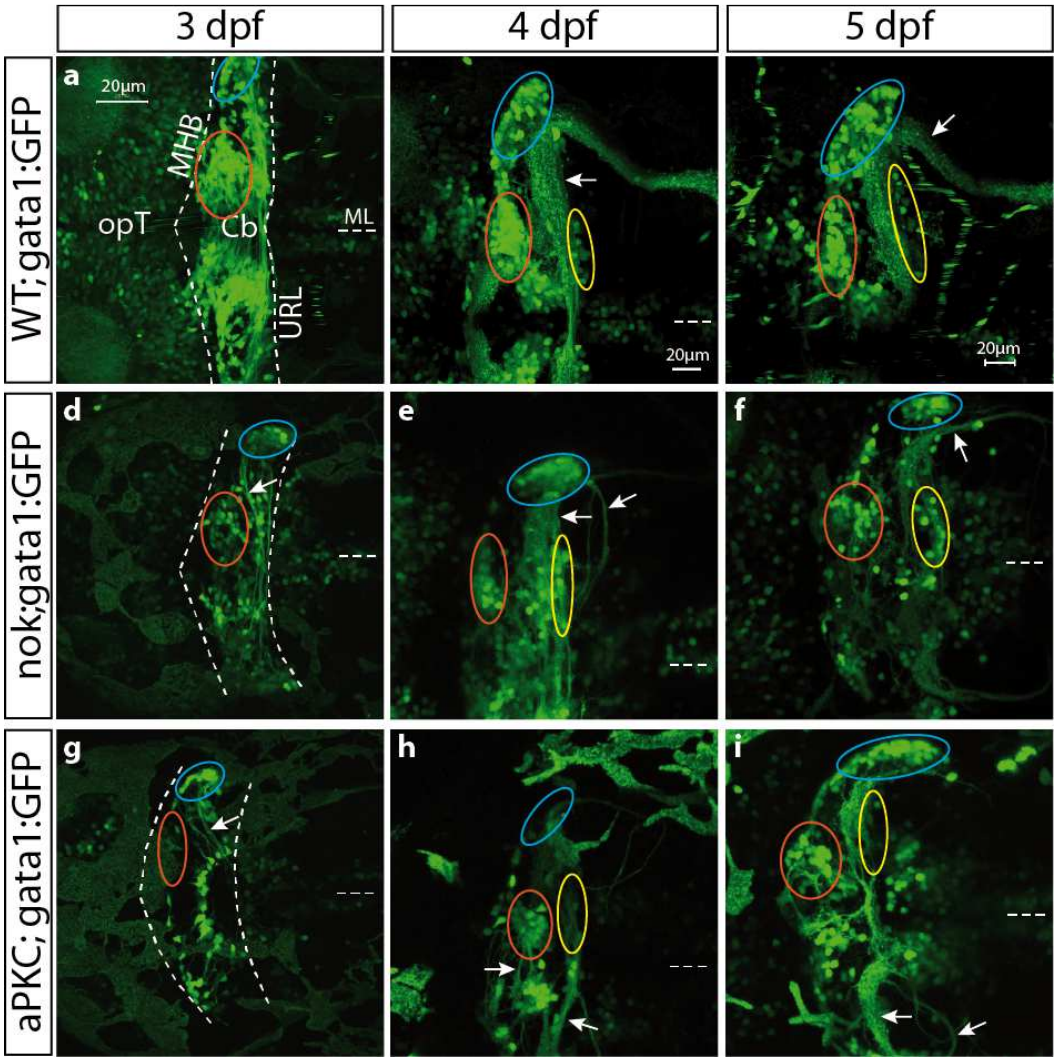

Figure 3.8: The number of GC is reduced in the mutants and GCs are localized partly at divergent areas compared to wt.
Dorsal view of the cerebellum of *Tg(gata1:GFP)* in *wt* (a-c), *nok*$^{-/-}$ (d-f) or *apkci*$^{-/-}$ (g-h) background, displaying GFP expression in cerebellar GCs (encircled). a-c) In *wt*, GFP expression and onset of migration started at 48 hpf and GCs migrated into three clusters: dorsomedial (orange circle),

dorsoposterior (yellow circle) and ventrolateral (blue circle). Parallel fibers were visible at 3 dpf and the prominent dorsal commissure and dorsal projection were apparent at 4 dpf (arrows). b-i) In *nok*$^{-/-}$ and *apkci*$^{-/-}$ GFP expression and onset of migration started approximately one day later and the amount of GCs was markedly reduced compared to *wt* throughout all stages. Cluster formation (circles) and outgrowth of parallel fibers (arrows) occurred in both mutants, but displayed a more disorganized shape and arrangement than in *wt*, indicating problems in path finding of migrating GCs.
Cb - cerebellum, MHB - mid-hindbrain boundary, OpT - optic tectum, URL - upper rhombic lip.
Scale in mutants similar to *wt* at the correspoding age.

To make use of this knowledge for this research project, zebrafish carrying a mutant *apkci* allele were bred with fish homozygous for the transgene *gata1*:GFP. Subsequently, identified carriers for *gata1*:GFP and a mutant *apkci* allele were than inbred in order to obtain homozygous mutant offspring (*apkci*$^{-/-}$ or *nok*$^{-/-}$) expressing GFP in granule cells. This way it was possible to follow migration of GCs in a mutant background and compare it to *wt* migration behaviour.

It has been shown previously by our group (Volkmann et al. 2008) that GCs migrate into three different clusters later contributing to distinct cerebellar compartments. In the mutants the cluster formation was affected. Depending on the embryo, clusters were not prominent in the mutants regarding the size and number of GFP expressing cells (fewer than in wt) and hence the outline of the region they occupied differed strongly between embryos, especially for the dorsomedial (orange circles) and dorsoposterior cluster (yellow circles). The formation of the ventrolateral clusters was less affected but still the number of GFP expressing cells was reduced (fig. 3.8, blue circles). This again was in accordance with the differentiation analysis of GCs in the mutants compared to *wt* (s. chapter 3.4). On account of the later initiation of differentiation, protrusion formation also lacked behind by about one day, but parallel fibres were emanating in the mutants starting from 3 dpf onwards (fig. 3.8 a-i, arrows). Taken together GCs were altered in both mutant strains, *apkci*$^{-/-}$ and *nok*$^{-/-}$, regarding granule cell number, onset of migration and cluster formation.

3.6 The number of GCs in *apkci* mutants is reduced by increased cell death and a decreased cell proliferation

The results of the experiments performed so far made it obvious that the number of GCs was reduced in *apkci*$^{-/-}$ and *nok*$^{-/-}$ embryos, which could not exclusively be explained by a delayed differentiation. To elucidate the reason for this reduced GC number, cell death, cell proliferation and Purkinje cell development were investigated. Because *apkci*$^{-/-}$ embryos

showed the stronger phenotype in the expression analysis of GCs differentiation marker genes (chapter 3.4) and because *apkci* is expressed in migrating GCs, further experiments focused on this mutant line.

3.6.1 Cell Death Analysis in the Cerebellum

First, increased cell death was addressed as one reason for the reduced number of granule cells. Therefore, an Acridine Orange (AO) staining was performed at different developmental stages (fig. 3.9). AO binds to nucleic acid and can only do so if nuclear membranes are broken down, which is a characteristic sign for cell death. Throughout all developmental stages analysed (48 hpf, 3 dpf, 4 dpf, 5 dpf), cell death in *apkci*$^{-/-}$ embryos was significantly increased compared to *wt* (p=0.007, 0.011, 0.030, 0.038, respectively, significance was calculated using the students t-test; fig. 3.10).

One has to keep in mind though, that this staining is not selectively marking GCs but all cell types dying. Acridine Orange has an emission maximum at 525 nm and is in the same emission range of GFP. Hence, it cannot be used together with the transgenic line *Tg(gata1:GFP)* in which only GCs in the cerebellum express GFP. Nevertheless, AO was not restricted to one area, but evenly distributed throughout the cerebellum. Therefore, it is likely that all cerebellar cell types, and hence GCs were affected by increased cell death.

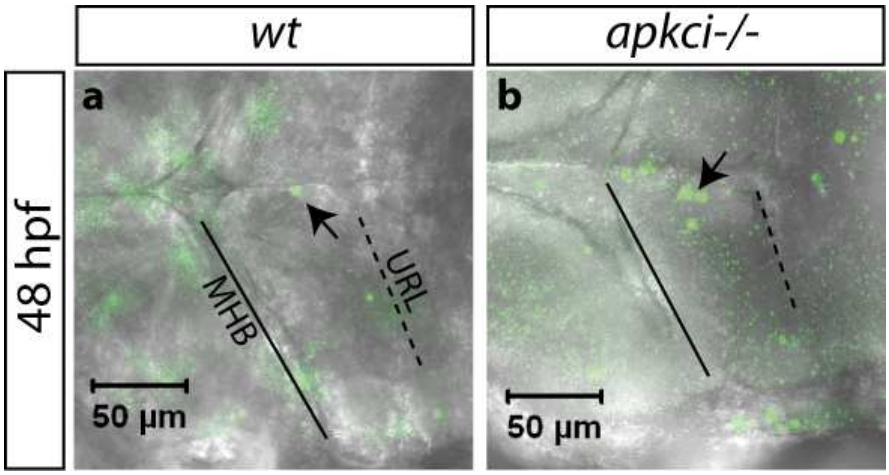

Figure 3.9: Acridine Orange staining to analyse cell death in the developing cerebellum
a-b) Dorsal view of Acridine Orange staining (arrows) on 48 hpf embryos. Cell death was increased in the cerebellum of apkci mutants. Maximal projections of confocal LSM z-stacks.

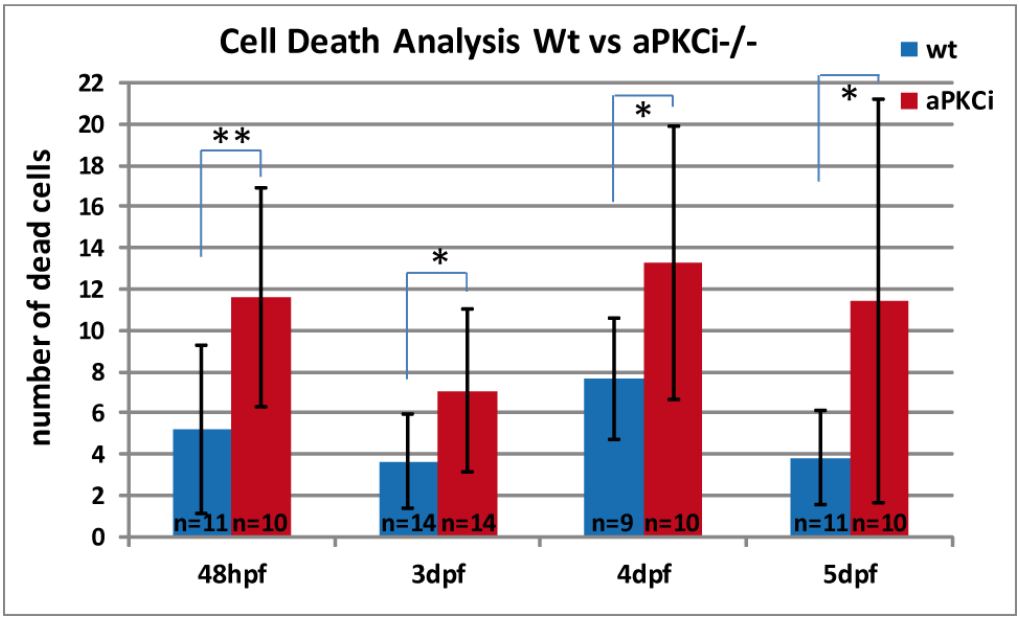

Figure 3.10: Cell death analysis in *wt* and *aPKCi*$^{-/-}$ embryos
Cell death was analysed by subjecting living embryos to an Acridine Orange staining. At all developmental stages investigated (2, 3, 4, 5 dpf) cell death rate was significantly increased in *apkci*$^{-/-}$ compared to *wt* embryos (p=0.007; 0.011; 0.030; 0.038, respectively).

3.6.2 Cell proliferation Analysis in the Cerebellum

Besides increased cell death, a further reason for the reduced cell number observed in *apkci* mutant embryos could be a reduction in cell proliferation. Even though no severe impairment of the proliferation zone was observed by the expression of *atoh1a* (chapter 3.4), proliferation was addressed, by performing a whole-mount fluorescent antibody staining against phospho-Histone H3 (pH3), which marks mitotic cells in late G2/M-phase of the cell cycle (Hendzel et al. 1997).

Cell proliferation rate

Cells expressing pH3 were counted in the cerebellum of *apkci*$^{-/-}$ and *wt* embryos. The counting (fig. 3.11) revealed that there was no significant difference at 24 hpf in the extent of cell proliferation in the cerebellar primordium between *wt* and *apkci*$^{-/-}$ embryos. However, cell proliferation decreased significantly (p=0.024) in *apkci*$^{-/-}$ compared to *wt* embryos from 48 hpf onwards, a developmental stage when the cerebellum begins to generate the vast numbers of GCs. Even less proliferation could be observed at 3 dpf and 4 dpf (p=0.007 and p=0.00001), when GC proliferation in *wt* reaches its peak.

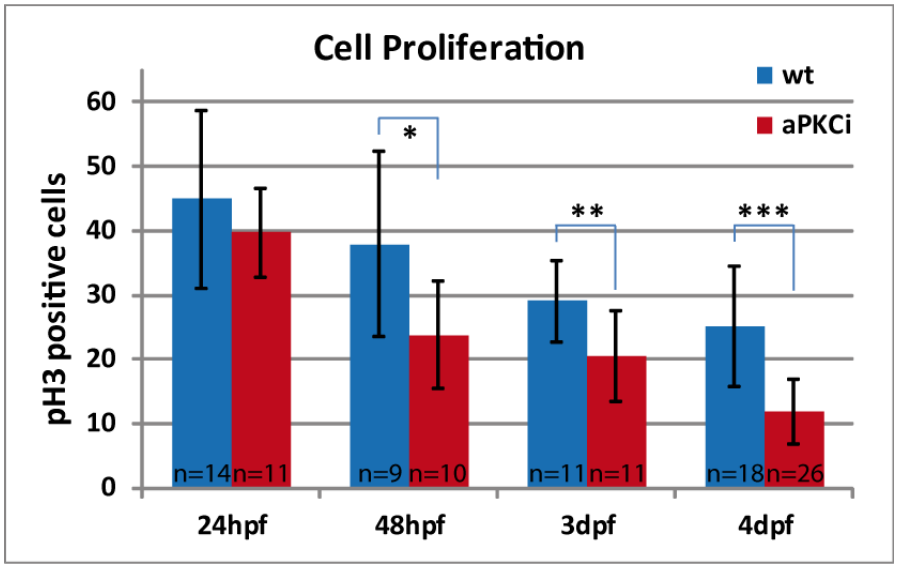

Figure 3.11: Cell proliferation is decreased in the cerebellum of *apkci*$^{-/-}$ embryos
Cell proliferation was analysed doing an α-pH3 staining and counting all labelled cells in the cerebellum. At 24 hpf the amount of dividing cells was comparable between *wt* and *apkci*$^{-/-}$ embryos. Starting from 48 hpf cell proliferation decreased continuously in *apkci* mutants (p=0.024) and was highly significantly lower at 3 and 4 dpf compared to *wt* (p=0.007; 0.00001).

From this analysis it cannot be concluded though, that the reduced rate of proliferation specifically applies for GCs. However, α-pH3 staining was reduced throughout the cerebellum and not localized to certain areas, suggesting that the reduction of cell proliferation affected all cerebellar cell populations that arise from day 2 onwards. At this developmental stage GCs, which are by far the most numerous neuronal cells in the cerebellum, start to be generated. Therefore, it was most likely that the rate of GC proliferation was decreased. Taken together increased cell death and decreased cell proliferation are a plausible cause for a reduced GCs number in *apkci*$^{-/-}$ embryos.

Localization of proliferating cells

In 24 hpf *wt* embryos, pH3 positive cells were located along the URL (fig. 3.12 a, arrows) which was expected, because proliferation of progenitors in early neuroepithelia takes place at the apical surface (Frade et al. 2002). The same pattern was observed in *apkci*$^{-/-}$ embryos (fig. 3.12 b), suggesting intact tissue polarity for this early stage. At 48 hpf pH3 positive cells were no longer restricted to the URL, but appeared additionally throughout the cb in *wt* and in *apkci*$^{-/-}$ embryos (fig. 3.12 c, d; arrowheads).

In addition, an antibody staining with Proliferating-Cell-Nuclear-Antigen (PCNA) was performed. PCNA is a marker for cells in S-phase (Celis and Celis 1985).

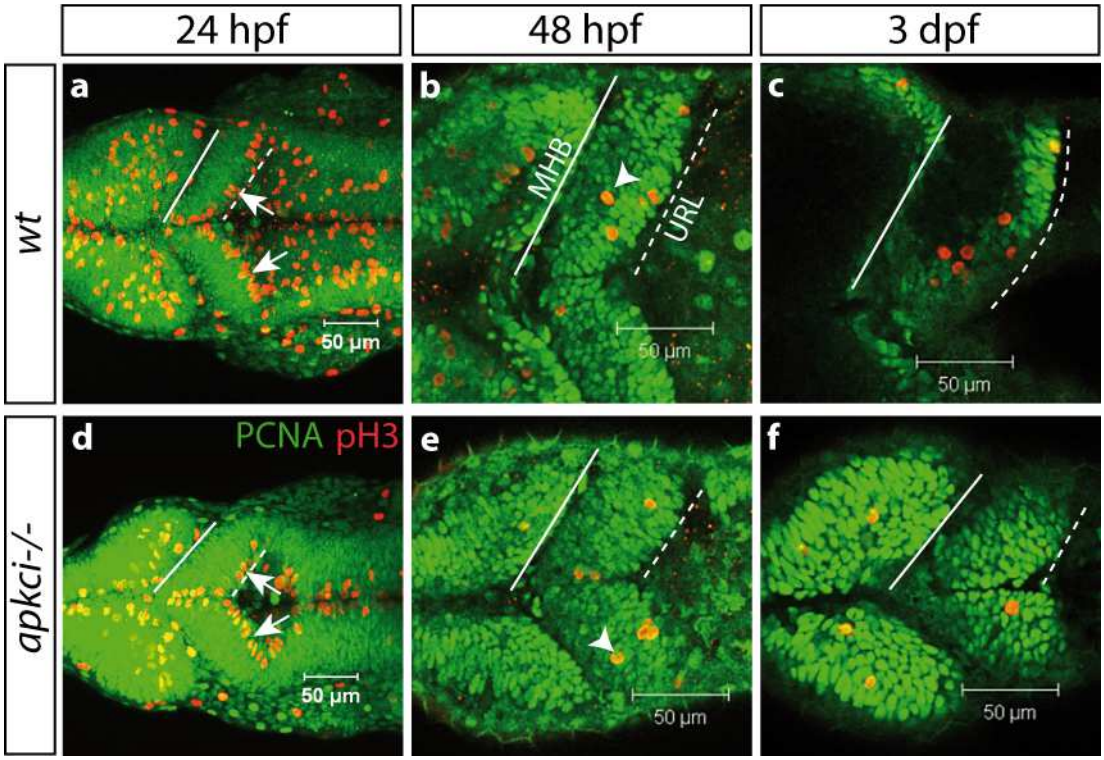

Figure 3.12: Cell cycle analysis illustrates the same pattern in *apkci* mutants like in *wt* embryos
a-b) Maximum projection of confocal z-stacks of 24 hpf *wt* and *apkci* mutant embryos. PCNA expression (green) spanned the whole width from URL to MHB, depicting the pseudo-stratified appearance of the early neuroepithelium. Phospho-histone 3 (red) is only expressed along the URL in apical dividing progenitors in both phenotypes. c-d) Confocal section of 48 hpf old embryos. In *wt* and *apkci* mutant embryos, PCNA expressing cells were observed in dorsal layers of the cb from the URL to the MHB; and pH3 positive cells are no longer restricted to the URL, but appeared throughout the cb (arrowheads), indicating an existing EGL in the zebrafish embryo.
MHB - mid-hindbrain boundary, URL - upper rhombic lip.

Because of occurring interkinetic nuclear movement (INM) from apical to basal lamina and back in progress of cell cycle (s. chapter 1.7), S-phase nuclei were distributed throughout the cerebellum from URL to MHB in *wt* embryos at 24 hpf (fig. 3.12 a, green). The same pattern was observed for *apkci*$^{-/-}$ embryos.

At 48 hpf S-phase nuclei were still covering the complete dorsal cerebellar surface in *wt* and *apkci*$^{-/-}$ embryos (fig. 3.12 c, d), whereas in ventral regions of the cb S-phase nuclei were more restricted to the ventricular side (not shown). This is interesting with respect to the question, whether a transient external granular layer (EGL) exists in zebrafish or not. The observed α-PCNA signal covering the dorsal cb, together with the α-pH3 staining at 48 hpf revealing cell division apart from the URL, would argue in favour for an existing EGL. At 3 dpf PCNA staining in *wt* embryos seems to get more restricted to the ventricular site also in the dorsal cb

with a diameter of ~5 cell somata (Figure 3.12 c), indicating the progressive development from a monolayer to a multi-layered tissue architecture.

3.6.3 Purkinje Cell Development

A research study in mice concluded that a massive cell death of glutamatergic cells (amongst others GCs) occurred, if *ptf1a* derived cells like PCs were completely missing, due to lack of synaptic connections (Hoshino et al. 2005); this is not shown for zebrafish so far, but it should be likely comparable, because these synaptic connections are the same in the zebrafish (Bae et al. 2009). To investigate the possibility that the observed increased rate of cell death in the mutants is caused by affected PCs, the development of PCs was analysed.

As a first step (comparable to chapter 3.4) the expression of several differentiation marker genes for Purkinje cells was analysed by whole mount mRNA *in situ*-hybridization in *wt* and *apkci*$^{-/-}$ embryos.

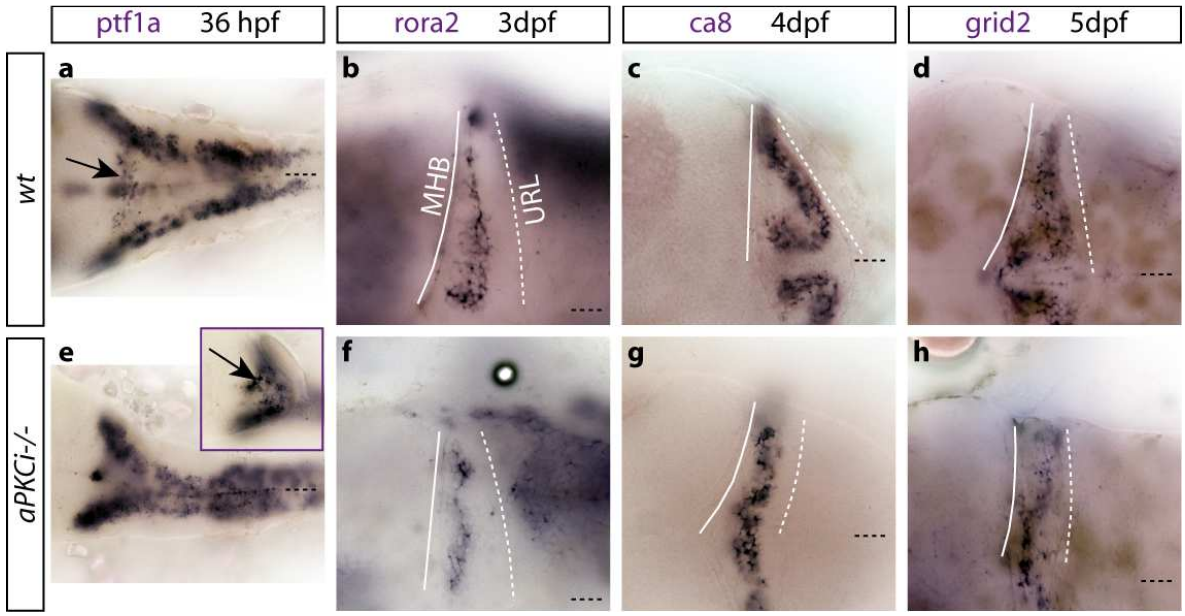

Figure 3.13: Purkinje cells differentiate in *apkci* mutants.
Dorsal views of whole-mount mRNA *in situ*-hybridization on zebrafish embryos. In *wt*, expression of *ptf1a* appeared along the ventricular zone of the hindbrain ventricle, thus in the cerebellar primordium (a, arrow). In *apkci*$^{-/-}$ expression was visible mostly in a broad line along the midline (e), but also in the cerebellar primordium (e, arrow in small image). The expression pattern of *rora2*, *ca8* and *grid2* in *wt* (b, c and d) was each highly reproducible, whereas in *apkci*$^{-/-}$ the pattern varied strongly between embryos within the same batch. Nevertheless expression of all three genes was present in *apkci* mutants at all tested developmental stages (3, 4 and 5 dpf), but in fewer cells compared to *wt* embryos. MHB - mid-hindbrain boundary, URL - upper rhombic lip; a, e) 20x; b-d), f-h) 40x objective, Zeiss Axioplan micrsoscope.

The proliferation marker *ptf1a* is expressed along the ventricular zone where Purkinje cells (PC) proliferate, just below the expression zone of *athoh1a* (URL), which is the proliferation zone of GCs (Wullimann et al. 2011). In wt embryos *ptf1a* was expressed along the ventricular zone of the hindbrain neuroepithelium and the cerebellar anlage, thereby displaying a trigonal shape (fig. 3.13 a). In *apkci*$^{-/-}$ embryos expression could be seen in a broad stripe along the midline in the hindbrain region, which was slightly divided in two parts at the anterior hindbrain region (fig. 3.13 e). Expression in the cerebellar primordium could be observed as well (fig. 3.13 e, arrow in small picture), indicating the presence of a ventricular proliferative zone for GABAergic neurons.
The expression of the three distinct differentiation marker genes for PCs, *carbonic anhydrase 8* (*ca8*) (Bae et al. 2009), *retinoid-related orphan receptor alpha* (*rora2*) and *glutamate receptor δ2* (*grid2*) (Mikami et al. 2004; Katsuyama et al. 2007) was analysed each at 3, 4 and 5 dpf. At all stages expression of these marker genes was visible in *wt* and *apkci* mutant embryos (fig. 3.13 b-d and f-h). Although a robust expression was visible, the number of cells displaying mRNA-expression was reduced in *apkci*$^{-/-}$ embryos compared to *wt*. The expression pattern in *wt* was continuous in a clearly restricted area and similar between embryos stained for the same marker gene, whereas in the mutants the pattern looked patchier and varied from embryo to embryo. But differentiation of PCs seemed not to be altered.

In addition to the *in situ*-hybridization, an antibody staining against Zebrin2 was performed. Zebrin2 is the protein encoded by the gene *aldolase C* (Ahn et al. 1994). Expression was robust in *apkci*$^{-/-}$ embryos at developmental stages 3, 4 and 5dpf, here exemplarily shown for 4 dpf (fig. 3.14 b), but again fewer cells were labelled compared to *wt*, as shown by the mRNA expression analysis above. However, the antibody staining clearly outlined the emanating axons to the vestibular nucleus comparable between *wt* and mutants (fig. 3.14 a, b, arrow). A double staining of PCs and GCs in *wt* and *apkci* mutant background of the *Tg(gata1:GFP)* line revealed the positioning of both cell types to each other within the cerebellum. During the development of wt embryos, PCs migrate from ventral to dorsal to the final Purkinje cell layer, and GCs *vice versa* from dorsal to more ventral regions to the inner granule cell layer in the medial corpus cerebelli. Consequently, in the end PCs reside dorsally to GCs ((Wullimann et al. 1996); fig. 3.14 c). This was also the case in *apkci* mutants (fig. 3.14 d, arrows), i.e. PCs migrated to dorsal regions above GCs.

In summary, PCs in mutants seemed to develop quite normal during the developmental stages investigated, and were thus no likely cause for the altered development of granule cells in *apkci* mutants.

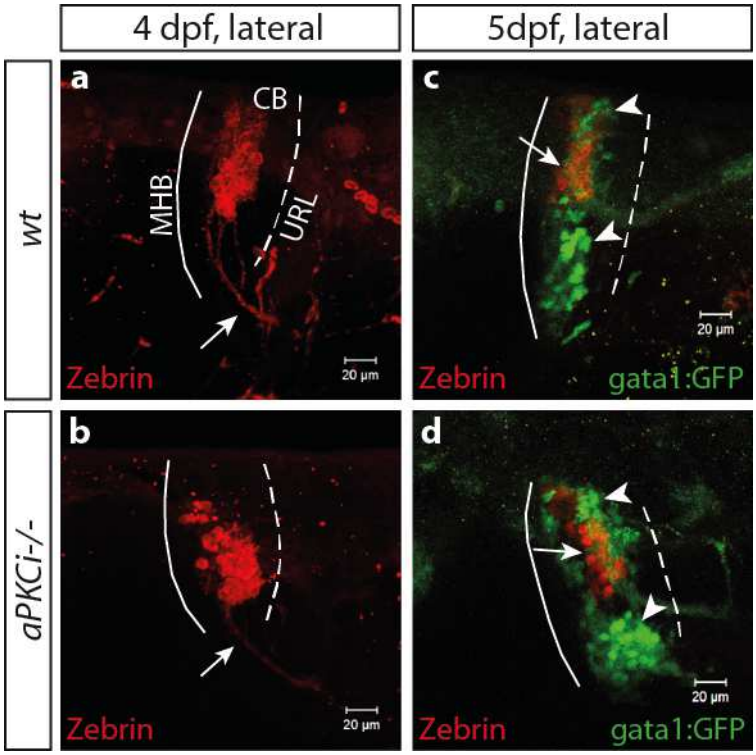

Figure 3.14: Expression of the PC specific marker protein Zebrin2
Lateral view of 4 and 5dpf old *wt*,*gata1:GFP* and *apkci*$^{-/-}$,*gata1:GFP* embryos subjected to an antibody staining against Zebrin2 and GFP. The expression pattern at 4 dpf was comparable between *wt* (a) and *apkci*$^{-/-}$ (b) and axons were emanating (a and b, arrows). A double staining of PCs (red, arrows) and GCs (green, arrowheads) revealed that their cell bodies were placed in the same relation comparing *wt* and *apkci*$^{-/-}$ (c and d). CB - cerebellum, MHB - mid-hindbrain boundary, URL - upper rhombic lip.

3.7 Migration of Granule Cells in the Cerebellum of *apkci* mutants

The major goal of this work was to address a potential role of apkci in regulating GC migration. For this reason, time-lapse recordings of embryos of the transgenic *gata1*:GFP strain in *wt* and *apkci* mutant background (s. chapter 3.5) were performed using confocal laser scanning microscopy, and subsequently single cells were manually tracked over time using ImageJ software (http://imagej.nih.gov/ij/). Cells were chosen randomly preferably nearer to the midline than to lateral regions (fig. 3.15 a, e; coloured dots), because of the stronger

phenotype expected based on the differentiation analysis (chapter 3.4) and the characterization of the *Tg(gata1:GFP)* line (chapter 3.5). Ahead of tracking, the movie was subjected to the plugin 'stackreg'. This plugin counterbalances the movement of recorded samples (caused by the living embryo), by comparing successive frames. Otherwise this movement would have sophisticated the results of cell tracking. Subsequently, cells were manually tracked using the plugin 'Manual tracking'. Finally, the software calculated the migrated distance between frames and the speed of migration and displayed the covered migratory paths (fig. 3.15 b, f). Tracking occurred over a time period of 17 hours. In total 26 cells in 4 *wt* embryos and 25 cells in 3 *apkci* mutants were tracked, and the total migrated distance and mean velocity in 17 hours were determined for each cell. The linear distance between start- and endpoint of migration was measured with the ImageJ software, too, using the 'set scale' and 'straight' tool. Figure 3.15 shows exemplarily for each phenotype the first and last frame of tracking, the resulting path and the mean values of the tracking. Exemplary movies can be viewed on the attached DVD.

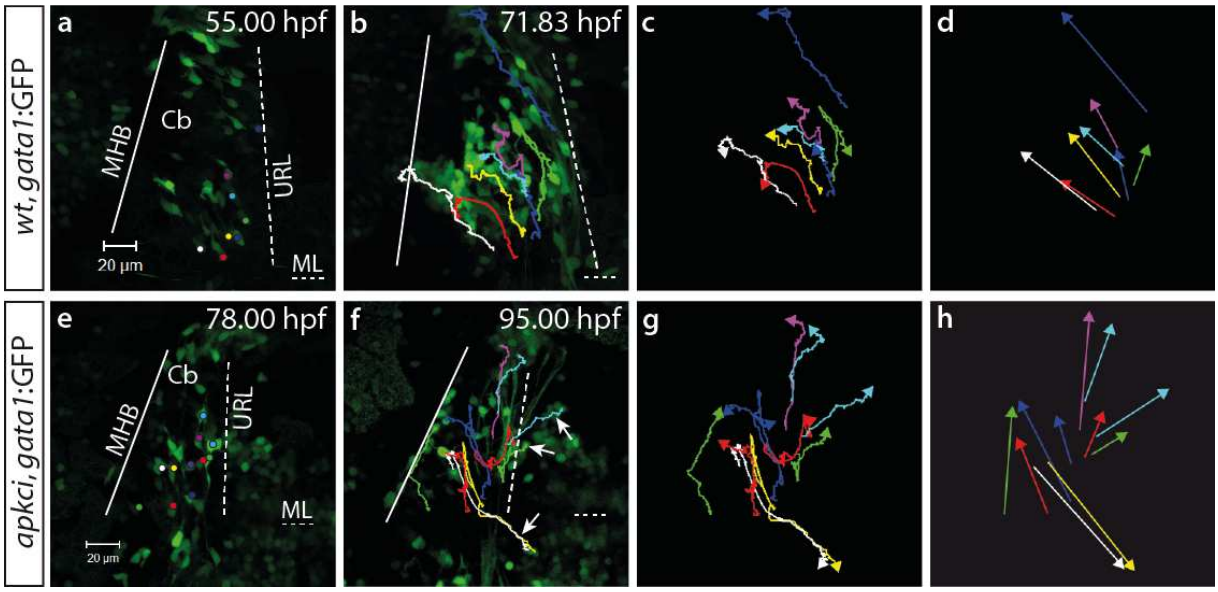

i)	total distance µm	start - end µm	Velocity µm/min
***wt* (n=26)**	468.31	35.79	0.46
***apkci* (n=25)**	510.45	36.36	0.51
ttest (*p*-value)	0.270	0.936	0.195

Figure 3.15: Time-lapse recordings of *tg(gata1:GFP)* in *wt* and *apkci* mutant background
a, b) Dorsal view of the cerebellum of a *wt,gata1:GFP* embryo, scale 20µm. a) Recording started at 55 hpf. b, c) Displaying the tracking of GCs revealed that they migrated predominantly towards the MHB and to the lateral cluster, without dramatic changes in direction. d) Thus migration of all cells is directed anterior and slightly lateral, besides cells contributing to the dorsoposterior cluster (green line). e, f) Dorsal view of the cerebellum of a *apkci,gata1:GFP* embryo. e) Because of the delayed start of migration compared to *wt* recording started at 78 hpf. f) Mostly GCs migrated to the MHB and

lateral clusters, but an increased number of cells often changed direction and even crossed the URL and emigrated to ectopic positions in the hindbrain (arrows). g) Thus the displayed migration paths were disordered and (h) pointed in all directions. See movies 1, 2, 3, 4 on attached DVD (movie legend at chapter 5.2). CB - cerebellum, MHB - mid-hindbrain boundary, URL - upper rhombic lip.

Recordings of *wt,gata1:GFP* embryos (movie 1) started around 55 hpf, when already several GCs expressed GFP (fig. 3.15 a). The tracing (shown exemplarily in movie 2) revealed that a cell of a *wt* embryo migrated in average 468.31 µm in 17 hours with a speed of 0.46µm/min. The average linear distance between start- and endpoint of the observed migration period was ~36 µm (for summary see fig. 3.15 i). The total migration distance seemed to be very long compared to the direct linear distance, but the granule cells always moved a little for and backward or to the side and back, even in the stationary phase of the saltatory migration mode of GCs. Because the tracking was done by clicking in the centre of the cell, instead of moving the cursor only at an actual migration step, these high values were reached.
In *apkci* mutants similar results were obtained by the manual tracking. On account of the later start of migration of GCs in the mutants, recordings were started one day later around 78 hpf (movie 3). The results of the tracing (movie 4) revealed a mean total migration distance of 510.45 µm in 17 hours with a velocity of 0.51 µm/min. The linear distance between start- and endpoint was also ~36 µm, similar to *wt*, while the total migration distance and speed were somewhat increased compared to wt.

However, observing the displayed migration paths (fig. 3.15 c, g), differences became obvious. In *wt* (fig. 3.15c; movie 2) cells migrated predominantly in a straight direction on one of the following described paths. Either a cell migrated to the MHB and the ventrolateral cluster (white and red track), or to the MHB and then to the lateral cluster (pink; recording was longer than tracking), or directly to the lateral cluster (blue), or the cell stayed at the URL in the dorsoposterior cluster (not shown). Sometimes a cell on the way to the MHB turned back to the URL and contributed in the end to the dorsoposterior cluster (green track). In the end all arrows, generated by connecting start- and endpoint, pointed to the MHB and slightly lateral away from the midline, besides the cells contributing to the dorsoposterior cluster (fig. 3.15 d).

In *apkci* mutants (fig. 3.15 g; movie 4) many cells migrated to the MHB (lower red track) and the lateral cluster (pink) as well. But more cells than in wt (observation by eye) turned on

their way back and forth, hence changing direction of migration and moving longer distances. Strikingly, some of the cells migrating backwards to the URL even crossed this apical tissue border and migrated into hindbrain regions to ectopic locations. This contributed to the above observed reduced number of GCs in the cerebellum of *apkci* mutants compared to *wt*. When emigrated granule cells came to a halt in the hindbrain, they rounded up and stayed there for the entire duration of the time lapse recording. Because of this disordered migration the vectors pointed in all directions at the end of tracking (fig. 3.15 h). Another observation was that GCs seemed to lose contact to each other during migration more often than in wt, and suddenly migrated in opposite directions.

In summary, migration of GCs in *apkci* mutants was not hindered regarding motility and velocity. However, keeping direction of migration was impaired and some cells even migrated to ectopic positions, penetrating the border between separated brain compartments.

3.8 GCs might escape through gaps appearing in the apical border between cerebellum and hindbrain in *apkci* mutants

Discovering the escaping cells, the question raised how it was possible that cells leave the cerebellum, thereby crossing the border between two tissues. Grant and Moens (Grant and Moens 2010) demonstrated, that migrating facial branchiomotor neurons in the zebrafish hindbrain can escape through gaps in the basal lamina, which appear in *apkc-iota+zeta* double morphants but not in *wt*. In accordance to this, we investigated the appearance of the apical border in *apkci* mutants compared to *wt*. To achieve this, an antibody staining against ZO-1 (zonula occludens-1) was performed. ZO-1 is a marker for the apical residing tight junctions in epithelia tissues (Stevenson et al. 1986) and hence suitable to outline the apical border of the cerebellum and its integrity (fig. 3.16 a, c, e).

At 24 hpf ZO-1 was located along the open ventricles in both, *wt* and *apkci*$^{-/-}$ embryos and no disruption in the URL was visible (fig. 3.16 a, b). Starting from 48 hpf (not shown), when the ventricles are closing again, holes appeared in the apical border of the mutants, whereas it remained a continuous line between cerebellum and hindbrain in *wt*. At 3 and 4 dpf even large gaps were visible in the URL of *apkci*$^{-/-}$ embryos (fig. 3.16 d and f, arrows). These gaps are most likely generated through the incomplete opening of the ventricle. Therefore no clear separation of the cerebellum and the hindbrain arises over large areas and cerebellar GCs can easily emigrate into the adjacent hindbrain.

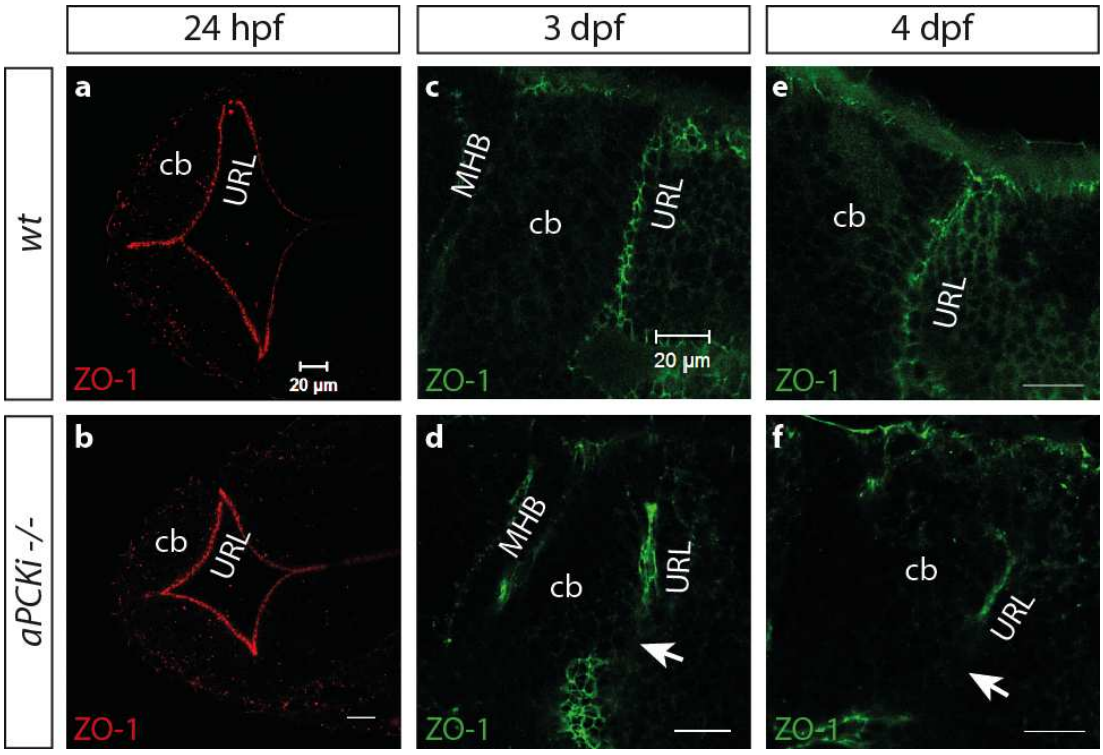

Figure 3.16: Outline of apical borders visualized by an antibody staining against ZO-1.
Dorsal view of zebrafish embryos subjected to an antibody staining against ZO-1. At 24 hpf the 4th ventricle is clearly outlined in a continuous line in *wt* (a) and *apkci* mutants (b). At later stages the URL stayed a continuous border between cb and hb in *wt* embryos (c and e), whereas is *apkci* mutants gaps were visible (d and f, arrows) and the ZO-1 staining pattern looked more patchy.
CB - cerebellum, MHB - mid-hindbrain boundary, URL - upper rhombic lip. Scale a-f: 20µm.

3.9 The role of aPKCi in Direct Migration of Granule Cells

3.9.1 Test of the mutated protein aPKCi2A for usage as a dominant negative inhibitor to intrinsic aPKCi

To address whether aPKCi acts cell autonomously regarding migration, aPKCi should be inactivated in individual cells. To achieve this, a mutated version of aPKCi, called aPKCi2A, was generated by site directed mutagenesis and a primer pair according to Rohr et al. (Rohr et al. 2006) (s. 2.2.4.4), who showed that embryos injected with *apkci2A* mRNA resembled the phenotype of *apkci* mutants. Subdomain VIII of the protein kinases plays an important role in recognition of peptide substrates, of which the highly conserved Ala-Pro-Glu ('APE') motif faces the cleft (Hanks and Hunter 1995). Therefore the APE motif was changed to Ala-Ala-Ala ('AAA') by the mutagenesis approach. To test the functionality of aPKCi2A in the cerebellum, injections of *apkci2A* mRNA were performed. The resulting phenotype within the first 24 hours copied convincingly the phenotype of *apkci* mutants (s. fig. 3.17, compare to

fig.Figure 1.10). In *apkci2A* mRNA injected embryos the 4th ventricle was only opening at interval regions along the midline and not as a whole compared to *wt* (fig. 3.17 a', b', arrowhead). Also, unlike in *wt*, the retinal pigment epithelium was not completely pigmented (fig. 3.17 a', b', arrow) and an oedema was formed at the heart region in injected embryos (fig. 3.17 a', b', asterisk).

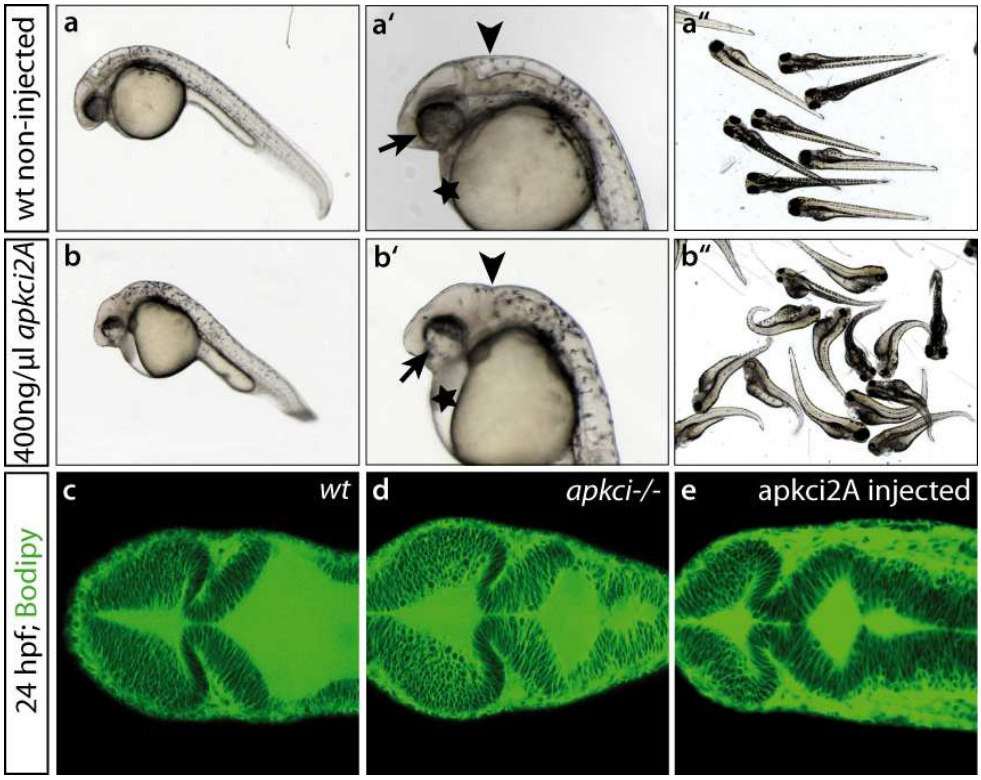

Figure 3.17: aPKCi2A mRNA injection resembles the phenotype of *apkci* mutants
Comparison of non-injected (a-a'') and *apkci2A*-mRNA injected (b-b'') wt embryos. Injection occurred in the one-cell stage and images were taken 24 h later. b') Injection of *apkci2A*-mRNA led to a reduced inflation of the hindbrain ventricle (arrowhead), an incomplete pigmentation of the retinal pigment epithelium (arrow) and heart oedema (asterisk). c-e) A dorsal view of Bodipy ceramide staining visualized the similar defects in ventricle inflation caused by *apkci2A*-mRNA injection (e) or non-functional aPKCi in the mutants (d) compared to wt (c).

A staining with Bodipy ceramide clearly outlined defects in midline separation and ventricle inflation comparable to *apkci* mutants (s. fig. 3.17 c-e). Injections of GFP encoding mRNA, which were performed as a control, did not resemble the phenotype (not shown). This suggested that aPKCi2A indeed functions as a dominant-negative version to aPKCi. However, a final proof would require the injection of both *apkci2A* mRNA and *wt apkci* mRNA together and to observe, if the phenotype is rescued.

3.9.2 aPKCi does probably not act cell-autonomous in directed cell migration

The advantage of electroporation compared to injections at the single cell stage of the embryo is, that cells can be manipulated in a mosaic manner at a selected time point of choice. This allows temporal control over the start of interference of developmental processes within the embryo. In consequence, the embryo develops normally until the time-point of electroporation. ´

In order to manipulate only GCs a transgenic line was used, which expresses the yeast transcriptional activator Gal4 and a fluorescence reporter (UAS:mCherry) under control of the GC specific zic4 promotor (*Tg(zic4:Gal4, UAS:mCherry)*). In combination, the electroporated plasmids (fig. 3.18) contained the Gal4 dependent UAS (Upstream Activating Sequence) domain in front of the transgene (*apkci* or *apkci2A*). To be able to follow electroporated cells, the injected plasmids co-expressed the fluorescent reporter Venus fused to *unc-76* localizing to the cell membrane and the cytoplasm, but being excluded from the nucleus (Dynes and Ngai 1998). The gene of interest and the reporter were under control of the same 4xUAS and spaced by a T2A sequence. During translation of the mRNA-transcript into a peptide, the T2A domain leads to a break between the reporter (UncVenus) and the transgene (aPCKi or aPKCi2A). Therefore both proteins are expressed in a stoichiometric ratio. A strong fluorescence thus indicates strong transgene expression.

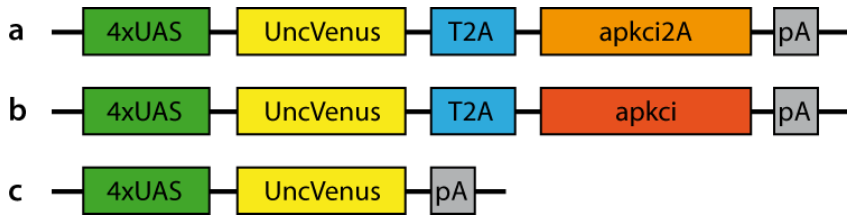

Figure 3.18: Gal4 dependent Electroporation Vectors
a-c) The expression vectors contained a 4xUAS Gal4 recognition site and coding region for the reporter protein UncVenus. a) contained the mutant variant aPKCi2A to block cell intrinsic aPKC function and b) the wt version aPKC for overexpression experiments; c) was used as a control.

Injection of the plasmid into the hindbrain ventricle and electroporation were performed in *wt* embryos around 36 hpf ahead of the start of migration of GCs, which takes place at 48 hpf. Therefore, early neuronal development would not be affected by influencing aPKCi function. 4xUAS:UncVenus-T2A-aPKCi2A would block intrinsic aPKCi function and single altered cells could be followed in a *wt* environment. In contrast 4xUAS:UncVenus-T2A-aPKCi

electroporated into *apkci*$^{-/-}$ embryos would lead to single cells expressing aPKCi in an otherwise mutant background. As a control experiment a plasmid only containing 4xUAS:UncVenus was used.

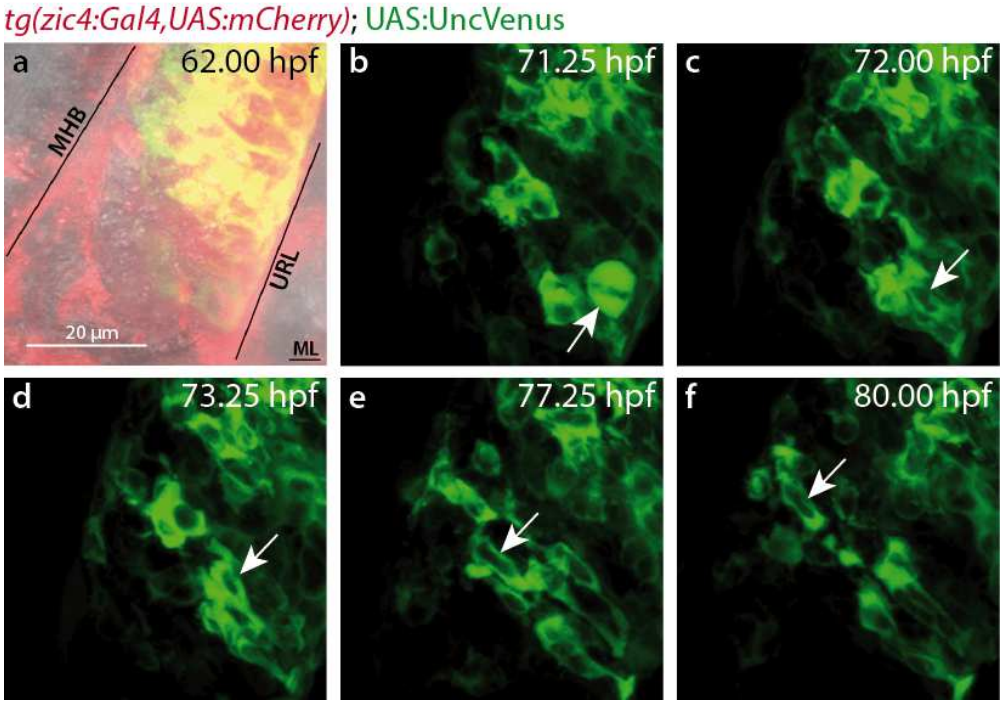

Figure 3.19: Electroporation of 4xUAS:UncVenus in *Tg(zic4:Gal4,UAS:mCherry)*
Time lapse recording of a dorsal view of a part of the cerebellum of *Tg(zic4:Gal4,UAS:mCherry)* embryos electroporated with *4xUAS:UncVenus*. Cells expressing the plasmid appear yellow (a). GC behavior is shown exemplary for one cell (arrows). A GC precursor was dividing (b, arrow) and afterwards both daughter GCs were migrating towards the MHB, here visible for one cell (c-f, arrows), in a saltatory motion (supplementary movie 5).
Hpf – hours post fertilization, MHB – mid-hindbrain boundary, URL – upper rhombic lip.

Time-lapse recordings by confocal laser scanning microscopy of the control experiment revealed that granule cells expressing only the reporter UncVenus (fig. 3.19 a (yellow), b-f (green)) in wt background showed similar behaviour as observed in the transgenic line *Tg(gata1:GFP)*. At the dorsal view of the cerebellum of electroporated embryos one could observe that GCs were dividing (fig. 3.19 b, arrow) and differentiated neurons detached from the URL and migrated towards the MHB (fig. 3.19 c-f, arrows) or into lateral clusters (not shown). Many cells stayed stationary in one place or often moved only for and backwards, still attached to the URL (supplementary movie 5).

A similar result regarding division (fig. 3.20 b-d) and migration of GCs (fig. 3.20 e-f) was observed for the electroporation with the mutant variant aPKCi2A into wt background. GCs expressing aPKCi2A exhibited the same mode of elongation and rounding up of saltatory

migration steps and extended and retracted protrusions (supplementary movie 6). A similar ratio between moving and stationary cells was observed by eye compared with the electroporation of the control plasmid. This indicated that aPKCi had no cell-autonomous function in directed cell migration.

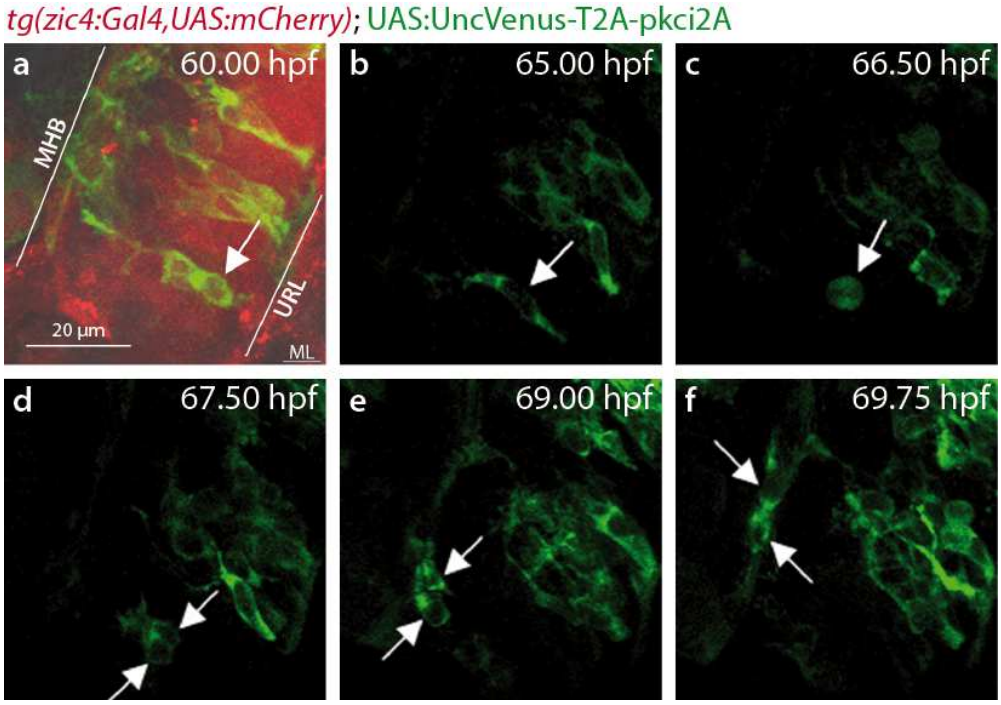

Figure 3.20: Electroporation of 4xUAS:UncVenus-T2A-apkci2A in *Tg(zic4:Gal4,UAS:mCherry)*
Time lapse recording of a dorsal view of a part of the cerebellum of *Tg(zic4:Gal4,UAS:mCherry)* embryos electroporated with *4xUAS:UncVenus-T2A-apkci2A*. Cells expressing the plasmid appear yellow (a). GC behavior is shown exemplary for two cells (arrows). A GC precursor was dividing (a-b, arrow) and afterwards both daughter cells were migrating towards the MHB (d-f, arrows), in a saltatory motion (supplementary movie 6). Hpf – hours post fertilization, MHB – mid-hindbrain boundary, URL – upper rhombic lip.

Furthermore, a few injections of wt *apkci* in mutants were tried. Preliminary results varied strongly from embryo to embryo. Either most labelled cells were rounded up or were long stretched and connected by protrusions to both, URL and MHB. Cells were predominantly completely stationary, but in two recordings a cell, weakly labelled, migrated into the lateral cluster.

In summary these results suggest, that apkci is probably not necessary cell autonomously for granule cell migration, but rather in a tissue autonomous manner. The phenotype observed with the *Tg(gata1:GFP)* strain in *apkci* mutant background (s. 3.7), i.e. GCs often changing direction and migration to ectopic positions, would then be caused by lost tissue integrity.

4 Discussion

4.1 Morphology of wt and mutant cerebella

With this work we showed that the development of the cerebellum in *apkci* and *nok* mutants is severely altered. Because the hindbrain ventricle did not inflate properly and the midline was not separating completely, a reduced rotation of the cerebellar primordium was the result and no clear boundary between cb and hb arose. The polarity proteins MPP5 (Nok) and aPKCi play an important role in specifying epithelial apico-basal polarity (for review see Margolis and Borg 2005; Suzuki and Ohno 2006; Assémat et al. 2008). This polarity is necessary to set up the midline of the neural tube, which is subsequently necessary for a clear midline separation during ventricle inflation (Lowery and Sive 2005; Lowery et al. 2009). It was shown by Lowery et al. (2005), that in the rhombencephalon of *nok* mutants nuclear positioning is disorganized, and staining with junctional markers revealed no continuous midline, which might explain the failure in midline separation. In *apkci* mutants a continuous midline was present but still separation was impaired (this work and Lowery et al. 2009). At a small area including rhombomere 1 and 2 a small 4th ventricle opened, but the midline stayed fused at several points. In contrast the 4th ventricle in *wt* opened wide along the hindbrain. The weaker phenotype of *apkci* mutants compared to *nok* is likely explainable by the isoform aPKCζ, which probably compensated to some extent for the lost aPKCi function, because both isoforms have partially redundant functions, at least shown for retinogenesis in zebrafish (Cui et al. 2007).

However, although initially junctions are formed in *apkci* mutant zebrafish embryos, it was observed that apical junctions get progressively lost in the retina and also neural tube starting from 2 dpf (Horne-Badovinac et al. 2001). This could explain the inability to establish a clear apical boundary between the cerebellum and the hindbrain upon ventricle closure observed in the *apcki* mutants. In *wt* this boundary became evident around 3dpf. In *nok* mutants hardly any midline separation occurred, and therefore no morphological boundary between cb and hb, normally visible by cellular membrane staining, could arise.

Another observation by the performed Bodipy Ceramide staining was the reduced brain size in the mutants compared to *wt*. Measurements at 4 dpf revealed that the lateral expansion of the cerebellum in the mutants was significantly smaller, which could also be explained by the

reduced ventricle inflation and subsequent no or only minor rotation of the cerebellar anlage from an anterior-posterior to a medio-lateral orientation. That the cerebellum of *mpp5* mutants was in tendency smaller than that of *apkci* mutants favoured this argumentation, because ventricle inflation was most severely impaired in *nok* mutants.

Remarkably, although the re-orientation of the cerebellar primordium was affected and apico-basal polarity was absent (*nok*) or got successively lost (*apkci*) in the mutants, some typical cerebellar tissue organization was recognizable at later differentiation stages. A molecular layer was detectable (although it was patchy and never reached the expansion compared to *wt*) and parallel fibres of GCs emanated and formed a dorsal commissure, although less pronounced than in wt. A double staining of GCs and PCs confirmed the impression of principal cerebellar tissue organization in *apkci* mutants, because those cell types were located correctly with respect to each other.

4.2 Expression profile of *nok* and *apkci* in the cerebellum

GC development in *wt* zebrafish has been already well characterized by our group (Volkmann et al. 2008). GCs have to migrate long distances from their place of origin to their final position within the brain network. For this directed migration GCs likely require to establish a polarity with a leading and trailing process. Thus, GCs are well suited to investigate a possible role of aPKCi and MPP5 in neuronal migration. But first, the expression of both proteins within GCs had to be confirmed.

In situ-hybridization and antibody staining in 1-3 dpf *wt* embryos showed that *nok* was localized at the URL of the cerebellum. Expression within the cerebellum was not apparent. Contrary aPKCi not only localized along the URL, but was distributed throughout the cerebellum and the whole brain. This is consistent with other research studies, which suggest a role for MPP5 only in apcio-basal polarity by localizing the apical complex to tight junctions, whereas aPKCi is a highly conserved polarity protein throughout *C. elegans*, *D. melanogaster* and vertebrates (Henrique and Schweisguth 2003; Macara 2004) and is involved in different mechanisms in which polarity plays an important role, for example cell migration or proliferation (Hurd et al. 2003; Margolis and Borg 2005; Suzuki and Ohno 2006; Assémat et al. 2008).

In order to dissect whether aPKCi is expressed in GCs an antibody staining against aPKCi was conducted. Indeed, with the used aPKCi antibody a signal within GCs was observed.

However, later analysis of the epitope sequence revealed that the obtained signal could not be stated as specific aPKCi expression with certainty. The antibody used was raised against the C-terminus of the aPKCi protein, which is, however, highly similar to the C-terminus of aPKCζ. This made it likely that both aPKC isoforms were detected. A request to BD laboratories revealed that they have not tested the specific binding so far.

Nevertheless, it is very likely that the isoform *apkci* is expressed throughout the brain, and therefore within GCs, based on the whole-mount *in situ*-hybridization with an *apkci* ribo-probe. To obtain a better idea of the possible different distribution of *apkci* and *apkcζ* expression one should perform an *in situ*-hybridization with an *apkcζ* antisense riboprobe and compare the result with the expression pattern of *apkci*. Further, the western blot to test the ability of the aPKCi and aPKCλ antibodies to detect zebrafish aPKCζ should be repeated. First trials did not work, only unspecific signals were obtained with both antibodies. Meanwhile antibodies against the N-terminus or the middle region of aPKCi are available and should be tested in zebrafish, because the N-terminus is more divergent from aPKCi to aPKCζ and should guarantee more specificity. These experiments are necessary in order to clarify if aPKCi and aPKCζ could have potentially a functional redundancy also in the cerebellum, like it was shown for zebrafish eye development (Cui et al. 2007), in order to be able to better interpret functional studies in the cerebellum.

4.3 Granule cell development

To investigate cerebellar GC differentiation in *apkci*$^{-/-}$ and *nok*$^{-/-}$ embryos, the onset and pattern of distinct genes, expressed successively during GC maturation (Volkmann et al. 2008), was analysed by *in situ*-hybridization.

In *nok*$^{-/-}$ embryos, expression of all addressed genes was present ranging from *atonal homolog 1a* (*atoh1a*), that is expressed in progenitor cells of the URL, to the terminal differentiation marker *gaba$_A$ receptor α6 subunit* (*gaba$_A$ Rα6*) of GCs, the latter indicating the formation of synapses with GABAergic neurons like PCs. A difference between *nok*$^{-/-}$ and *wt* embryos was the extent of expression of these genes. Especially the expression of the late differentiation markers *vesicular glutamate receptor 1* (*vglut1*) and *gaba$_A$ Rα6* at 4 and 5 dpf, respectively, revealed fewer cells expressing these genes in *nok* mutants, leading to a patchy pattern compared to area-wide expression in *wt* embryos. This suggested problems in terminal differentiation and / or an increased rate of cell death in GCs that lacked functional MPP5.

In *apkci*$^{-/-}$ embryos only the expression level of *athoh1*a and *neuroD* were comparable with *wt*, however the pattern was aberrant. *Atoh1a* expression depicted the missing ventricle inflation, which was also the case for *nok* mutants. Instead of lining the trigonal shape of the 4th ventricle as in wt, the expression in the mutants was apparent in one broad stripe-like domain along the dorsal midline. Remarkably, in *apkci*$^{-/-}$ embryos expression of *vglut1* was only observed in ventro-lateral regions and not in the dorso-medial part of the cerebellum; and expression of *gaba$_A$ Rα6* was not visible at all in the cerebellum, indicating either massive GC death, failure in or delayed onset of terminal differentiation. Subsequent expression analysis of *vglut1*at developmental stage 5 and 6 dpf excluded the possibility of later onset of expression, because in both stages expression was not observed in the dorso-medial part of the cerebellum and development is only delayed by one day in the mutants. In contrast the expression of the postmitotic marker gene *neuroD* was robust throughout all stages. However this does not exclude the possibility of cell death, as new GC are generated until the juvenile stage and could constantly replenish the pool of *neuroD* expressing cells. The vast majority of GCs in *wt* zebrafish migrates between 48 hpf and 3-4 dpf (Volkmann et al. 2008) and the broad expression domain of *neuroD* observed at 5 dpf in *apkci* mutants could also represent this peak of migrating GCs, if the delayed development of one day in the mutants is taken into account. Nevertheless the number of cells expressing *neuroD* in *wt* was never reached in the mutants. Taken together, the reduced number of cells expressing the marker genes and the missing expression of *vglut1* and *gaba$_A$ Rα6* indicated less cell proliferation and increased cell death. In addition a failure in terminal differentiation of GCs and therefore a failure in reaching a neurotransmitter identity were apparent.

Atypical PKCs and other apical located proteins are thought to play a role in early determination, during progenitor division. Dependent on the distribution of apical proteins the descendant becomes a neuronal cell or stays mitotically active (Alexandre et al. 2010; Willardsen and Link 2011). However nothing is reported of aPKC playing a role in later differentiation so far. But considering that aPKC is able to translocate to the nucleus (Perander et al. 2001; White et al. 2002) a role in differentiation might be possible.

4.4 Possible mechanisms leading to a reduced GC number

A reduced GC number became also obvious by analysing GC development with help of the transgenic strain *Tg(gata1:GFP)*. In this line GFP is only expressed in GCs in the cerebellum

and using this line it was demonstrated that GCs migrate into three distinct clusters, which can be recognized easily (Volkmann et al. 2008). Carriers of the mutant *apkci* or *nok* allele were crossed with fish of the *Tg(gata1:GFP)* line. Subsequently, GFP positive embryos with a homozygous mutant background were analysed at different developmental stages ranging from 3-5 dpf. It turned out that GC number and final positioning especially in the medial clusters were severely altered in both mutants. In embryos displaying a strong mutant phenotype, clusters were scarcely recognizable, which was a first hint of impaired directed GC migration. In embryos with a milder phenotype GCs mainly migrated into the described three clusters, but these were clearly reduced in size. These observations further strengthened the notion that GC cell death was probably increased and proliferation of GC progenitors decreased. Because of the stronger impairment in differentiation of GCs in *apkci* compared to *nok* mutants, and because of the most likely expression of *apkci* in migrating granule cells, further research was focussed on *apkci*$^{-/-}$ embryos.

4.4.1 Cell death is increased in the cerebellum of *apkci*$^{-/-}$ embryos

The findings of a reduced GC number and a smaller cerebellar size in *apkci* mutants compared to wt, led to investigation of cell death. Acridine Orange staining revealed increased rate of cell death from 48 hpf onwards in the cerebellum of *apkci* mutants compared to wt embryos. Because embryos die latest at 6 dpf, it was not surprising to find increased cell death. We rather expected an even higher number of dying cells at 5 dpf in *apkci*$^{-/-}$ embryos compared to *wt* than observed, because of the daily increasing maimed appearance of mutant embryos. One explanation could be that apoptotic cells are recognized quickly and removed efficiently by microglia through phagocytosis (Kettenmann 2007; Peri and Nüsslein-Volhard 2008).

Although the staining did not selectively mark GCs, it was likely that GCs were affected, as dying cells were equally distributed throughout the cerebellum. To overcome the problem that GC death could not be evaluated selectively we tried to use AnnexinV Cy5, another marker for cell death with an emission range in the far red. Unfortunately, several trials with different conditions gave no recordable signal so far.

In this context it is interesting to mention that aPKCi seems to be involved in apoptosis and also promotes tumour development (Fields et al. 2007; Kim et al. 2007). A research study showed that Par6, aPKC and GSK-3ß regulate cell death in a 3D model of epithelial

morphogenesis of MDCK cells. In this system inhibition of aPKC promotes cell death (Kim et al. 2007). This, besides many other effects of dysfunctional aPKCi and the involved pathways, could be one explanation for the early cell death of mutant embryos. Further, overexpression of aPKCi promotes tumour progression in many tissues including the brain, because aPKCi activates multiple signalling pathways that confer resistance to apoptosis induced for example by carcinogens and chemotherapeutic agents, and therefore promotes cell survival (Murray et al. 2011). In turn disruption of aPKCi expression blocks multiple aspects of abnormal tissue growth in human *in vitro* models and in nude mice (Fields et al. 2007), further supporting a regulatory role for aPKCi in cell death.

4.4.2 Cell proliferation is decreased in the cerebellum of *apkci*$^{-/-}$ embryos

With respect to the observation that cell death was less increased than expected, based on the malformations of mutant embryos, we looked for further explanation for the reduced GC number. As a logic following step, cell proliferation was investigated next. A reduced number of GCs became obvious earliest around 3 dpf, when the vast majority of GCs are born.

To analyse cell proliferation an immuno-staining against Phospho-Histone H3 (pH3), a marker for late G2/M-phase of the cell cycle (Hendzel et al. 1997), and against the S-phase marker Proliferating-Cell-Nuclear-Antigen (PCNA) (Celis and Celis 1985) was conducted. The number of proliferating cells marked by pH3 was counted. The rate of proliferating cells decreased constantly from 48 hpf until 4 dpf significantly in *apkci* mutant compared to wt. This is the time span, when GC proliferation in *wt* reaches its peak. To selectively count GC precursors (GCPs) this experiment should be repeated in the transgenic line *Tg(gata1:GFP)*. Nevertheless, comparable with the Acridine Orange staining the equally distributed reduction of proliferating cells in wt and mutant embryos and the fact that GCs are the most numerous neurons, which are generated during the time period investigated, lead to the conclusion that it was most likely that GCPs were affected by decreased proliferation. Taken together increased cell death and decreased cell proliferation explained the reduced occurrence of GC and the smaller size of the cerebellum in the mutants.

Another aspect to explain a reduced GC number could be alterations in the division mode of precursor cells. It was shown for zebrafish that neurogenesis in the retina of aPKCi mutants was initiated normally, but subsequently the proportion of progenitor cells that divide neurogenically was significantly reduced, instead more proliferative progenitors were

segregated (Baye and Link, 2007). Further it was demonstrated, that cell fate decision of apical epithelial progenitors is, amongst others, dependent on the distribution and localization of polarity proteins during division (Alexandre et al. 2010; Willardsen and Link, 2011). Lost aPKCi function could lead to aberrant localization of further apical polarity proteins, and therefore contribute to a shift in the modes of progenitor division. A shift towards more proliferative progenitor segregation could explain a reduced number of GCs in the cerebellum of *apkci*$^{-/-}$ embryos. However, the strong level of *neuroD* expression observed at 3 dpf in *apkci* mutants implies a high number of postmitotic URL descendants, i.e. postmitotic GCs.

The pH3 counting demonstrated a rather normal proliferation rate around 24 hpf, when tegmental hindbrain nuclei neurons are born. But at 48 hpf proliferation was decreased when GC proliferation occurs. A study in *Drosophila* stated that neuroblasts (progenitors of *Dros.* neuronal cells) exit cell cycle earlier in embryos mutant for aPKC and also in larval eye imaginal discs (Rolls et al. 2003). An early cell cycle exit consequently leads to fewer cells proliferating. This explanation would fit better with our observation in the zebrafish cerebellum of an initially normal proliferation rate followed by a progressive reduction of cells proliferating, than the above mentioned possibly altered division mode.

4.4.3 Basic tissue organization is reached in *apkci* mutants

The areas of proliferation were similar between wt and *apkci* mutants, especially obvious at early stages (24-48 hpf). This was interesting because it further supported the impression of correct tissue architecture although an apical polarization factor was missing and brain morphogenesis was impaired by reduced ventricle inflation. But, as already mentioned, aPKCζ could likely compensate to some extent for the non-functional aPKCi in the early embryo. In addition, the initial formation of tight junctions and their only progressive loss would support the establishment of early tissue polarity and therefore allow at least partial cerebellar organization.

Further, the staining with the proliferation markers was interesting in regard of the on-going discussion whether an EGL does exist (Wullimann et al. 2011) in zebrafish or not (Chaplin et al. 2010). In mammals GCPs form a transient external granule cell layer (EGL), which spans the whole surface of the cerebellum. The EGL is unique relating to the fact that progenitor cells stay mitotically active after leaving the apical proliferation zone (Chédotal, 2010). The PCNA labelling together with the pH3 staining which was conducted in this work indicated a transient EGL in wt zebrafish. PCNA expressing cells spanned the whole surface of the

cerebellum and also pH3 staining aside the URL was observed. This is similar in *apkci* mutants, but because of the delayed development by one day, the EGL is still visible at 3 dpf. And again the observed similarities between wt and *apkci*$^{-/-}$ embryos demonstrated that correct organization of cerebellar tissue is partly achieved in the mutants.

4.4.4 Purkinje Cells develop rather normal in *apkci* mutants

The final maturation of neurons depends on synaptic contact with their afferents and efferents. For example, when *ptf1a* derived cells like PCs are completely missing in the brain of mice, a massive cell death of glutamatergic cells is the consequence, due to lack of synaptic connections (Hoshino et al. 2005). Furthermore, proliferation of GC progenitors in mammals is crucially dependent on Sonic hedgehog (Shh) released by PCs. The primary cilium of GCPs (found on mostly all eukaryotic cells) is necessary for recognizing Shh, which subsequently induces proliferation (Spassky et al. 2008). *Shh* expression was also confirmed in zebrafish (Babaryka, 2009; Wullimann et al. 2011). Therefore, it was necessary to exclude the possibility that the main interaction partner of GCs, the Purkinje cells, were severely altered and hindered GC development.

As a first step *in situ*-hybridizations with distinct genes expressed in PCs during different stages of their development were conducted. The signal obtained with a riboprobe of *ptf1a,* which is expressed in ventricular zone progenitors, was prominent in *apkci*$^{-/-}$ embryos comparable in strength to the signal in *wt* embryos. The pattern was divergent, though, as the ventricle did not inflate to its full extent in the mutants, leading to a broad stripe of expression instead of the trigonal shape like observed in *wt*. The expression of *grid2, rora2* and *ca8* was apparent in *apkci*$^{-/-}$ embryos throughout 3-5 dpf, demonstrating differentiation of PCs, but the number of cells expressing these genes was reduced. The expression of the glutamate receptor (grid2) is an indicator that a neurotransmitter identity is reached and therefore PCs develop normal in *apkci*$^{-/-}$ embryos, despite deviance in total number of cells and slight pattern divergence compared to wt. In addition, a double staining of PCs and GCs revealed that PCs migrated to correct positions with respect to GCs, meaning PCs resided dorsal to GCs in the medial corpus cerebelli. Gross localization is reached, but is nevertheless not totally correct and might impair interaction between GCs and PCs.

To rule out impairment by missing synaptic contact one could investigate the molecular layer, formed by dendritic trees of PC and parallel fibres of GCs more closely. For example by

applying synaptic and PC marker on *wt;gata1:GFP* and *apkci;gata1:GFP* embryos and subject them to high resolution imaging.

In summary, the observed lower number of GCs is caused by increased cell death and a reduced rate of cell proliferation, the latter probably caused by an earlier cell cycle exit of neuronal progenitor cells. Embedded into the context of published literature this suggests a cell-autonomous function for aPKCi in cell survival signalling.

4.5 Migration of Granule Cells

In *wt* embryos GCs follow straight paths during migration, mostly without changing direction. GCs migrate from the URL towards the MHB or in ventro-lateral regions of the cerebellum (Volkmann et al. 2008, this work). In contrast, migration of GCs in *apkci*$^{-/-}$ embryos was rather disorganized. Migrating cells often changed direction, especially when they lost contact to other cells. Motility itself was therefore not altered by GCs missing functional aPKCi, but migration in a directional manner was scarcely occurring. Still, the speed and total migration distance were even slightly increased in the mutants, the latter reflecting probably the increased changing of direction of GCs in *apkci* mutants. Migration into the lateral cluster was hardly affected or less affected than in medial cerebellar regions. Cells contributing to the lateral cluster migrated in a direct fashion, which was already indicated by the results of the differentiation analysis of GCs. In parachute mutants, GCs of the lateral cerebellar region were less affected as well. Parachute mutants possess a mutated version of Cadherin-2, which was shown to be important for cell-cell adhesion during GC chain migration (Rieger et al. 2009). It is, however, not clear why lateral migrating GCs are less impaired.

A role for aPKCi in cell orientation during migration was proposed by a study investigating neuronal precursors in the chicken cerebellum. The orientation of the tip of the leading process was inhibited and its branching aberrant, if a dominant-negative version of Par6 formed a defective complex with aPKC (Sakakibara and Horwitz, 2006), whereas the formation of the leading process was not altered. In our studies, elongation and therefore polarization and protrusion formation was observed as well. Hence, confused directional changes and migration to ectopic positions could have been caused by defective leading tip orientation.

4.6 GCs emigrate into hindbrain through holes in apical border

The most striking observation of the cell tracing in the gata:GFP line, was GCs migrating across the border from the cerebellum into the hindbrain, which never occurred in wt and indicates severe impairment in cerebellar tissue integrity. The Bodipy ceramide staining already outlined a disrupted cell alignment along the border between cerebellum and hindbrain. In addition, a recent research study reported holes in the basal lamina in double apkci/apkcζ morphant zebrafish embryos (Grant and Moens, 2010). Consequently we investigated the integrity of the URL in *apkci*$^{-/-}$ embryos. Therefore an immuno-staining against the apical located zonula occludens-1 (ZO-1), a tight junction marker, was performed. It became obvious that the URL was often not a continuous border in *apkci*$^{-/-}$ mutants. This partial loss of tissue integrity was likely caused by the early incomplete midline separation and probably also by the progressive loss of tight junctions in the neural tube of *apkci* mutant embryos observed by others (Horne-Badovinac et al. 2001; Lowery et al. 2009). This result provides a good explanation for the phenomena of escaping GCs. In order to confirm that GCs migrated through these holes, we tried to monitor GC during migration by microscopy and fixate the embryo when a GC would escape into the hindbrain. Finally a ZO-1 antibody staining would have been conducted. However, first trials in capturing a cell while escaping were not successful. Granule cells escape to rarely and at not defined time-points. Further GC emigrated rather fast and finally rounded up, making them indistinguishable from cells of the hindbrains expressing GFP as well. In the end, there was simply not enough time left within this thesis to observe GC migration in more embryos.

4.7 aPKCi in directed cell migration - cell autonomous?

Because of the observed migration phenotype in apkci mutants the question was raised whether aPKCi has a cell autonomous function in directed cell migration. To survey this possibility we wanted to manipulate only single cells in an otherwise wt environment. Therefore we electroporated a dominant negative version of aPKCi called aPKCi2A. Supposedly, both aPKC variants are blocked, because of partly the same interaction partners and substrates. The ‘APE’-motif in the catalytic centre of the kinase domain, which was mutated, is also conserved in aPKCζ. To proof that aPKCi2A blocks intrinsic aPKC function, mRNA coding for the dominant-negative version was injected into one-cell stage embryos. The obtained phenotype at 24 hpf resembled convincingly the phenotype of *apkci* mutant

embryos. To finally confirm the dominant-negative properties a rescue experiment should be conducted. That would mean to inject *apkci* mRNA with the same ratio as *apcki2A* mRNA and monitor if the phenotype is rescued.

It turned out however, that GCs expressing apkci2A behaved like *wt* GCs. Manipulated GCs proliferated, elongated, formed a leading process, migrated to the MHB and their final positions and retracted the leading process upon leaving the MHB. Therefore single cells or also cell clusters missing aPKC function can migrate normally in a *wt* environment, indicating that aPKCi does not have a cell autonomous function in regard to cell migration. However, that does not rule out the already mentioned possibility that aPKCi is involved in the orientation of the tip of the leading process, shown for cerebellar explants of chickens (Sakakibara and Horwitz, 2006), although both aPKC variants (aPKCi and aPKCζ) seemed to be inhibited like in our study. GCs in the early zebrafish cerebellum move along each other by collective cell migration without using glial fibres for guidance (Rieger et al. 2009). In our electroporation experiment, this coherent chain migration might have helped aPKCi deficient cells to migrate directionally along not affected *wt* cells. In turn this would mean that intrinsic leading tip orientation is not crucially important for directed cerebellar GC migration. Especially if one considers that the formation of the leading process per se was not altered by missing aPKC function in the chicken explants (Sakakibara and Horwitz, 2006) and judging from our experiments (personal observation).

These results demonstrate in addition, that electroporation is a good approach to examine functions of genes more stringently by choosing the time point of interference and thereby excluding some of the pleiotropic effects of a protein, for example roles in the early development of organs. This is one advantage over cell transplantation between embryos, which however has its own usefulness. Within this work, transplantation of cells of *apkci* mutant *gata1:GFP* embryos into wt embryos would have made certain, that only aPKCi function was missing, and not both aPKC variants. In addition, transplantation would have guaranteed a complete loss-of- function of aPKCi, whereas electroporation led to divergent expression rates between manipulated cells, judged by the expression of the reporter gene Unc:Venus. Thus, aPKCi function is not completely blocked for certain in electroporated cells. However, transplanted cells would lack aPKCi from the beginning, and it could be possible that other cell types in the surrounding of GCs were mutant for *apkci*. In contrast, by combining electroporation and the Gal4-system we certainly affected only one cell type and

excluded the possibility that other cell types were affected and hindered GC behaviour. But, with the electroporation approach we most likely blocked also aPKCζ. Still, in case of a gene broadly expressed in early development and necessary to establish polarity of early epithelial tissue, electroporation would be the better approach to examine developmental later gene functions for cell migration or differentiation. Considering above arguments it would be worth trying to find another dominant-negative aPKCi variant that does only block aPKCi and not aPKCζ function. This could be achieved by altering the N-terminal region of aPKCi. This region consists of binding domains for interaction partners, and differs more strongly from the corresponding aPKCζ sequence. The dominant-negative aPKCi2A used in this work was chosen because of its reported functionality and creating and testing other possible variants would not have been possible within the time schedule of this work.

Another interesting site aspect would be to look for differentiation of the electroporated cells. Terminal differentiation of GCs in *apkci*$^{-/-}$ embryos did not occur, which points to a cell-autonomous function of aPKCi. A study in the zebrafish eye suggests a cell-autonomous function of aPKCi for differentiation of retinal pigmented epithelial cells (Cui et al. 2007). But considering the strongly divergent results for the GC migration behaviour of mutant *apkci, gata1:GFP* embryos and the behaviour of electroporated cells in *wt* background, it could be possible that there is also a difference in the ability of GCs to differentiate in the two systems. That means that GCs lacking aPKCi function might differentiate in wt background. This could be investigated by *in situ*-hybridization with marker genes for GC differentiation, like it was performed in this work to analyse GC development in *mpp5* and *apkci* mutant embryos compared to *wt*.

In summary more experiments are needed to clarify whether the functions of aPKCi and MPP5 in cerebellar GC development are cell autonomous or not. If a gene affects so many developmental processes and is expressed in mostly all cells in many organs, it is not easy to investigate its role for one particular developmental aspect. Electroporation could be a good solution for such cases, but has to be carefully controlled for specificity in time, cell type and affected gene. Within this work, I optimized the conditions for electroporation and based on this, I further revealed that the cell type specific Gal4 expression in combination with UAS coding plasmids could be used for manipulating only cells of interest (see also Hoegler, 2011)

The first important observation of this work was impaired terminal differentiation of GCs in *apkci* mutants, but additional experiments must be conducted to elucidate to which extend this was caused by a lost cell-autonomous function of aPKCi.

The second important observation based on this work is, that aPKCi is not important for cell motility. It might however facilitate GC orientation during migration by orientating the leading tip and regulating the number of its protrusions formed (Sakakibara and Horwitz, 2006). In addition it might help migrating GCs to keep contact to neighbouring migrating cells to allow chain migration. However, if aPKCi function was only suppressed in a mosaic manner, so that manipulated GCs migrated in an otherwise *wt* background, other factors seemed to compensate for missing aPKCi function during directed GC migration.

5 Appendix

5.1 Supplementary Figures

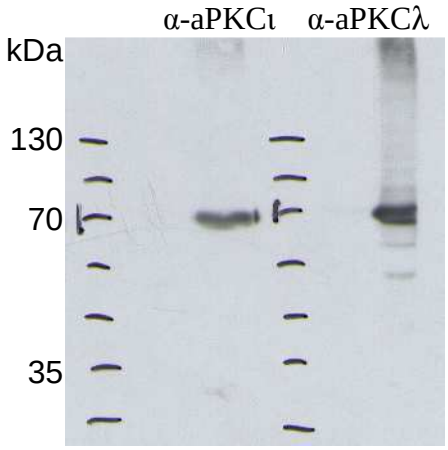

Figure 5.1: Western Blot Analysis to test cross-reactivity of the α-aPKCι and α-aPKCλ antibodies (BD #610175, #610207) with zebrafish aPKCi

```
1   ygmckeglrpgdttstfcgtpnyiapeilrgedygfsvdwwalgvlmfem 50     zf aPKCi
    |||||||||||||||||||||||||||||||||||||||||||||||||||
1   ygmckeglrpgdttstfcgtpnyiapeilrgedygfsvdwwalgvlmfem 50  human aPKCi

51  magrspfdivgssdnpdqntedylfqvilekqiriprslsvkaasvlkgf 100
    ||||||||||||||||||||||||||||||||||||||||||||||||.|
51  magrspfdivgssdnpdqntedylfqvilekqiriprslsvkaasvlksf 100

101 lnkeskerlgchpqtgfadimahpffrnvdwdlmeqkqvvppfkpnisge 150
    |||:.|||||||||||||||..||||||||||:||||||||||||||||
101 lnkdpkerlgchpqtgfadiqghpffrnvdwdmmeqkqvvppfkpnisge 150

151 fgldnfdaqftn 162
    |||||||:||||
151 fgldnfdsqftn 162
```

```
Gap_penalty: 10.0
Extend_penalty: 0.5
Identity: 155/162 (95.7%)
Similarity: 158/162 (97.5%)
Gaps: 0/162 ( 0.0%)
```

Figure 5.2: Comparison of the amico acid sequence of the zebrafish aPKCi and human aPKCi recognized by the tested α-aPKCι antibody.
Analysis was performed by using EMBOSS Needle (http://www.ebi.ac.uk/Tools/psa/emboss_needle/)
Zebrafish (zf) aPKCi: NP_571930.2
Human aPKCi: NP_002731.4

```
1   ygmckegirpgdttstfcgtpnyiapeilrgedygfsvdwwalgvlmfem 50     zf aPKCζ
    |||||||:||||||||||||||||||||||||||||||||||||||||||
1   ygmckeglrpgdttstfcgtpnyiapeilrgedygfsvdwwalgvlmfem 50  human aPKCi

51  magrspfdii--tdnpdmnteeylfqvilekpiriprslsvkaasvlkgf 98
    |||||||||:  :||||.|||:|||||||||.|||||||||||||||.|
51  magrspfdivgssdnpdqntedylfqvilekqiriprslsvkaasvlksf 100

99  lnkdpkerlgcqvqtgftdikshtffrsidwdqleqkqvtppfkpqitdd 148
    ||||||||||..||||.||:.|.|||::|||.:|||||.|||||.|:.:
101 lnkdpkerlgchpqtgfadiqghpffrnvdwdmmeqkqvvppfkpnisge 150

149 yglenfdtqftnep 162
    :||:|||:||||
151 fgldnfdsqftn—162
```

```
Gap_penalty: 10.0
Extend_penalty: 0.5
Identity: 135/164 (82.3%)
Similarity:148/164 (90.2%)
Gaps: 4/164 ( 2.4%)
```

Figure 5.3: Comparison of the amico acid sequence of the zebrafish aPKCζ and human aPKCi recognized by the tested α-aPKCι antibody
Analysis was performed by using EMBOSS Needle
Zebrafish aPKCζ: NP_001025262.1
human aPKCi: NP_002731.4

```
1   ygmckeglrpgdttstfcgtpnyiapeilrgedygfsvdwwalgvlmfem 50    zf aPKCi
    |||||||:||||||||||||||||||||||||||||||||||||||||||
1   ygmckegirpgdttstfcgtpnyiapeilrgedygfsvdwwalgvlmfem 50    zf aPKCζ

51  magrspfdivgssdnpdqntedylfqvilekqiriprslsvkaasvlkgf 100
    |||||||||:  :||||.|||:|||||||||.|||||||||||||||||
51  magrspfdii--tdnpdmnteeylfqvilekpiriprslsvkaasvlkgf 98

101 lnkeskerlgchpqtgfadimahpffrnvdwdlmeqkqvvppfkpnisge 150
    |||:.||||||..||||.||.:|.|||::|||.:|||||.|||||.|:.:
99  lnkdpkerlgcqvqtgftdikshtffrsidwdqleqkqvtppfkpqitdd 148

151 fgldnfdaqftn-- 162
    :||:|||.||||
149 yglenfdtqftnep 162
```

```
Gap_penalty: 10.0
Extend_penalty: 0.5
Identity: 134/164 (81.7%)
Similarity: 147/164 (89.6%)
Gaps: 4/164 ( 2.4%)
```

Figure 5.4: Comparison of the amico acid sequence of the zebrafish aPKCi and zebrafish aPKCζ recognized by the tested α-aPKCι antibody
Analysis was performed by using EMBOSS Needle
Zebrafish aPKCi: NP_571930.2
Zebrafish aPKCζ: NP_001025262.1

Danio rerio aPKCi (NP_571930.2)

```
  1 mptlrdstms hpgenphqvr vkayyrgdim ithfepsisy eglcnevrdm csmdndqlft
 61 mkwideegdp ctvssqlele ealrlyelnk dseliihvfp cvpekpgmpc pgedksiyrr
121 garrwrklyy atghafqakr fnrrahcaic tdriwglgrq gykcinckll vhkkchklvt
181 vecgrqviqd pmigridpgs thpehpdqvl gkknstesin hegeeheavg sresgkavss
241 lglidfdllr vigrgsyakv llvrlkkter iyamkvvkke lvnddedidw vqtekhvfeq
301 asnhpflvgl hscfqtesrl ffvieyvngg dlmfhmqrqr klpeeharfy saeislalny
361 lhergiiyrd lkldnvllds eghikltdyg mckeglrpgd ttstfcgtpn yiapeilrge
421 dygfsvdwwa lgvlmfemma grspfdivgs sdnpdqnted ylfqvilekq iriprslsvk
481 aasvlkgfln keskerlgch pqtgfadima hpffrnvdwd lmeqkqvvpp fkpnisgefg
541 ldnfdaqftn epiqltpddd davkkidqse fegfeyinpl lmsaeecv
```

Danio rerio aPKCζ (NP_001025262.1)

```
  1 mpvsngsmmd lpseyvkika hyggdmlisd ldlaltytev ckevremcgv rketpitlkw
 61 iddegdpcti ssqmeleeaf riysrsrhsg lllhvfpsip ekpgmpcpge dksiyrrgar
121 rwrklyrvng hlfqakrfnr kaycghcser iwglgrqgyk cinckllvhk rchklvpltc
181 qrhmdpvmps qeplvdddks geevelpped pedtdaipvp flahnrkvek aeddsedlka
241 vvdgiegiqi sqclglgdfd lirvigrgsy akvllvrlkk neqiyamkvv kkelvhdded
301 idwvqtekhv feqastnpfl vglhscfqte srlflvieyv nggdlmfhmq rqrklpeeha
361 rfyaaeicia lnflhekgii yrdlkldnvl ldqdghiklt dygmckegir pgdttstfcg
421 tpnyiapeil rgedygfsvd wwalgvlmfe mmagrspfdi itdnpdmnte eylfqvilek
481 piriprslsv kaasvlkgfl nkdpkerlgc qvqtgftdik shtffrsidw dqleqkqvtp
541 pfkpqitddy glenfdtqft nepvqltpdd edvikridqs efegfeyinp lllsteetv
```

Homo sapiens aPKCi (NP_002731.4)

```
  1 mptqrdsstm shtvagggsg dhshqvrvka yyrgdimith fepsisfegl cnevrdmcsf
 61 dneqlftmkw ideegdpctv ssqleleeaf rlyelnkdse llihvfpcvp erpgmpcpge
121 dksiyrrgar rwrklycang htfqakrfnr rahcaictdr iwglgrqgyk cinckllvhk
181 kchklvtiec grhslpqepv mpmdqssmhs dhaqtvipyn psshesldqv geekeamntr
241 esgkassslg lqdfdllrvi grgsyakvll vrlkktdriy amkvvkkelv nddedidwvq
301 tekhvfeqas nhpflvglhs cfqtesrlff vieyvnggdl mfhmqrqrkl peeharfysa
361 eislalnylh ergiiyrdlk ldnvlldseg hikltdygmc keglrpgdtt stfcgtpnyi
421 apeilrgedy gfsvdwwalg vlmfemmagr spfdivgssd npdqntedyl fqvilekqir
481 iprslsvkaa svlksflnkd pkerlgchpq tgfadiqghp ffrnvdwdmm eqkqvvppfk
541 pnisgefgld nfdsqftnep vqltpddddi vrkidqsefe gfeyinpllm saeecv
```

Figure 5.5: Complete protein sequence of aPKCs of *Danio rerio* and *H. sapiens*

5.2 Movie Legend

Movie 1: wt;gata1_GC migration
Time-lapse recording of a transgenic *wt;gata1:GFP* embryo from 55-72 hpf. Dorsal view of the cerebellum. The movie shows early GC migration and the migration path of selected GC in the final frame.

Movie 2: wt,gata1_GC tracing
Time-lapse recording of a transgenic *wt;gata1:GFP* embryo from 55-72 hpf. Dorsal view of the cerebellum. Throughout the movie the tracing of selected GC is depicted.

Movie 3: has,gata1_GC migration
Time-lapse recording of a transgenic *has;gata1:GFP* embryo from 78-95 hpf (17 hours). Dorsal view of the cerebellum. The movie shows early GC migration and the migration path of selected GC in the final frame.

Movie 4: has,gata1_GC tracing
Time-lapse recording of a transgenic *wt;gata1:GFP* embryo from 78-95 hpf (17 hours). Dorsal view of the cerebellum. Throughout the movie the tracing of selected GC is depicted.

Movie 5: wt,zic4_UncVenus-Control
Time-lapse recording of an transgenic *wt;zic4:Gal4,UAS:mCherry* embryo injected with the expression vector pCS-4xUAS:UncVenus. Control movie to show migration of electroporated GCs without affected functionality of aPKCi. The embryo was injected into the 4^{th} ventricle and subjected to electroporation at ~36 hpf. The movie shows the dorsal view of one hemisphere of the cerebellum recorded from 70-80 hpf.

Movie 6: wt,zic4_UncVenus-aPKCi2A
Time-lapse recording of an transgenic *wt;zic4:Gal4,UAS:mCherry* embryo injected with the expression vector pCS-4xUAS:UncVenus-T2A-aPKCi2A. The movie shows migration of electroporated GCs with inhibited function of aPKCi. The embryo was injected into the 4^{th} ventricle and subjected to electroporation at ~36 hpf. The movie shows the dorsal view of one hemisphere of the cerebellum recorded from 60-80 hpf.

5.3 Abbreviations

AA	amino acid	LSM	laser scanning microscope
AcO	Acridine Orange	MeOH	methanol
aPKC	atypical protein kinase	met	metencephalon
ATP	adenosine triphosphate	MHB	mid-hindbrain boundary
BCIP	5-bromo-4-chloro-3'-indolyphosphate p-toluidine	ML	molecular layer
		mRNA	messenger RNA
bp	base pair	NBT	nitro-blue tetrazolium chloride
BSA	bovine serum albumine		
cb	cerebellum	NGS	normal goat serum
CNS	central nervous system	*nok*	*nagie oko*
LRL	lower rhombic lip	OpT	optic tectum
DMSO	dimethylsulfoxid	PBS	phosphate-buffered saline
DNA	deoxyribonucleic Acid	PC	Purkinje cell
DNase	desoxyribonuclease	PCL	Purkinje cell layer
dNTP	deoxynucleotide triphosphate	PCNA	Proliferating-Cell-Nuclear-Antigen
dpf	days past fertilization	PCR	polymerase chain reaction
EGL	external granular layer	PFA	paraformaldehyde
EtOH	ethanol	pH3	phosphp-histone H3
ENU	N-ethyl-N-nitrosourea	PTU	phenylthiourea
GC	granule cell	PTW	PBS with Tween
GCP	granule cell precursor	Rh	rhombencephalon
GFP	green fluorescent protein	RNA	ribonucleic acid
has	*heart & soul*	RNase	ribonuclease
hb	hindbrain	rpm	rounds per minute
hpf	hours past fertilization	RT	room temperature
IGL	inner granular layer	RT-PCR	reverse transcription PCR
INM	interkinetic nuclear movement	Tg	transgenic
		UAS	upstream activating sequence
IsO	isthmic organiser		
4thV	fourth ventricle	URL	upper rhombic lip
kDa	kilo dalton	VZ	ventricular zone
LB	Luria-Bertani medium	*wt*	*wildtype*

5.4 References

Ahn, AH; Dziennis, S; Hawkes, R and Herrup, K (1994). The cloning of zebrin II reveals its identity with aldolase C. Development 120(8): 2081-2090.

Alexandre, P; Reugels, AM; Barker, D; Blanc, E and Clarke, JDW (2010). Neurons derive from the more apical daughter in asymmetric divisions in the zebrafish neural tube. Nat Neurosci 13(6): 673-679.

Assémat, E; Bazellières, E; Pallesi-Pocachard, E; Le Bivic, A and Massey-Harroche, D (2008). Polarity complex proteins. Biochimica et Biophysica Acta (BBA) - Biomembranes 1778(3): 614-630.

Babaryka, A (2009). Characterisation of the zebrafish cerebellar efferent system. Dissertation. Technische Universität München.

Bae, Y-K; Kani, S; Shimizu, T; Tanabe, K; Nojima, H; Kimura, Y; Higashijima, S-i and Hibi, M (2009). Anatomy of zebrafish cerebellum and screen for mutations affecting its development. Developmental Biology 330(2): 406-426.

Bahn, S; Harvey, RJ; Darlison, MG and Wisden, W (1996). Conservation of γ-Aminobutyric Acid Type A Receptor α6 Subunit Gene Expression in Cerebellar Granule Cells, Blackwell Science Ltd. 66**:** 1810-1818.

Baye, LM and Link, BA (2007). Interkinetic Nuclear Migration and the Selection of Neurogenic Cell Divisions during Vertebrate Retinogenesis. J. Neurosci. 27(38): 10143-10152.

Benton, R and Johnston, DS (2003). Drosophila PAR-1 and 14-3-3 Inhibit Bazooka/PAR-3 to Establish Complementary Cortical Domains in Polarized Cells. Cell 115(6): 691-704.

Bolivar, F; Backman, K and Ray, W (1979). [16] Plasmids of Escherichia coli as cloning vectors. Methods in Enzymology, Academic Press. Volume 68: 245-267.

Bullock, WO; Fernandex, JM and Short, JM (1987). Xl1-Blue: A High Efficiency Plasmid Transforming recA Escherichia coli Strain With Beta-Galactosidase Selection BioTechniques 5: 376-379.

Campbell, HR; Meek, J; Zhang, J and Bell, CC (2007). Anatomy of the posterior caudal lobe of the cerebellum and the eminentia granularis posterior in a mormyrid fish. The Journal of Comparative Neurology 502(5): 714-735.

Celis, JE and Celis, A (1985). Cell cycle-dependent variations in the distribution of the nuclear protein cyclin proliferating cell nuclear antigen in cultured cells: subdivision of S phase. Proceedings of the National Academy of Sciences 82(10): 3262-3266.

Chaplin, N; Tendeng, C and Wingate, RJT (2010). Absence of an External Germinal Layer in Zebrafish and Shark Reveals a Distinct, Anamniote Ground Plan of Cerebellum Development. The Journal of Neuroscience 30(8): 3048-3057.

Chédotal, A (2010). Should I stay or should I go? Becoming a granule cell. Trends in Neurosciences 33(4): 163-172.

Chenn, A; Zhang, YA; Chang, BT and McConnell, SK (1998). Intrinsic Polarity of Mammalian Neuroepithelial Cells. Molecular and Cellular Neuroscience 11(4): 183-193.

Costa, MR; Wen, G; Lepier, A; Schroeder, T and Götz, M (2008). Par-complex proteins promote proliferative progenitor divisions in the developing mouse cerebral cortex. Development 135(1): 11-22.

Cox, DN; Seyfried, SA; Jan, LY and Jan, YN (2001). Bazooka and atypical protein kinase C are required to regulate oocyte differentiation in the Drosophila ovary. Proceedings of the National Academy of Sciences 98(25): 14475-14480.

Cui, S; Otten, C; Rohr, S; Abdelilah-Seyfried, S and Link, BA (2007). Analysis of aPKCι and aPKCλ reveals multiple and redundant functions during vertebrate retinogenesis. Molecular and Cellular Neuroscience 34(3): 431-444.

Distel, M; Babaryka, A and Köster, RW (2006). Multicolor in vivo time-lapse imaging at cellular resolution by stereomicroscopy. Developmental Dynamics 235(4): 1100-1106.

Distel, M; Hocking, JC; Volkmann, K and Köster, RW (2010). The centrosome neither persistently leads migration nor determines the site of axonogenesis in migrating neurons in vivo. The Journal of Cell Biology 191(4): 875-890.

Dynes, JL and Ngai, J (1998). Pathfinding of Olfactory Neuron Axons to Stereotyped Glomerular Targets Revealed by Dynamic Imaging in Living Zebrafish Embryos. Neuron 20(6): 1081-1091.

Etienne-Manneville, S and Hall, A (2003). Cdc42 regulates GSK-3[beta] and adenomatous polyposis coli to control cell polarity. Nature 421(6924): 753-756.

Feigin, ME and Muthuswamy, SK (2009). Polarity proteins regulate mammalian cell-cell junctions and cancer pathogenesis. Current Opinion in Cell Biology 21(5): 694-700.

Fields, A; Frederick, L and Regala, R (2007). Targeting the oncogenic protein kinase Cι signalling pathway for the treatment of cancer. Biochemical Society Transactions 35(5).

Frade, JM; Azmitia, EC; DeFelipe, J; Jones, EG; Rakic, P and Ribak, CE (2002). Chapter 5 Interkinetic nuclear movement in the vertebrate neuroepithelium: encounters with an old acquaintance. Progress in Brain Research, Elsevier. Volume 136: 67-71.

Fukata, M; Nakagawa, M and Kaibuchi, K (2003). Roles of Rho-family GTPases in cell polarisation and directional migration. Current Opinion in Cell Biology 15(5): 590-597.

Gómez, A; Durán, E; Salas, C and Rodríguez, F (2010). Cerebellum lesion impairs eyeblink-like classical conditioning in goldfish. Neuroscience 166(1): 49-60.

Grant, P and Moens, C (2010). The neuroepithelial basement membrane serves as a boundary and a substrate for neuron migration in the zebrafish hindbrain. Neural Development 5(1): 9.

Hanks, S and Hunter, T (1995). Protein kinases 6. The eukaryotic protein kinase superfamily: kinase (catalytic) domain structure and classification. The FASEB Journal 9(8): 576-596.

Harris, TJC and Peifer, M (2005). The positioning and segregation of apical cues during epithelial polarity establishment in Drosophila. The Journal of Cell Biology 170(5): 813-823.

Hendzel, MJ; Wei, Y; Mancini, MA; Hooser, AV; Ranalli, T; Brinkley, BR; Bazett-Jones, DP and Allis2, CD (1997). Mitosis-specific phosphorylation of histone H3 initiates primarily within pericentromeric heterochromatin during G2 and spreads in an ordered fashion coincident with mitotic chromosome condensation. Chromosoma 106(6): 348-360.

Henrique, D and Schweisguth, Fo (2003). Cell polarity: the ups and downs of the Par6/aPKC complex. Current Opinion in Genetics & Development 13(4): 341-350.

Hibi, M and Shimizu, T (2012). Development of the cerebellum and cerebellar neural circuits. Developmental Neurobiology 72(3): 282-301.

Horne-Badovinac, S; Lin, D; Waldron, S; Schwarz, M; Mbamalu, G; Pawson, T; Jan, Y-N; Stainier, DYR and Abdelilah-Seyfried, S (2001). Positional cloning of heart and soul reveals multiple roles for PKCi in zebrafish organogenesis. Current Biology 11(19): 1492-1502.

Horne-Badovinac, S; Rebagliati, M and Stainier, DYR (2003). A Cellular Framework for Gut-Looping Morphogenesis in Zebrafish. Science 302(5645): 662-665.

Hoshino, M; Nakamura, S; Mori, K; Kawauchi, T; Terao, M; Nishimura, YV; Fukuda, A; Fuse, T; Matsuo, N; Sone, M; Watanabe, M; Bito, H; Terashima, T; Wright, CVE; Kawaguchi, Y; Nakao, K and Nabeshima, Y-i (2005). Ptf1a, a bHLH Transcriptional Gene, Defines GABAergic Neuronal Fates in Cerebellum. Neuron 47(2): 201-213.

Hurd, TW; Gao, L; Roh, MH; Macara, IG and Margolis, B (2003). Direct interaction of two polarity complexes implicated in epithelial tight junction assembly. Nat Cell Biol 5(2): 137-142.

Hurov, JB; Watkins, JL and Piwnica-Worms, H (2004). Atypical PKC Phosphorylates PAR-1 Kinases to Regulate Localization and Activity. Current Biology 14(8): 736-741.

Ito, M (2008). Control of mental activities by internal models in the cerebellum. Nat Rev Neurosci 9(4): 304-313.

Izumi, Y; Hirose, T; Tamai, Y; Hirai, S-i; Nagashima, Y; Fujimoto, T; Tabuse, Y; Kemphues, KJ and Ohno, S (1998). An Atypical PKC Directly Associates and Colocalizes at the Epithelial Tight Junction with ASIP, a Mammalian Homologue of Caenorhabditis elegans Polarity Protein PAR-3. The Journal of Cell Biology 143(1): 95-106.

Joberty, G; Petersen, C; Gao, L and Macara, IG (2000). The cell-polarity protein Par6 links Par3 and atypical protein kinase C to Cdc42. Nat Cell Biol 2(8): 531-539.

Johansson, A; Driessens, M and Aspenstrom, P (2000). The mammalian homologue of the Caenorhabditis elegans polarity protein PAR-6 is a binding partner for the Rho GTPases Cdc42 and Rac1. Journal of Cell Science 113(18): 3267-3275.

Joyner, AL (1996). Engrailed, Wnt and Pax genes regulate midbrain-hindbrain development. Trends in Genetics 12(1): 15-20.

Joyner, AL; Liu, A and Millet, S (2000). Otx2, Gbx2 and Fgf8 interact to position and maintain a mid-hindbrain organizer. Current Opinion in Cell Biology 12(6): 736-741.

Kani, S; Bae, Y-K; Shimizu, T; Tanabe, K; Satou, C; Parsons, MJ; Scott, E; Higashijima, S-i and Hibi, M (2010). Proneural gene-linked neurogenesis in zebrafish cerebellum. Developmental Biology 343(1-2): 1-17.

Kaslin, J; Ganz, J; Geffarth, M; Grandel, H; Hans, S and Brand, M (2009). Stem Cells in the Adult Zebrafish Cerebellum: Initiation and Maintenance of a Novel Stem Cell Niche. The Journal of Neuroscience 29(19): 6142-6153.

Kato, K (1990). Novel $GABA_A$ receptor α subunit is expressed only in cerebellar granule cells. Journal of Molecular Biology 214(3): 619-624.

Katsuyama, Y; Oomiya, Y; Dekimoto, H; Motooka, E; Takano, A; Kikkawa, S; Hibi, M and Terashima, T (2007). Expression of zebrafish ROR alpha gene in cerebellar-like structures. Developmental Dynamics 236(9): 2694-2701.

Kera, SA; Agerwala, SM and Horne, JH (2010). The Temporal Resolution of In Vivo Electroporation in Zebrafish: A Method for Time-Resolved Loss of Function. Zebrafish 7(1): 97-108.

Kettenmann, H (2007). Neuroscience: The brain's garbage men. Nature 446(7139): 987-989.

Kim, M; Datta, A; Brakeman, P; Yu, W and Mostov, KE (2007). Polarity proteins PAR6 and aPKC regulate cell death through GSK-3beta in 3D epithelial morphogenesis. J Cell Sci 120(14): 2309-2317.

Kim, S; Lehtinen, MK; Sessa, A; Zappaterra, MW; Cho, S-H; Gonzalez, D; Boggan, B; Austin, CA; Wijnholds, J; Gambello, MJ; Malicki, J; LaMantia, AS; Broccoli, V and Walsh, CA (2010). The Apical Complex Couples Cell Fate and Cell Survival to Cerebral Cortical Development. Neuron 66(1): 69-84.

Kimmel, CB; Ballard, WW; Kimmel, SR; Ullmann, B and Schilling, TF (1995). Stages of embryonic development of the zebrafish. Developmental Dynamics 203(3): 253-310.

Kosodo, Y; Roper, K; Haubensak, W; Marzesco, A-M; Corbeil, D and Huttner, WB (2004). Asymmetric distribution of the apical plasma membrane during neurogenic divisions of mammalian neuroepithelial cells. EMBO J 23(11): 2314-2324.

Köster, RW (2006). Quo vadis, neuron? Biospektrum(5).

Köster, RW and Fraser, SE (2006). FGF Signaling Mediates Regeneration of the Differentiating Cerebellum through Repatterning of the Anterior Hindbrain and Reinitiation of Neuronal Migration. The Journal of Neuroscience 26(27): 7293-7304.

Krauss, S; Maden, M; Holder, N and Wilson, SW (1992). Zebrafish pax[b] is involved in the formation of the midbrain-hindbrain boundary. Nature 360(6399): 87-89.

Lemmers, C; Michel, D; Lane-Guermonprez, L; Delgrossi, M-H; Médina, E; Arsanto, J-P and Le Bivic, A (2004). CRB3 Binds Directly to Par6 and Regulates the Morphogenesis of the Tight Junctions in Mammalian Epithelial Cells. Molecular Biology of the Cell 15(3): 1324-1333.

Long, Q; Meng, A; Wang, H; Jessen, JR; Farrell, MJ and Lin, S (1997). GATA-1 expression pattern can be recapitulated in living transgenic zebrafish using GFP reporter gene. Development 124(20): 4105-4111.

Lowery, LA; De Rienzo, G; Gutzman, JH and Sive, H (2009). Characterization and Classification of Zebrafish Brain Morphology Mutants. The Anatomical Record: Advances in Integrative Anatomy and Evolutionary Biology 292(1): 94-106.

Lowery, LA and Sive, H (2005). Initial formation of zebrafish brain ventricles occurs independently of circulation and requires the nagie oko and snakehead/atp1a1a.1 gene products. Development 132(9): 2057-2067.

Lüddens, H; Pritchett, DB; Kohler, M; Killisch, I; Keinanen, K; Monyer, H; Sprengel, R and Seeburg, PH (1990). Cerebellar GABAA receptor selective for a behavioural alcohol antagonist. Nature 346(6285): 648-651.

Macara, IG (2004). Parsing the Polarity Code. Nat Rev Mol Cell Biol 5(3): 220-231.

Machold, R and Fishell, G (2005). Math1 Is Expressed in Temporally Discrete Pools of Cerebellar Rhombic-Lip Neural Progenitors. Neuron 48(1): 17-24.

Malicki, J; Neuhauss, SC; Schier, AF; Solnica-Krezel, L; Stemple, DL; Stainier, DY; Abdelilah, S; Zwartkruis, F; Rangini, Z and Driever, W (1996). Mutations affecting development of the zebrafish retina. Development 123(1): 263-273.

Margolis, B and Borg, J-P (2005). Apicobasal polarity complexes. Journal of Cell Science 118(22): 5157-5159.

Marín, O; Valiente, M; Ge, X and Tsai, L-H (2010). Guiding Neuronal Cell Migrations. Cold Spring Harbor Perspectives in Biology 2(2).

Martini, FJ; Valiente, M; López Bendito, G; Szabó, G; Moya, F; Valdeolmillos, M and Marín, O (2009). Biased selection of leading process branches mediates chemotaxis during tangential neuronal migration. Development 136(1): 41-50.

Mikami, Y; Yoshida, T; Matsuda, N and Mishina, M (2004). Expression of zebrafish glutamate receptor δ2 in neurons with cerebellum-like wiring. Biochemical and Biophysical Research Communications 322(1): 168-176.

Miyata, T; Maeda, T and Lee, JE (1999). NeuroD is required for differentiation of the granule cells in the cerebellum and hippocampus. Genes & Development 13(13): 1647-1652.

Moens, CB and Prince, VE (2002). Constructing the hindbrain: Insights from the zebrafish. Developmental Dynamics 224(1): 1-17.

Mugnaini, E; Sekerková, G and Martina, M (2011). The unipolar brush cell: A remarkable neuron finally receiving deserved attention. Brain Research Reviews 66(1-2): 220-245.

Murray, NR; Kalari, KR and Fields, AP (2011). Protein kinase Cι expression and oncogenic signaling mechanisms in cancer. Journal of Cellular Physiology 226(4): 879-887.

O'Hara, FP; Beck, E; Barr, LK; Wong, LL; Kessler, DS and Riddle, RD (2005). Zebrafish Lmx1b.1 and Lmx1b.2 are required for maintenance of the isthmic organizer. Development 132(14): 3163-3173.

Pan, N; Jahan, I; Lee, J and Fritzsch, B (2009). Defects in the cerebella of conditional *Neurod1* null mice correlate with effective *Tg(Atoh1-cre)* recombination and granule cell requirements for *Neurod1* for differentiation. Cell and Tissue Research 337(3): 407-428.

Pellettieri, J and Seydoux, G (2002). Anterior-Posterior Polarity in C. elegans and Drosophila--PARallels and Differences. Science 298(5600): 1946-1950.

Perander, M; Bjorkoy, G and Johansen, T (2001). Nuclear Import and Export Signals Enable Rapid Nucleocytoplasmic Shuttling of the Atypical Protein Kinase Cλ. Journal of Biological Chemistry 276(16): 13015-13024.

Peri, F and Nüsslein-Volhard, C (2008). Live Imaging of Neuronal Degradation by Microglia Reveals a Role for v0-ATPase a1 in Phagosomal Fusion In Vivo. Cell 133(5): 916-927.

Qiu, R-G; Abo, A and Martin, GS (2000). A human homolog of the C. elegans polarity determinant Par-6 links Rac and Cdc42 to PKCζ signaling and cell transformation. Current Biology 10(12): 697-707.

Rhinn, M; Lun, K; Amores, A; Yan, Y-L; Postlethwait, JH and Brand, M (2003). Cloning, expression and relationship of zebrafish gbx1 and gbx2 genes to Fgf signaling. Mechanisms of Development 120(8): 919-936.

Rieger, S; Senghaas, N; Walch, A and Köster, RW (2009). Cadherin-2 Controls Directional Chain Migration of Cerebellar Granule Neurons. PLoS Biol 7(11): e1000240.

Rodríguez, F; Durán, E; Gómez, A; Ocana, FM; Álvarez, E; Jiménez-Moya, F; Broglio, C and Salas, C (2005). Cognitive and emotional functions of the teleost fish cerebellum. Brain Research Bulletin 66(4-6): 365-370.

Rohr, S; Bit-Avragim, N and Abdelilah-Seyfried, S (2006). Heart and soul/PRKCi and nagie oko/Mpp5 regulate myocardial coherence and remodeling during cardiac morphogenesis. Development 133(1): 107-115.

Rolls, MM; Albertson, R; Shih, H-P; Lee, C-Y and Doe, CQ (2003). Drosophila aPKC regulates cell polarity and cell proliferation in neuroblasts and epithelia. The Journal of Cell Biology 163(5): 1089-1098.

Rupp, RA; Snider, L and Weintraub, H (1994). Xenopus embryos regulate the nuclear localization of XMyoD. Genes & Development 8(11): 1311-1323.

Sakakibara, A and Horwitz, AF (2006). Mechanism of polarized protrusion formation on neuronal precursors migrating in the developing chicken cerebellum. J Cell Sci 119(17): 3583-3592.

Santos, N and Reiter, JF (2008). Building it up and taking it down: The regulation of vertebrate ciliogenesis. Developmental Dynamics 237(8): 1972-1981.

Sato, T; Joyner, AL and Nakamura, H (2004). How does Fgf signaling from the isthmic organizer induce midbrain and cerebellum development? Development, Growth & Differentiation 46(6): 487-494.

Schier, AF; Neuhauss, SC; Harvey, M; Malicki, J; Solnica-Krezel, L; Stainier, DY; Zwartkruis, F; Abdelilah, S; Stemple, DL; Rangini, Z; Yang, H and Driever, W (1996). Mutations affecting the development of the embryonic zebrafish brain. Development 123(1): 165-178.

Schüller, U; Kho, AT; Zhao, Q; Ma, Q and Rowitch, DH (2006). Cerebellar 'transcriptome' reveals cell-type and stage-specific expression during postnatal development and tumorigenesis. Molecular and Cellular Neuroscience 33(3): 247-259.

Sgaier, SK; Lao, Z; Villanueva, MP; Berenshteyn, F; Stephen, D; Turnbull, RK and Joyner, AL (2007). Genetic subdivision of the tectum and cerebellum into functionally related regions based on differential sensitivity to engrailed proteins. Development 134(12): 2325-2335.

Sgaier, SK; Millet, S; Villanueva, MP; Berenshteyn, F; Song, C and Joyner, AL (2005). Morphogenetic and Cellular Movements that Shape the Mouse Cerebellum: Insights from Genetic Fate Mapping. Neuron 45(1): 27-40.

Solecki, DJ; Trivedi, N; Govek, E-E; Kerekes, RA; Gleason, SS and Hatten, ME (2009). Myosin II Motors and F-Actin Dynamics Drive the Coordinated Movement of the Centrosome and Soma during CNS Glial-Guided Neuronal Migration. Neuron 63(1): 63-80.

Soloff, RS; Katayama, C; Lin, MY; Feramisco, JR and Hedrick, SM (2004). Targeted Deletion of Protein Kinase C i Reveals a Distribution of Functions between the Two Atypical Protein Kinase C Isoforms. The Journal of Immunology 173(5): 3250-3260.

Spalice, A; Parisi, P; Nicita, F; Pizzardi, G; Del Balzo, F and Iannetti, P (2009). Neuronal migration disorders: clinical, neuroradiologic and genetics aspects. Acta Pædiatrica 98(3): 421-433.

Spassky, N; Han, YG; Aguilar, A; Strehl, L; Besse, L; Laclef, C; Romaguera Ros, M; Garcia-Verdugo, JM and Alvarez-Buylla, A (2008). Primary cilia are required for cerebellar development and Shh-dependent expansion of progenitor pool. Developmental Biology 317(1): 246-259.

Stainier, DY; Fouquet, B; Chen, JN; Warren, KS; Weinstein, BM; Meiler, SE; Mohideen, MA; Neuhauss, SC; Solnica-Krezel, L; Schier, AF; Zwartkruis, F; Stemple, DL; Malicki, J; Driever, W and Fishman, MC (1996). Mutations affecting the formation and function of the cardiovascular system in the zebrafish embryo. Development 123(1): 285-292.

Stevenson, BR; Siliciano, JD; Mooseker, MS and Goodenough, DA (1986). Identification of ZO-1: a high molecular weight polypeptide associated with the tight junction (zonula occludens) in a variety of epithelia. The Journal of Cell Biology 103(3): 755-766.

Suzuki, A; Hirata, M; Kamimura, K; Maniwa, R; Yamanaka, T; Mizuno, K; Kishikawa, M; Hirose, H; Amano, Y; Izumi, N; Miwa, Y and Ohno, S (2004). aPKC Acts Upstream of PAR-1b in Both the Establishment and Maintenance of Mammalian Epithelial Polarity. Current Biology 14(16): 1425-1435.

Suzuki, A and Ohno, S (2006). The PAR-aPKC system: lessons in polarity. J Cell Sci 119(6): 979-987.

Suzuki, A; Yamanaka, T; Hirose, T; Manabe, N; Mizuno, K; Shimizu, M; Akimoto, K; Izumi, Y; Ohnishi, T and Ohno, S (2001). Atypical Protein Kinase C Is Involved in the Evolutionarily Conserved Par Protein Complex and Plays a Critical Role in Establishing Epithelia-Specific Junctional Structures. The Journal of Cell Biology 152(6): 1183-1196.

Tabuse, Y; Izumi, Y; Piano, F; Kemphues, KJ; Miwa, J and Ohno, S (1998). Atypical protein kinase C cooperates with PAR-3 to establish embryonic polarity in Caenorhabditis elegans. Development 125(18): 3607-3614.

Tamai, H; Shinohara, H; Miyata, T; Saito, K; Nishizawa, Y; Nomura, T and Osumi, N (2007). Pax6 transcription factor is required for the interkinetic nuclear movement of neuroepithelial cells. Genes to Cells 12(9): 983-996.

Taverna, E and Huttner, WB (2010). Neural Progenitor Nuclei IN Motion. Neuron 67(6): 906-914.

Tsai, L-H and Gleeson, JG (2005). Nucleokinesis in Neuronal Migration. Neuron 46(3): 383-388.

Umeshima, H; Hirano, T and Kengaku, M (2007). Microtubule-based nuclear movement occurs independently of centrosome positioning in migrating neurons. Proceedings of the National Academy of Sciences 104(41): 16182-16187.

Valiente, M and Marín, O (2010). Neuronal migration mechanisms in development and disease. Current Opinion in Neurobiology 20(1): 68-78.

Volkmann, K; Chen, Y-Y; Harris, MP; Wullimann, MF and Köster, RW (2010). The zebrafish cerebellar upper rhombic lip generates tegmental hindbrain nuclei by long-distance migration in an evolutionary conserved manner. The Journal of Comparative Neurology 518: 2794-2817.

Volkmann, K; Rieger, S; Babaryka, A and Köster, RW (2008). The zebrafish cerebellar rhombic lip is spatially patterned in producing granule cell populations of different functional compartments. Developmental Biology 313(1): 167-180.

Wang, VY; Rose, MF and Zoghbi, HY (2005). Math1 Expression Redefines the Rhombic Lip Derivatives and Reveals Novel Lineages within the Brainstem and Cerebellum. Neuron 48(1): 31-43.

Wei, X and Malicki, J (2002). nagie oko, encoding a MAGUK-family protein, is essential for cellular patterning of the retina. Nat Genet 31(2): 150-157.

Westerfield, M (1995). The Zebrafish Book. A Guide for the Laboratory Use of Zebrafish (Danio rerio). Eugene, University of Oregon Press

White, WO; Seibenhener, ML and Wooten, MW (2002). Phosphorylation of tyrosine 256 facilitates nuclear import of atypical protein kinase C. Journal of Cellular Biochemistry 85(1): 42-53.

Willardsen, MI and Link, BA (2011). Cell biological regulation of division fate in vertebrate neuroepithelial cells. Developmental Dynamics 240(8): 1865-1879.

Wingate, R (2005). Math-Map(ic)s. Neuron 48(1): 1-4.

Wodarz, A; Ramrath, A; Grimm, A and Knust, E (2000). Drosophila Atypical Protein Kinase C Associates with Bazooka and Controls Polarity of Epithelia and Neuroblasts. The Journal of Cell Biology 150(6): 1361-1374.

Wullimann, MF (1998). The central nervous system. The Physiology of Fishes. D. H. Evans. Boca Raton, Florida, CRC Press.

Wullimann, MF; Mueller, T; Distel, M; Babaryka, A; Grothe, B and Köster, RW (2011). The long adventurous journey of rhombic lip cells in jawed vertebrates: a comparative developmental analysis. Frontiers in Neuroanatomy 5.

Wullimann, MF; Rupp, B and Reichert, H (1996). Neuroanatomy of the zebrafish brain: a topological atlas. Basel, Birkhäuser Verlag.

Wurst, W and Bally-Cuif, L (2001). Neural plate patterning: Upstream and downstream of the isthmic organizer. Nat Rev Neurosci 2(2): 99-108.

Yamaguchi, M; Imai, F; Tonou-Fujimori, N and Masai, I (2010). Mutations in N-cadherin and a Stardust homolog, Nagie oko, affect cell-cycle exit in zebrafish retina. Mechanisms of Development 127(5-6): 247-264.

5.5 Eidesstattliche Erklärung

Hiermit erkläre ich an Eides statt, dass ich die vorliegende Dissertation gemäß der Prüfungsordnung der TU München selbstständig, ohne unzulässige fremde Hilfe und unerlaubte Hilfsmittel angefertigt habe.

München, den

_____

(Anna-Lena Kerner)

5.6 Danksagung

Ich danke Prof. Dr. Reinhard Köster für die gute Betreuung, sein Verständnis und die Aufnahme in seine Arbeitsgruppe.

Ich danke meinem Doktorvater Prof. Dr. Wolfgang Wurst für die Möglichkeit in seinem Institut meine Doktorarbeit anfertigen zu können.

Ich danke ganz besonders meinen Kollegen, ohne deren Unterstützung und Hilfsbereitschaft in jeglicher Hinsicht, sowie gute Laune, Scherze, Musikeinlagen usw. diese Arbeit nicht fertig geworden wäre. Vielen lieben Dank an Katrin, Jen, Enrico, Niklas, Martin, Rosi, Christiane, Thomas, Petra, Andreas, Kazuhiko und Changsheng.

Vielen Dank auch an die Tierpflegerinnen (Yvonne, Heike, Anni, Sylvie, Vera) ohne deren unermüdlichen Einsatz zum Wohlergehen der Fische nichts möglich oder vieles um einiges mühsamer und zeitraubender gewesen wäre, und die immer für einen Scherz zu haben waren.

Ich danke Dr. Daniela Vogt Weisenhorn und Elisabeth Güll für ihr offenes Ohr und Verständnis.

Ich danke herzlichst meinen Freunden für die moralische Unterstützung, die oft nötig war. Und dafür, dass sie immer zu mir gehalten haben. Rosi, Christiane, Christine, Marcus, Anja, Korinna, Veronika, Franzi, André, Sabine und Steffi und allen anderen. Rosi, vielen lieben Dank für den mega krass coolen super schönen Doktorhut.

Ich danke von ganzem Herzen meiner Familie, dass sie mich in einer schwierigen Phase aufgefangen hat, und dass ich immer auf sie zählen konnte.
Meinen Eltern Annemarie und Hans-Jürgen, sowie meinen Geschwistern Eva und Matthias.